

DOTTORATO DI RICERCA IN
Scienze Chimiche

Ciclo XXV

Settore Concorsuale di afferenza: 03/C1

Settore Scientifico disciplinare: CHIM/06

TITOLO TESI

**Reactivity of activated electrophiles and
nucleophiles: labile intermediates and
properties of the reaction products**

Presentata da: Zanna Nicola

Coordinatore Dottorato

Prof. Adriana Bigi

Relatore

Dott. Carla Boga

Co-Relatore

Prof. Luciano Forlani

Esame finale anno 2013

Table of contents

PREFACE

Chapter 1: A general overview on the electrophilic and nucleophilic aromatic substitution reactions

- 1.1 Electrophilic Aromatic Substitution Reactions (SE_{Ar})
- 1.2 Nucleophilic Aromatic Substitution Reaction (SN_{Ar})

Chapter 2: The proton dance in tris(dialkylamino)benzenes

- 2.1 The interactions of proton with tris(dialkylamino)benzenes
 - 2.1.1 Protonation of symmetric tris(dialkylamino)benzene derivatives
 - 2.1.2 Effect of the temperature's change
 - 2.1.3 Protonation of asymmetric tris(dialkylamino)benzenes
 - 2.1.4 X-Ray diffraction analysis
- 2.2 First X-ray structure of the Wheland complex in azo-coupling reaction

Chapter 3: 2,4-dipyrrolidine-1,3-thiazole as a new supernucleophile

- 3.1 Synthesis and characterization of ultrastable W-M complexes
- 3.2 A theoretical study on the structure, energetic and properties of the W-M complexes
 - 3.2.1 Theoretical structures
 - 3.2.2 Energetic Along Reaction's Pathways and Functional Benchmark
 - 3.2.3 Electronic Properties

Chapter 4: Solid state fluorescence in protonated azobenzenes

- 4.1 Coupling reaction of 1,3,5-trimethoxybenzene and diazonium salt derivatives
- 4.2 Fluorescence of azobenzene derivatives
- 4.3 Experimental and theoretical structures of azobenzene derivatives

Chapter 5: Multiple applications for a new class of azobenzene derivatives

- 5.1 The textile-dyeing property
- 5.2 The pH indicator property
- 5.3 Formation of fluorescent nanoparticles
 - 5.3.1 Preparation of fluorescent nanoparticles
 - 5.3.2 UV-Visible analyses
 - 5.3.3 Size measurement
 - 5.3.4 Fluorescence analyses

Chapter 6: Phospha Michael-type reaction of bidentate nucleophiles

- 6.1 Brief summary of used reagents
- 6.2 Reactions between 1,2-diaza-1,3-dienes (DDs) and bis(diphenyl) phosphines
 - 6.2.1 Reactions carried out with equimolar amount of DDs and diphosphines
 - 6.2.2 Reactions carried out with DDs and diphosphines in a 2/1 relative molar ratio
- 6.3 Reactions between 1,2-diaza-1,3-dienes and diphenyl phosphino amines

Chapter 7: Interaction between gliadins and coumarin: a joint theoretical and experimental study

- 7.1 Coumarin (3-EcC) and Glia at neutral pH
 - 7.1.1 Raman and IR vibrational results
 - 7.1.2 NMR Results
- 7.2 Coumarin (3-EcC) and Glia at acidic pH
 - 7.2.1 Raman Results
 - 7.2.2 NMR Results
- 7.3 Cyanidin (Cya) and Glia at acidic pH
 - 7.3.1 Raman Results
 - 7.3.2 NMR Results

7.4 A complex between coumarin and cyanidin? Influence on gliadin (GliA)
secondary structure

7.4.1 Raman Results

7.4.2 NMR Results

7.4.3 UV-Vis analysis

7.4.4 Theoretical calculation

Chapter 8: Theoretical study on the spectroscopic properties of iron complexes

8.1 Computational methods

8.2 Functionals benchmarking

8.3 Transition analyses

Preface

During my time as Ph.D. student I worked in the Forlani-Boga's research group. From a long time the research group's interest lies in the study of nucleophilic/electrophilic aromatic substitution reactions in particular from a mechanistic point of view.

These reactions were studied a lot in the past since aromatic compounds became building blocks for the development of materials with large applications. The accurate knowledge of their reactivity had a crucial and strategic role for the improvement of yields and number of steps in the industrial context.

From an academic point of view, a lot of more detailed studies were carried out with the aim of rationalize the basic reactions of aromatic rings such as nucleophilic and electrophilic substitutions. These studies were done to better understand the effects of substituents on the activation and regioselectivity of the attack by means of both electrophilic and nucleophilic reagents. The kinetic analyses were for a long time the only way to give an explanation to these questions, which also corroborated the simple approach of the number of resonance structures describing the system.

Afterwards, more sophisticated techniques allowed to identify some reaction's intermediates, which expanded the knowledge about aromatic substitution reactions. But even much more is to be discovered, and we tried to do it with the newest instruments that science give us.

For example, the Nuclear Magnetic Resonance (NMR) spectroscopy, which is actually among chemists the most used technique, allowed us to carry out the reactions directly in the NMR tube also at low temperature to letting us study the reaction's intermediates.

However our attention was mainly focused on the reactivity of superactivated aromatic systems. In spite of their high reactivity (hence the high reaction's rate), we were able to identify and in some case to isolate σ -complexes

until now only hypothesized. Interesting results comes from the study of the protonation of the supernucleophiles tris(dialkylamino)benzenes.

The goal of isolate stable σ -complexes was achieved thanks to a mindful design of these superactivated reagents, which was basically the main target of my Ph. D. research.

Furthermore we discovered, in some case fortuitously, some relevant properties and applications of the compounds we synthesized, such as fluorescence in solid state and nanoparticles or textile dyeing. We decided to investigate all these findings also by collaborating with other research groups.

Another collaboration with University of Urbino allowed us to investigate on the reactivity of 1,2-diaza-1,3-dienes toward nucleophiles such as amino and phosphine derivatives.

With the increasing power of computers and new methodologies such as Density Functional Theory (DFT) approach, computational chemistry has become actually an useful tool also for organic chemists which can easily carried out their studies by its own, looking for a support on the hypothesis based on the experimental data. Since the main topic of my Ph. D. thesis was the study on the reaction's mechanisms, I decided to begin a new path in the field of theoretical chemistry, with the aim and the hope to obtain important elucidation which could be able to help me in better describe the hypothesis based on my experimental data.

The choice of dedicate part of my research in the field of computational chemistry proceeded with a period in the "Laboratoire de Structure et Réactivité des Systèmes Moléculaires Complexes-SRSMC, Université de Lorraine et CNRS, France" in which I improved my knowledge about the topic, making a study on new iron complexes for the use as dyes in Dye Sensitized Solar Cells (DSSC). Furthermore, thanks to this new expertise, I was involved in a collaboration for the study of the ligands' interaction in biological systems.

This brief introduction is to explain the decision to separate the thesis in various chapters on the basis of the different research topics I have worked on.

Chapter 1

A general overview on the electrophilic and nucleophilic aromatic substitution reactions

Electrophilic and nucleophilic aromatic substitution reactions are probably the most studied reactions.^[1,2] The mechanism and the steps involved in both kinds of reactions is well known and largely reported in literature.

If we analyze in detail the mechanism of both types of reaction, we can observe that also if the intermediates have opposite charge, the reactive stages of reactions are the same. In the first step the electron-rich reagent interacts with the electron-poor one to give a charge transfer complex and then, with the formation of a real bond, the σ -complex is obtained.

The final product is obtained as a result of the departure of the leaving group or a simple atom, such in the case of hydrogen, which can be present in the reagent.

Starting from this consideration, new hypothesis about substitution reactions on aromatic substrate were elaborated; this prompted us to study more in deep the above mentioned reactions.

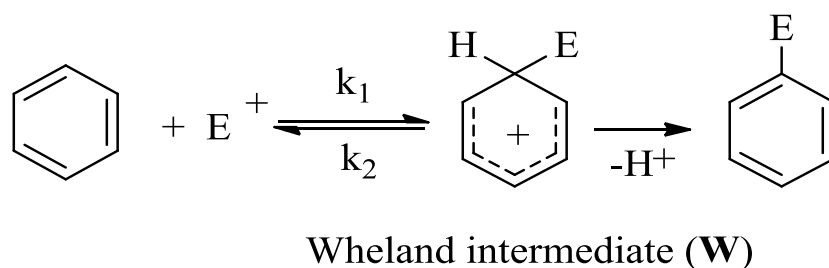
1.1 Electrophilic Aromatic Substitution Reactions (SE_{Ar})

The simplest example of this kind of reaction is the substitution of a proton on a benzene ring.

Benzene is the parent of all aromatic compounds; it is characterized by an high degree of electron's delocalization and a lower reactivity with respect to alkene and alkyne.

The evidence of the lower reactivity of aromatic hydrocarbon with respect to the unsaturated ones was observed from a long time: the electrophilic aromatic substitution is favored in the first case, while in the second case the electrophilic addition is preferred.

A detailed examination of the aromatic electrophilic substitution reaction show that the reaction between the aromatic ring and the electrophile bring at first to the formation of a positively charged intermediate usually called Wheland complex.^[3]



Scheme 1. General scheme for the electrophilic aromatic substitution reactions.

The cationic intermediate (or Wheland) possess a covalent bond between the electrophilic moiety and the aromatic ring in which one carbon atom change its hybridization from sp^2 to sp^3 .

The hybridization change by addition to the double bond and the break of the highly conjugated aromatic system make the σ -complex an high energy intermediate. (Figure 1).^[4]

Furthermore, the Wheland intermediate shows an higher stabilization respect to other cationic intermediates which are generated by addition reaction on unsaturated non-aromatic compounds. This stabilization is given by the possibility for the conjugate system to delocalize the charge on the other carbon atoms.^[1,2,4]

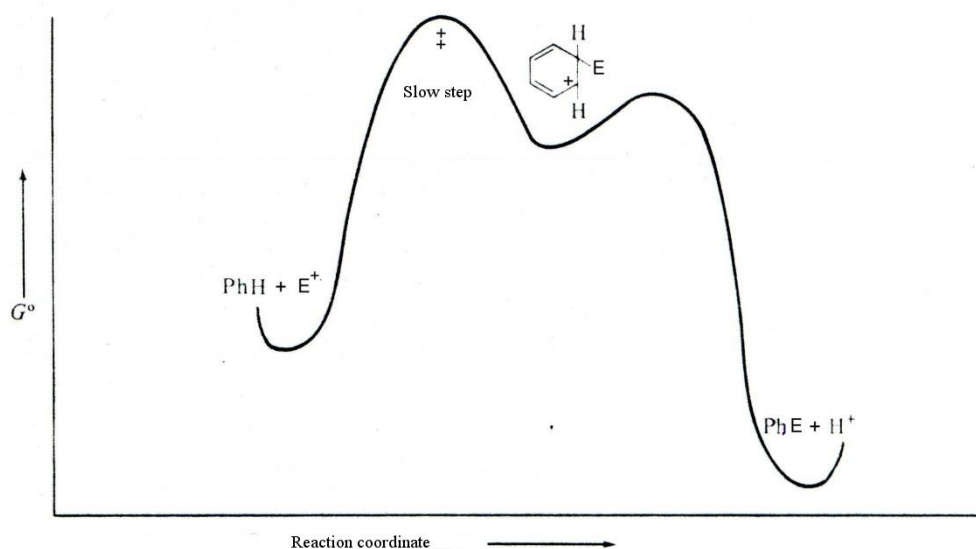


Figure 1. Energetic levels along the reaction coordinates for the electrophilic aromatic substitution reactions.

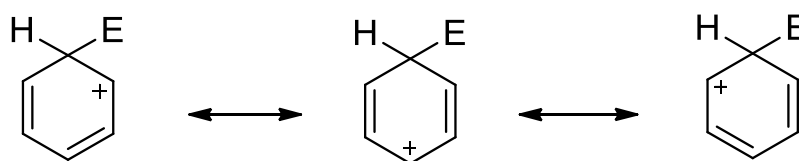


Figure 2. Resonance structures of the Wheland intermediate.

This intermediate usually leads to the proton elimination and the subsequent re-aromatization of the aromatic ring.

The literature reports induce to think that, because of the high rate of the proton elimination process from the intermediate, the σ -complex appears to be more similar to a transition state than to an intermediate.

However the proton substitution with deuterium show that in some cases the reaction's rate depends on the break of the C-H bond.^[5] It is still accepted the presence of two separate steps being the first the electrophilic attack on the aromatic ring and the second the proton departure, as shown in Figure 1.

However the σ -complex is an intermediate difficult to isolate because it is a species with a short lifetime for which the concentration result to be really low during the reaction.^[6]

The isolation and characterization of Wheland intermediate has been possible by the reaction of an electrophile with an hexa-substituted aromatic system. The cationic intermediate formed is moderately stable because of the presence of electron-donor groups in a conjugated position respect to the charge and the lack of easily removable proton.

An example of isolable intermediate comes from the reaction between an electrophile and hexamethyl-benzene, which lead to the formation of σ -complexes charaterizable by using spectroscopic techniques.^[7] Chloro-hexamethylbenzene, heptamethyl-benzene and nitro-hexamethyl-benzene cations (figure 3) were isolated and characterized by X-ray diffraction analysis.^[8a-b]

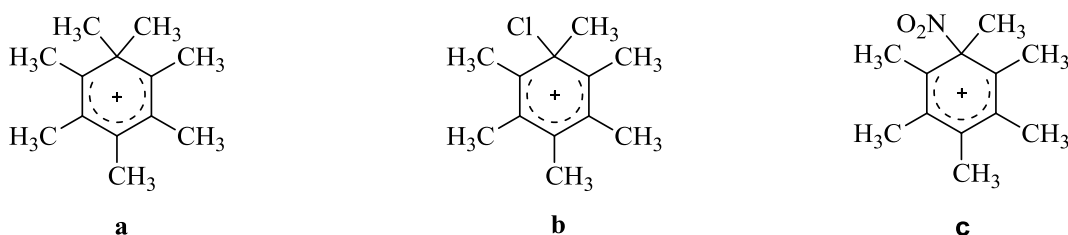
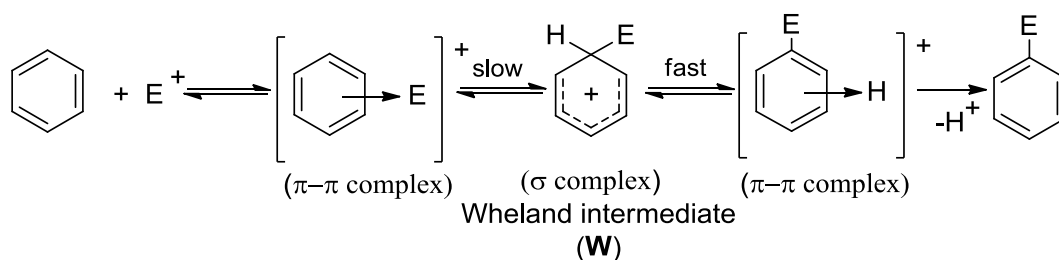


Figure 3. Heptamethyl-benzene (a), chloro-hexamethylbenzene (b), and nitro-hexamethyl-benzene (c) cations.

The energetic and reaction scheme depicted in Figure 1 and Scheme 1 respectively, show only one intermediate. Following studies carried out specially by J. K. Kochi showed the presence of four steps and three intermediates along the reaction pathways (scheme 2).^[9,10,11,12]



Schema 2. The general mechanism of aromatic substitution reactions.

The reaction's pathway reported in scheme 2 show that in a first step the electrophile get close to the π -electron of the aromatic systems, bringing to the formation of a donor-acceptor (**DA**) interaction. The complex formed is usually called π -complex which is not covalent in nature. In a donor-acceptor complex an interaction between the π cloud of the aromatic ring and the electrophile is formed in a reversible stage.

Hydrochloric acid and toluene form, for example, a π -complex at -78°C which is in equilibrium with starting materials.^[5]

In a **DA** complex the electrophile is not localized on a particular atom but is close to the π cloud of the aromatic ring. However some experimental evidence which involved electrophile such as Br^+ or NO_2^+ showed their preferential localization on a specific C-C bond preceding the formation of σ -complex.^[13]

The interaction in the π -complex is weak in nature, hence the energy of formation is low together with its activation energy. This implies that the rate of formation of the π -complex is not highly influenced by the substituent groups on the aromatic ring. However entropy can have a significant contribution related to the geometry of the system. In the case of proton this contribution is negligible because of its small size and the positive charge uniformly distributed on it.

Some π -complexes have been identified thanks to their property of showing charge transfer interactions, which can be easily observed as a result of the high absorption in the visible region of the electromagnetic spectra, hence resulting in strong colored compounds. In some cases they have been crystallized and analyzed by X-Ray diffraction spectroscopy.^[6,11,12,14]

Crystalline π -complexes were obtained from the reaction between picric acid and silver salts. It has been demonstrated that in π -complex between benzene and bromonium ion, the bromine atom is displaced in the middle of the π -electron cloud.^[1]

As abovementioned the next step of the reaction implies the formation of the new σ bond between the two substrates. These kind of intermediates are significantly different from the π -complexes, hence it can be possible to characterize it in a univocal way with spectroscopic technics. Until now nitrosation reactions are the only examples of electrophilic substitutions for which both π -complexes and σ -complexes have been identified and characterized by X-ray diffraction analysis and UV-visible spectroscopy.^[11,15,16]

The cyclohexadienic system formed from the evolution of the π -complex it is higher in energy respect to the starting aromatic compound; this means that the reaction can go on in both directions. This depends on the easiness with which the intermediate eliminate the electrophile or the proton also if usually the last is favored.

At last in the third step, together with the rearomatization process, the leaving group form a π -complex with the aromatic ring before it will be completely removed.

The formation of the Wheland intermediate is considered to be the slow stages of the reaction, with its energy close to that of transition state. A simplified energetic trend is reported in figure 4.

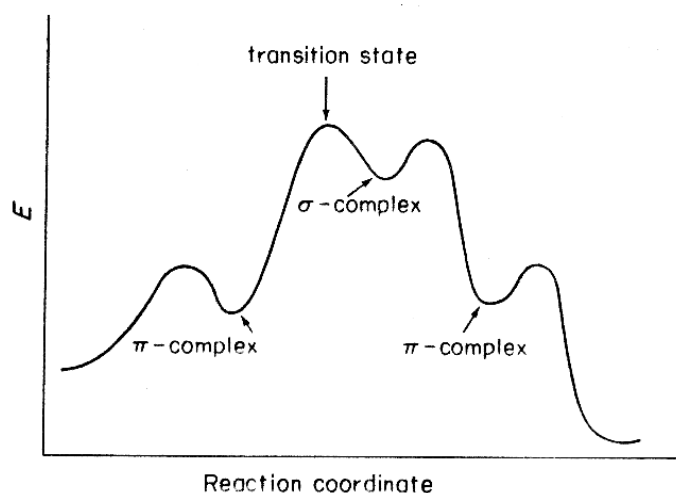


Figure 4. Energetic profile for SE_{Ar} .

The existence of the Wheland intermediate does not necessarily prove that the transition state is directly correlated with it. Dewar first discovered the existence of π -complexes along the reaction's coordinate and hypothesized that the reaction's rate could depend also on their stability.^[17]

In agreement with Hammond's postulate for which species closer in the reaction's coordinate with almost the same energy have similar geometry, it's clear that the transition state higher in energy will be similar to the intermediate with a comparable energy.

Hence it is possible to observe the following three situation.^[18]

1. Formation of the π -complex. In this case the transition state higher in energy is similar to the π -complex.^[19] The formation of this non-covalent interaction is fast and reversible and most of the time the equilibrium constant is very small. If the formation of the π -complex is the rate determining step there is no isotopic effect.

2. Formation of the Wheland intermediate. The transition state highest in energy is that before the formation of the Wheland intermediate.

It has been demonstrated that for some reactions a linear relationship between the rate of substitution and the relative stability of the σ -complex exist.

This give indication on the correlation between the transition state higher in energy and the Wheland intermediate.

3. Proton elimination. The usual assumption is that the proton departure occurs in a fast step. However it is possible that the transition state at higher energy could be the one before the proton elimination. The reaction is characterized by a strong isotopic effect which has been demonstrated by changing the proton of the substrate with deuterium; in this case the reaction's rate change. Assuming k_H the constant for the proton elimination and k_D the one for deuterium, if the ratio k_H/k_D is high (>2 , also if in some cases it can reach the values of 6-7) there is a prominent isotopic effect.^[2] In these case the reaction can undergoes basic catalysis phenomena. The energetic trend can be summarized as depicted in Figure 5.

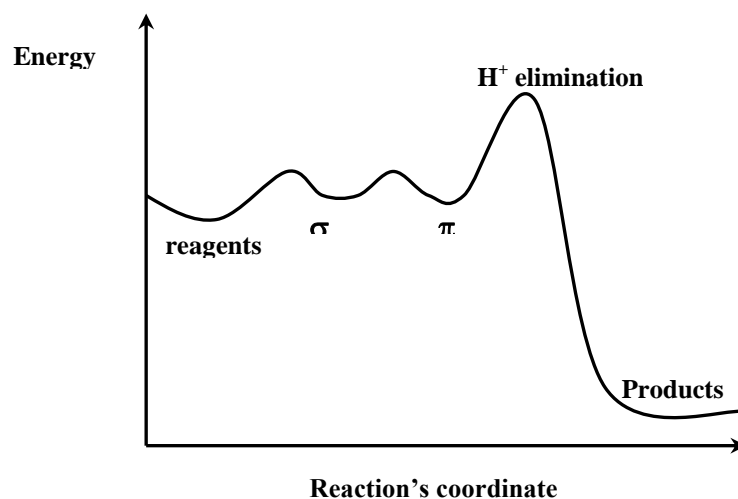


Figure 5. Energetic trend in SE_{Ar} in which the slow step is the proton elimination.

The nature of the electrophiles and the other substrates become of great importance to determine the slow stage. In some cases the electrophile can be a species which is generated in situ from reagents and it is present at low concentration. In the nitration reaction, for example, the attack is not performed by nitric acid but by the nitronium ion NO_2^+ , for which its formation is the rate determining step. Other factors, such as the nature of the solvent and the presence of acidic or basic condition, could influence the slow stage.^[2]

While considering the nature of the slow stages of the reaction we have not mentioned the importance of the substituents on the aromatic ring. They have a strong influence on the regioselectivity determining the resonance energy for the different Wheland complexes formed by the attack of the electrophile at the different position.^[18] In the presence of a strong electrophile the rate determining step can be the formation of the charge transfer complex; this can affect only the selectivity toward the substrate which becomes low.

Since the π -complex evolve toward the Wheland intermediate to obtain the substitution product, it is needed to take into account the substituent effect for the formation of the σ -complex.

If the substituent is an electron-donor, hence it is able to stabilize the positive charge, there is an high selectivity on the attack position: *ortho* and *para* are favored respect to *meta*.

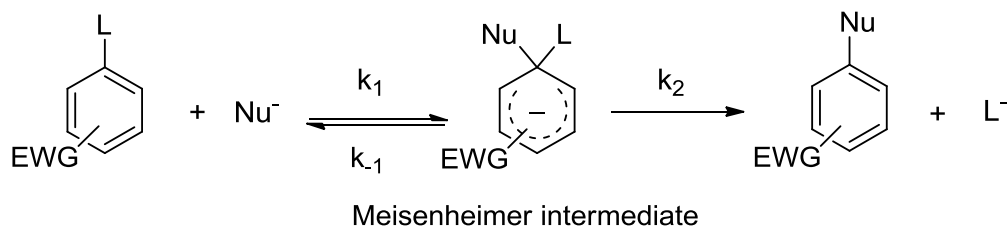
If the electrophile is weak, without considering the proton elimination step, it is the stability of the σ -complex to determine the selectivity on the attack.

The presence of an electron-donor substituent which stabilize the positive charge contribute to decrease the stability of the intermediate *para*>*ortho*>*meta* respectively with an high selectivity in the *para* position.

1.2 Nucleophilic Aromatic Substitution Reaction (S_NAr)

Benzene is an electron rich system: this feature lead to a deactivation toward nucleophilic substitution reactions due basically to the electrostatic repulsion between the π cloud and the nucleophile. However some electron-withdrawing substituents are able to reduce the electron density of the aromatic ring allowing it to interact with nucleophile.

The nucleophilic aromatic substitution reaction involve, following the mechanism proposed by Bunnett, two separate stages: the addition of the nucleophile and the elimination of the leaving group (Scheme 3).



Scheme 3. Simplified scheme for the nucleophilic aromatic substitution reaction.

It is a bimolecular reaction in which the first step is characterized by a negative charged intermediate usually called Meisenheimer complex or σ -complex. The process involved in this step is the formation of a σ -bond between the nucleophile and the aromatic ring. In the second step of the reaction the Meisenheimer complex lose the leaving group contemporary with the rearomatization process of the aromatic ring. Two reaction profiles could be observed on the basis of the energy of the transition states (Figure 6).

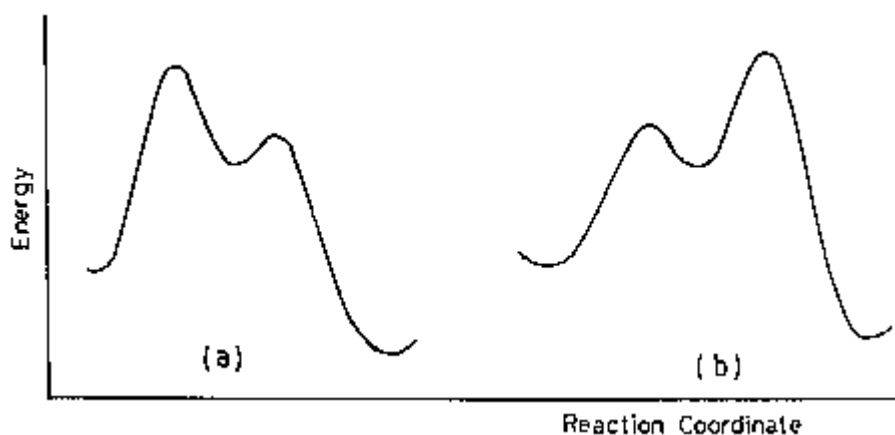


Figure 6. Energetic trend for S_NAr : (a) Transition state with energy comparable to the formation of the σ -complex. (b) Transition state with energy closer to the σ -complex decomposition.

If the nucleophile is neutral such in the case of alcohols and amines, a zwitterionic σ -complex in which the positive charge is localized on the heteroatom is obtained (Figure 7).

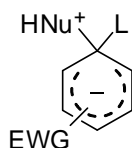
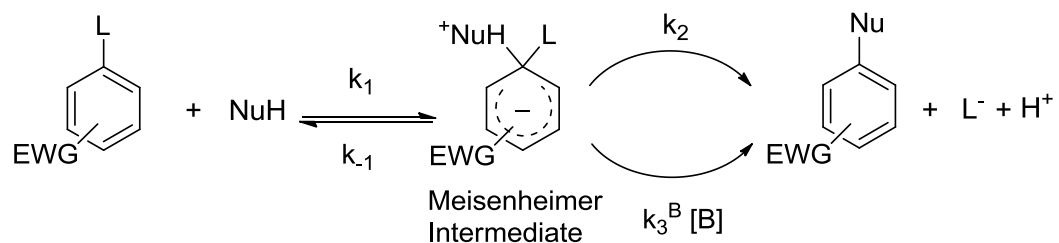


Figure 7. Meisenheimer intermediates.

Such kind of intermediates can contain acidic hydrogen atoms which allow the reaction to be easily catalyzed by means of bases (Scheme 4).



Scheme 4. S_NAr reaction with neutral nucleophiles possessing acidic hydrogens.

Different studies shown that, as in the case of electrophilic aromatic substitution reactions, also in the nucleophilic substitutions the formation of the Meisenheimer intermediate is preceded by donor-acceptor interactions with formation of π -complexes which in some cases have been characterized.^[20,21]

The presence of electron-withdrawing group on the aromatic ring activate the system but also help to stabilize the negative charge on the cyclohexadienilic intermediate, specially if it is in the *ortho* and *para* positions. While considering the resonance structures of the anion we can observe that the negative charge is localized in the *ortho* and *para* positions (Figure 18).

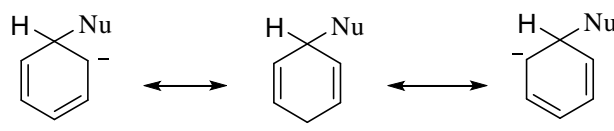


Figure 5. Resonance structure on the Meisenheimer intermediate.

The substitution of an hydrogen atom for an electron-poor system it is not a favored process because the hydride ion is a bad leaving group. This kind of nucleophilic substitution can take place only under particular experimental conditions. The general mechanism provides the formation of a σ -intermediate in a first step, followed by the system oxidation. The oxidation may occur spontaneously as a result of the species present in the reaction system as in the case of the reaction between *m*-dinitrobenzene and acetone in a basic environment. In this case the aromatic system act as the oxidizing agent, effect which can be easily observed by using an excess of *m*-dinitrobenzene. However it is possible to use external oxidizing agents which can be inorganic (H_2O_2 , hypochloride, alogens) or organic.

Electrophilic and nucleophilic aromatic substitution reactions (Figure 9 and 10 respectively) are generally treated separately because usually only one reagent is aromatic and it is the one who undergoes the substitution.

The course of both reactions is similar and involve the formation of an intermediate usually called σ -complex after the reagents' interaction. This kind of

intermediates possess for both reactions a covalent bond of a carbon atom in the aromatic ring which change hybridization from sp^2 to sp^3 . This change of hybridization as a result of the addition to a double bond and the π aromatic system break generate the σ -complex that is an high energy intermediate.

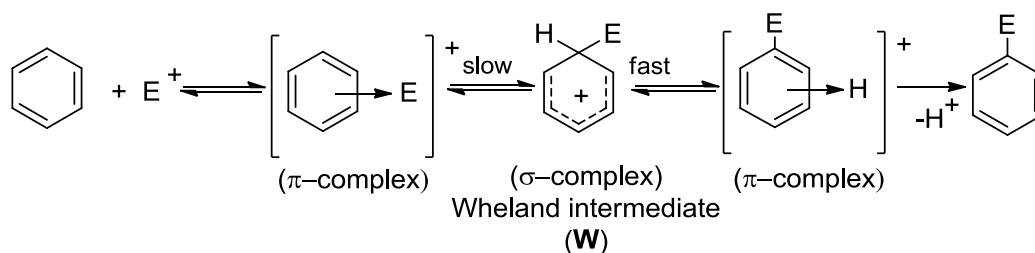


Figure 9. Classic mechanism of electrophilic aromatic substitution reactions.

The next step provides the elimination of a leaving group with the subsequent rearomatization and formation of the final product. In both cases a lot of stages are involved in the reaction, but only recently it has been possible to isolate π -complexes in nucleophilic aromatic substitution reactions.^[22]

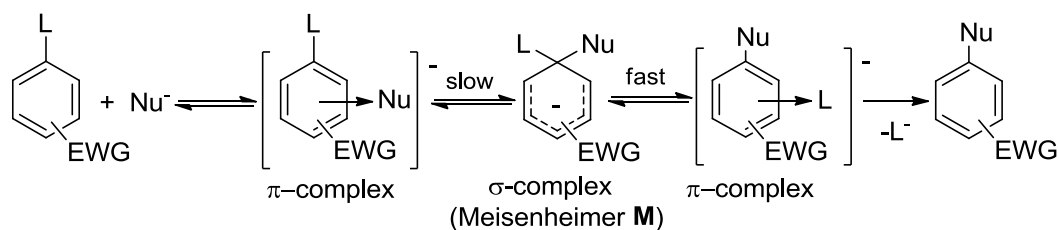


Figure 6. Classic mechanism of nucleophilic aromatic substitution reactions.

Modulating the steric and electronic properties of the substrates, using highly nucleophilic and electrophilic systems, it has been possible in the research group where I worked during my Ph.D., to isolate reaction's intermediate for both electrophilic and nucleophilic reactions and demonstrate with zwitterionic complexes named Wheland-Meisenheimer (Figure 11) that the difference between the two typology of reactions is simply a formality.

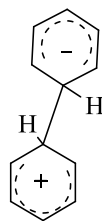


Figure 7. Example of a Wheland-Meisenheimer complex.

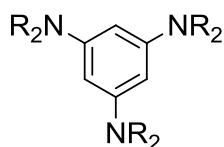
References

- [1] R.Taylor, *Electrophilic Aromatic Substitution*; John Wiley & Sons **1990**.
- [2] F.A.Carey, R.J. Sundberg, *Advanced Organic Chemistry Part A*, 3a ed; Plenum Press: New York and London, **1990**.
- [3] G. W. Wheland, *J. Am. Chem. Soc.*, **1942**, 64, 900
- [4] N.L. Allinger, M.P. Cava, D.C. De Jongh et al, *Chimica Organica*, 2a ed., Zanichelli, **1981**.
T.H.Lowry, K.S. Richardson, *Mechanism and Theory in Organic Chemistry*, 3a ed., Harper and Row Publisher: New York, **1987**.
- [5] P. Sykes *A guidebook to mechanism in organic chemistry*, 5a ed, Prentice Hall **1992**.
- [6] S.M. Hubig, J.K. Kochi, *J. Org. Chem.*, **2000**, 65, 6807.
- [7] G.A. Olah, R.H. Scholoshberg, R.D. Porter, Y.K. Mo, D.P. Kelly, G.D. Mateescu, *J. Am. Chem. Soc.*, **1972**, 94, 2034.
- [8] a) R. Rathore, J. Hecht, J.K. Kochi, *J. Am. Chem. Soc.* **1998**, 120, 13278; b) G.A.Olah, H.C: Lin, Y.K. Mo, *J. Am. Chem. Soc.*, **1972**, 94, 3667.
- [9] W. Lau, J.K.Kochi, *J. Am. Chem. Soc.*, **1986**, 108, 6720.
- [10] W. Lau, J.K.Kochi, *J. Am. Chem. Soc.*, **1984**, 106, 7100.
- [11] S.M. Hubig, J.K. Kochi, *J. Am. Chem. Soc.*, **2000**, 122, 8279.
- [12] S.Fukuzumi, J.K. Kochi, *J. Am. Chem. Soc.*, **1981**, 103, 7240.
- [13] S.V. Rosokha, J.K. Kochi, *J. Org. Chem.*, **2002**, 67,1727.
- [14] L. Forlani, *J. Phys. Org. Chem.*, **1999**, 12, 417.
- [15] K.Kim, J.K. Kochi, *J. Am. Chem. Soc.*, **1991**, 113, 4962.
- [16] E. Bosch, J.K. Kochi, *J. Org. Chem.*, **1994**, 59, 5573.
- [17] M.J.S. Dewar, *J. Chem. Soc.*, **1946**, 406, 777.
- [18] G.A. Olah., *Acc. Chem. Res.*, **1971**, 4, 240.
- [19] G.A. Olah, S. . Kuhn, e S. H. Flood, *J. Am. Chem. Soc.*, **1961**, 83, 4571.
- [20] S.K. Dotterer, R.L. Harris, *J. Org. Chem.*, **1988**, 53, 777-779.
- [21] R. Bacaloglu, C.A. Bunton, G. Cerichelli, *J. Am. Chem.Soc*, **1987**, 109, 21-623.
- [22] P. Sepulcri, R. Goumont, J.C. Hallè, E. Buncl, F. Terrier, *Chem. Comm.*, **1997**, 789-790

Chapter 2

The proton dance in tris(dialkylamino)benzenes

Benzene ring activated by the presence of several strongly electron-donating substituents allowed my research group to have important information on the separate steps of the electrophilic aromatic substitution reactions.^[1] To perform these studies they used a series of substrates bearing strongly electron-rich rings, such as 1,3,5-tris(dialkylamino)benzenes (Figure 1).



NR₂ = *N*-piperidinyl (1)

NR₂ = *N*-morpholinyl (2)

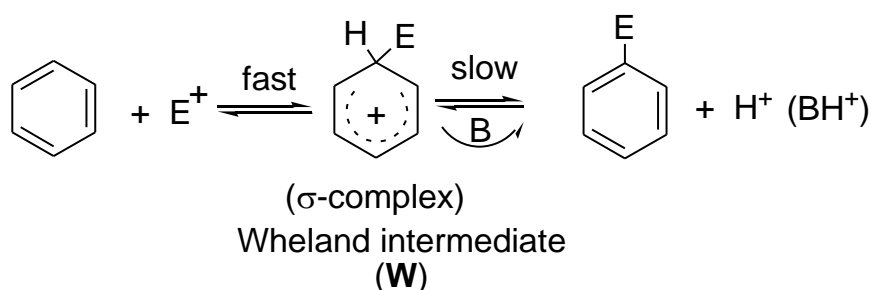
NR₂ = *N*-pyrrolidinyl (3)

Figure 1. Strongly activated aromatic nucleophilic reagents at the neutral carbon atom.

1,3,5-tris(dialkylamino)benzenes derivatives **1–3** were used to obtain moderately stable σ cationic complexes (the Wheland intermediates **W**) and, in particular, tris(*N*-pyrrolidinyl)benzene (**3**) affords σ complexes not only in protonation reactions,^[2-5] but also in alkylation reaction with alkyl halides^[4,6] and in halogenation reactions.^[7]

The combination of the supernucleophilic reagents **1–3** with superelectrophilic reagents (both at the neutral carbon atom) produced σ -complexes which are contemporaneously Wheland and Meisenheimer complexes (**WM**), as shown in Scheme 1 for the reaction between compounds **1–3** and 4,6-dinitrobenzofuroxan (**DNBF**).^[8]

process. Experimental evidences allowed us to state that the whole reaction is a reversible process in both steps.^[11]



Scheme 2. Mechanistic pathway for S_EAr reactions.

The presence of electron-donor groups on the benzene moiety such as in tris(dialkylamino)benzene derivatives allowed not only to characterize Wheland complexes by NMR spectroscopy, but, also to obtain their X-Ray molecular structures even if in a limited number of cases, probably due to the difficulty of growing crystals of X-ray quality. For example, 2,4,6-tris(pyrrolidino)cyclohexadienylium salts,^[3] 1-methyl-2,4,6-tris(pyrrolidino)cyclohexadienylium perchlorate,^[3] tris(*N,N*-dialkylamino)benzene chromium tricarbonyl complexes^[12] and *N,N,N'*-triphenyl-2,4,6-triamino cyclohexadienylium cation^[13] were isolated and investigated by X-ray diffraction analysis.

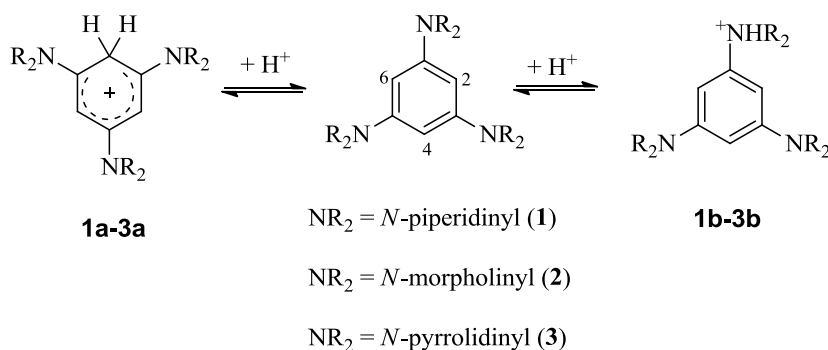
All these findings show the interesting properties of tris(dialkylamino)benzenes. In the next subchapters I present two studies which involve the tris(dialkylamino)benzene derivatives and their interactions with proton.

2.1 The interactions of proton with tris(dialkylamino)benzenes

Proton is the most simple and hard electrophilic reagent and it is of interest to investigate its affinity toward centers of different electronegativity and polarizability.

If the proton acceptor bears different basic centers, the proton may attack them depending on the availability of their lone pairs. This is the case of 1,3,5-tris(dialkylamino)benzenes, firstly studied by Effenberger.^[2]

1,3,5-Triaminobenzenes react with electrophilic reagents in two main ways: the attack on the carbon atoms of the aromatic ring and the attack on the nitrogen atoms of the amino group. When the proton is the electrophilic reagent, 1,3,5-triaminobenzene,^[14,15] as well as compounds **1**, **2**, and **3** of Scheme 3 can form σ -complexes **1a-3a** by protonation on the ring carbon atom and ammonium salts **1b-3b** by protonation of the amino group.^[4] Evidences of the presence of both equilibria of Scheme 3 were investigated from long time and are reported in the literature.^[2,4,14,15]



Scheme 3. Possible products of the attack of proton on compounds 1–3.

Knoche *et al.* reported^[16-18] a thermodynamic and kinetic studies on the protonation of tris(amino)benzenes **1**, **2**, and **3** in water/alcohols mixtures.

Data regarding the salification of tris(dialkylamino)benzenes by UV/Vis spectroscopic measurements^[16-18] clearly indicate the presence of three protonation steps. For this salification equilibrium the ¹H-NMR^[2,17,18] data reveal

the importance of the protonation at the nitrogen atoms, showing the magnetic equivalence of the three aromatic protons, indicating that the protonation site is undefined.

It has to be noted that σ -complexes derived from the protonation of some triaminobenzenes are stable, as, for example, in the case of *N,N',N''*-triphenyl-1,3,5-triaminobenzenes.^[19]

In previous studies^[1,9,11] the coupling between tris(dialkylamino)benzenes and arenediazonium salts afforded σ -complexes and no evidence of attack of the electrophilic reagent to the amino nitrogen atom was obtained. Also electrophilic neutral carbon reagents^[8,19,20,21] showed a similar reaction regarding the regioselectivity of the attack. On the contrary, alkylation of **1** is indicated^[2] to occur on the nitrogen atoms.

Previously, we reported that Wheland-Meisenheimer complexes (**WM**) can be formed from the reaction between tris(dialkylamino)benzenes and 4,6-dinitrobenzofuroxan (**DNBF**), a superelectrophilic reagent at the neutral carbon atom (Scheme 1).^[7] **WM** show an interesting dynamic process. In fact, when the ¹H-NMR spectrum of these complexes is recorded at room temperature, the protons bound to the trisaminobenzene moiety are equivalent. By lowering the temperature, **WM** shows a ¹H NMR spectrum in agreement with the structure depicted in Scheme 1 in which the bond between the superelectrophilic and the supernucleophilic reagents is in a definite position. An analogous behaviour was observed also in the reaction between compounds **1–3** and 4,6-dinitrotetrazolopyridine,^[22] a more powerful electrophile than **DNBF**.^[23]

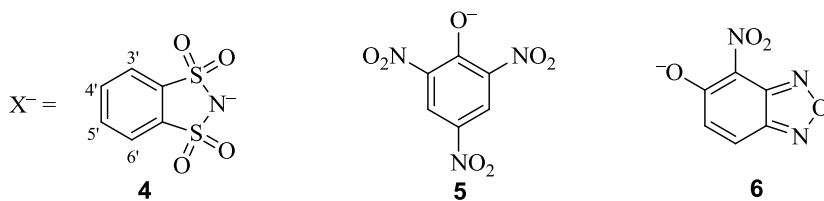
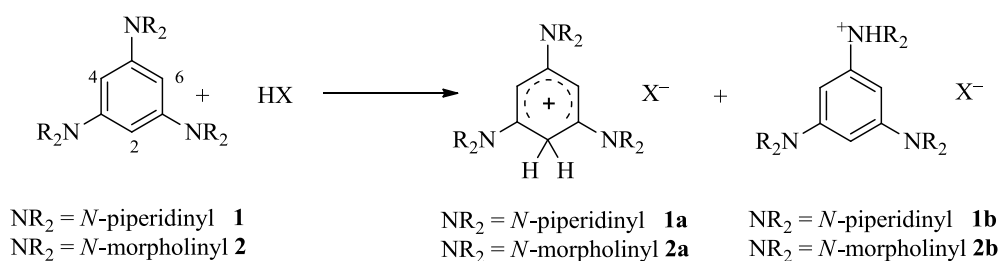
The “aromatic” carbon atom in position 7 of **DNBF** prefers the carbon atom of **1–3**, while the aliphatic carbon (sp³) of alkyl halides reacts on the nitrogen atom or at the carbon atom of the same compounds, depending on the amino substituent.^[2,6] This difference in regioselectivity of electrophilic species may be hardly explained by usual idea (basicity/acidity, polarizability, *etc.*).

With the purpose to provide further information on the mechanism of the electrophilic aromatic substitution reactions of considered substrates, we decided to investigate the protonation of tris(dialkylamino)benzenes with different acids.

Furthermore we report also some data on the alkylation reaction of these substrates.

2.1.1 Protonation of symmetric tris(dialkylamino)benzene derivatives

The addition at room temperature and directly in the NMR spectroscopy tube of a tris(dialkylamino)benzene solution (**1**, or **2**) in CDCl₃ (or in other solvents) to a solution containing an equimolar amount of *o*-benzendisulfonimide **4H** (or **5H** or **6H**, see Scheme 4) produced the appearance (in the ¹H NMR spectrum) of new signals different from those of starting materials.



HX = *o*-benzendisulfonimide (**4H**) HX = picric acid (**5H**) HX = 4-nitro-2,1,3-benzoxadiazol-5-ol (**6H**)

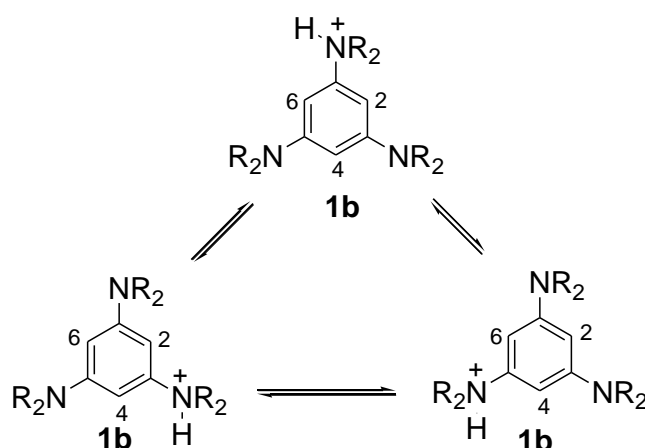
Scheme 4. Reactions between 1,3,5-(dialkylamino)benzene derivatives 1–3 and organic acids.

In agreement with that reported in literature using inorganic acids,^[4,16,17,18] from the reaction of compounds **1** and **2** with **4H** two kind of salts are formed, one arising from the attack of the electrophile H⁺ to the aromatic carbon atom and the second obtained from the attack to nitrogen atom of piperidine or morpholine moiety.

Differently from the previously observed behaviour of **WM** complexes (Scheme 1) in which all the C–H aromatic bonds of tris(alkylamino)benzene are magnetically equivalent at room temperature, the ¹H NMR spectrum of

compounds **1** and **2** after reaction with the proton to form a C–H bond agrees with formula **1a** and **2a**, indicating that the proton is in a fixed position.

On the contrary, compounds **1b** and **2b** show ^1H NMR signals indicating the presence of a mono-protonated salt in which the proton signals of benzene ring appear as a broad singlet at $\delta = 6.45$ ppm in CDCl_3 (see Table 1) integrating for three protons. This indicates the magnetic equivalence of the three aromatic protons suggesting that the center bearing the proton is undefined. The broad signals of the salt **1b** may arise from the fact that the aromatic protons are in a dynamic situation involving the shift of the proton from a nitrogen atom to another in positions 1, 3 and 5, as represented in Scheme 5. This behavior is comparable with that observed for complexes **WM**.



Scheme 5. Proposed dynamic process explaining the magnetic equivalence (observed in ^1H NMR experiments) of the three hydrogen atoms (H-2, H-4, and H-6) after reaction between compounds **1–3** and acid species **4H–6H**.

By summarizing, the NMR properties of the two kinds of salts **a** and **b** show that when H^+ attacks a carbon atom of the aromatic ring, the new C–H bond is in a fixed position and no dynamic phenomenon is observed and when the salification process occurs at the nitrogen atom the salt **b** undergoes a dynamic process. We were not able to stop this ‘proton dance’ by lowering the temperature (until -80 °C in CD_2Cl_2).

Another possible explanation of the spectral data observed might be the presence of an interaction between the π electrons of the benzene ring and the added proton.

A similar behaviour was previously observed by Effenberger and Niess^[2] in the reaction between perchloric acid and **1** in polar and proton-acceptor solvents: the ¹H NMR signal of aromatic protons was a singlet in [D₆]-acetone and in [D₆]-DMSO, while in CDCl₃ the proton appeared to be fixed on an amino group (δ = 7.90 (1H, N-H), 6.62 (s, 2H) and 5.37 (s, 1H).

The monoperchlorate of **1** was indicated to show, in [D₆]-DMSO and in [D₆]-acetone, rapid proton exchange among the amino groups and the behaviour showed by the system let the authors to observe “*there is a strong electronic disturbance of the π -electron system*”.^[2]

To further investigate on the regioselectivity of the attack to the ring carbon atom or to the nitrogen atom of the substituents of the tris(dialkylamino)benzenes **1** and **2** we planned to change the operative conditions, such as the solvent, the temperature and the electrophilic reagent. Table 1 reports a tentative to check the importance of the solvent in determining the relative amount of the two protonated species, the C-H and the N-H (**a/b**). On the basis of the rough definition of the polarity of the used solvent,^[25] in more polar solvents the equilibrium is shifted toward the **b** salt that results more polar than the **a** salt (C-H salt). Probably, in **a** the positive charge is more delocalized, and so more hidden to interactions with solvent than in **b** salt.

Table 1. Relative % ratio of C-H form versus N-H form of compounds **1 and **2** after salification with 4H at 25 °C in different solvents^[a]**

Compound↓ Solvent→	CDCl ₃	CD ₂ Cl ₂	CD ₃ CN	[D ₆]-DMSO
1a : 1b	12 : 88	8 : 92	48 : 52	n.d. : ≥ 99
2a : 2b	11 : 89	–	47 : 53	–

[a]. [1], [2], [3] = [4H] = 1.2 x 10⁻⁵ mol dm⁻¹ (as stoichiometric amount).

From data of Table 1 it is possible to state that **1** and **2** show very similar behaviours. In CDCl₃ (or CD₂Cl₂) and in [D₆]-DMSO, the dependence of the

ratios **1a:1b** (or **2a:2b**) from the solvent used indicates that the increase of the solvent polarity favours the protonated specie **b** (N-H) and, in agreement to these conclusion, we observed that also the addition of tetrabutylammonium bromide to enhance the polarity of the environment favours the species **b** (see Table 2).

Table 2. Relative ratio 1a and 1b after addition of tetrabutylammonium bromide in CD₃CN and in CDCl₃.^[a]

[TBAB] ^[b] 10 ³ x mol dm ⁻³	–	6.25	12.5	18.75	25.0	50.0
1a:1b (CD ₃ CN)	48:52	42:58	35:65	27:73	18:82	5:95
1a:1b (CDCl ₃)	12:88		10:90		2:98	

[a] [1] = [4H] = 1.2 x 10⁻⁵ mol dm⁻¹ (as stoichiometric amount). [b] TBAB = tetrabutylammonium bromide

In contrast, in CD₃CN (a more polar solvent than CDCl₃ or CD₂Cl₂, but less polar than DMSO^[25]) the ratio is about 50:50 for both, **1** and **2** salts. Probably, in this solvent some particular interaction/solvation processes are operating. Furthermore in CD₃CN, the addition of tetrabutylammonium bromide (TBAB) shifts the equilibrium from **a** to **b** (see Table 2).

In every case, the mixture of 1,3,5-tris(piperidinyl)benzene (**1**) (and all the other tris(dialkylamino)benzenes) and *o*-benzendisulfonimide (**4**) was prepared in 1:1 relative molar ratio. The addition of higher amount of acid (**4H**) until a 1:3 molar ratio, did not produce significant variation of NMR spectral data. However, the reported observations indicate the presence of an equilibrium between C-H and N-H species. In fact in the presence of the CH/ NH tautomerism shown in Scheme 3, when to the mixture of **1a** and **1b** in CDCl₃ is added a small amount of D₂O, the rapid exchange of both the sp³ protons of **1a** and of the three aromatic protons of the compound **1b** takes place and all the signals related to aromatic protons are strongly lowered.

With the aim to check the importance of the counter ion in the obtainment of the reported relative ratios **a** : **b** (**a** = C–H salt, **b** = N–H salt) and on the possible modification of chemical shift, we tried to change the acid. For this purpose we used picric acid (**5H**) and 4-nitro-5-hydroxybenzofurazane (**6H**) to

protonate compounds **1** and **2**. Table 3 shows the relative amount of the two protonated forms in CDCl₃ and in CD₃CN (the related ¹H NMR chemical shifts in CDCl₃ and in CD₃CN resulted to be poorly dependent on the acid used). In all cases an increase of the amount of **b** species with respect to the relative ratio shown in Table 1 was observed.

Table 3. Relative amount of species a and b (see Scheme 1) from salification of 1 and 2 with 5H and 6H.

Entry	Starting materials	Relative % amount of a : b in CDCl ₃	Relative % amount of a : b in CD ₃ CN
1	1 and 5H	1 : 99	30 : 70
2	2 and 5H	n.d. : ≥99	40 : 60
3	1 and 6H	1 : 99	25 : 75
4	2 and 6H	(n.d. : 99) ^[a]	(6 : 94) ^[a]

[a] Differences in chemical shifts are small with respect to those of starting compound.

In CD₃CN the relative ratio **a** : **b** of the morpholino derivative (entries 2 and 4) are significantly dependent on the used acid: picric acid **5H** enhance the protonation at the carbon atom respect to **4H**, even if the major protonated center is the nitrogen atom. A possible explanation of this behaviour may be in some specific interactions of **1a** with the anionic part of **5H**. In CD₃Cl no relevant influence of the negative counter ion was observed.

2.1.2 Effect of the temperature's change

The complexes **WM** between compounds **1**, **2**, or **3** and **DNBF** (see Scheme 1), show a dynamic process of the DNBF moiety on the tris(amino)benzene ring. This “motion” was observed through ¹H NMR spectrum, at room temperature, and it was stopped by a strong lowering of the mixture temperature.

The salification herein reported was carried out between equimolar amount of the tris(dialkylamino)benzenes **1** (and **2**) and the acid **4H** in different solvents directly in the NMR spectroscopy tube at various temperatures (in the range of +25°/ -80 °C in CD₂Cl₂, +25/ -55 °C in CDCl₃ and +25/ -10 °C in CD₃CN). If at these low temperatures the proton may stop its motion localizing it on one

nitrogen atom of salt **b** for a time at least comparable with the NMR time scale, different chemical shifts for the aromatic protons of the tris(dialkylamino)benzene moiety should be observed. In our experimental conditions we observed only one signal for aromatic protons of the tris(dialkylamino)benzene moiety. Since we have not evidence of the stop of the proton transfer, we deduce that the proton transfer from a nitrogen atom to another is a very easy and fast process.

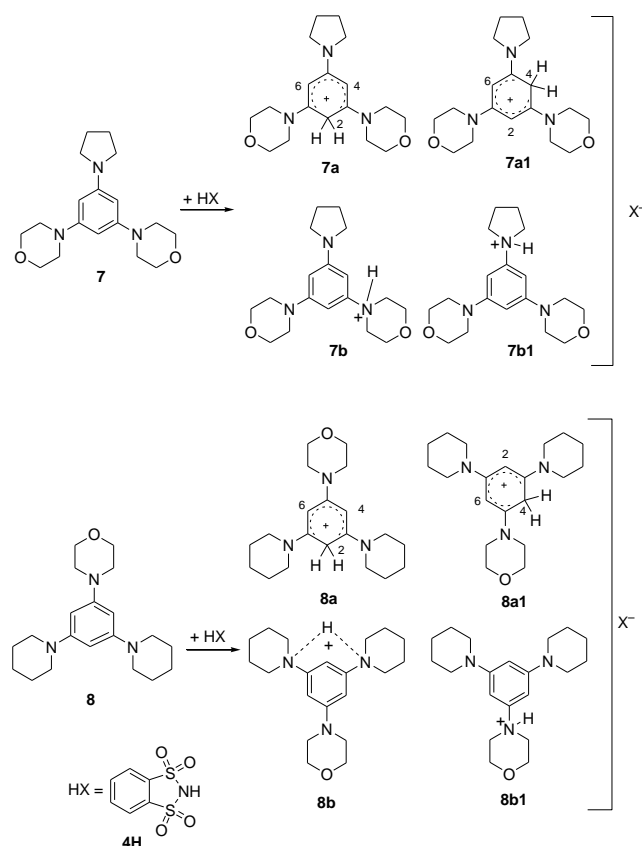
2.1.3 Protonation of asymmetric tris(dialkylamino)benzenes

Since the symmetry of the 1,3,5-tris(dialkylamino)benzenes **1–3** does not permit to discriminate the position of the attack of the electrophile, we checked the salification process between compound **4H** and two asymmetric bases, namely 4,4'-(5-pyrrolidin-1-yl-1,3-phenylene)dimorpholine (**7**) and 4-(3,5-dipiperidin-1-ylphenyl)morpholine (**8**), presenting two different kinds of nitrogen atoms and non-equivalent position of attack on the homocyclic aromatic ring. Scheme 6 reports the most probable protonation centres of **7** and **8**.

In CDCl₃, the mixture of **7** and **4H** affords the σ -complex **7a** deriving from the attack of the electrophile in para-position with respect to the pyrrolidine ring in equimolar amount with the nitrogen protonated salt and a minor amount of the complex **7a1** which show the proton bound in the ortho position with respect to the pyrrolidine ring. In principle, the formation of both salts (nitrogen protonated) **7b** and **7b1** (Scheme 6) is possible but from the spectral data it is difficult to discriminate the position of the proton on different nitrogen atoms. However, on the basis of the pK_a value of the nitrogen atom of the pyrrolidine (pK_a pyrrolidine = 19.58 in CH₃CN^[26]) with respect to that of the nitrogen atom of the morpholine (pK_a morpholine = 16.61 in CD₃CN^[26]), the preferential formation of **7b1** with respect to **7b** can be expected.

The ¹H NMR spectrum of the compound **8b** in CDCl₃ show two signals in the region of the protons bound to carbon atoms in position 2, 4 and 6 of the tris(dialkylamino)benzene ring. This agrees with the formation of two possible structures, one in which the proton is bonded to the nitrogen atom of the morpholine ring (**8b1**) and another in which the proton is shared between the two

nitrogen atoms of the piperidine rings (**8b**); also in this case, as for compound **7b**, it was not possible to distinguish between the two structures.



Scheme 6. Possible products from the salification of asymmetric tris(dialkylamino)benzenes **7 and **8** with compound **4H**.**

However, a comparison between the spectrum of the starting compound **8** and that of the reaction mixture revealed that in this latter case the ^1H NMR signals of the methylenic protons bound to the piperidine rings are broader with respect to those in compound **8**, while the methylene signals related to the morpholine ring are practically unchanged with respect to those of the starting compound **8**. From this observation it seems that the electrophile might be in common among the two piperidinic nitrogen atoms like in the structure **8b** represented in Scheme 6.

In CD_3CN , the ^1H NMR spectrum related to the protonation of **7** with **4H** shows a 70 : 30 relative ratio of compounds **7a** and **7a1**.

In CDCl_3 , the reaction between compound **8** and *o*-benzendisulfonimide **4H**, as well as with acids **5H** and **6H**, affords only the compound **8b**, while in CD_3CN also small amounts of the compounds **8a** and **8a1** are formed.

2.1.4 X-Ray diffraction analysis

While the crystal structures of some 1,3,5-tris(dialkyl)aminobenzene derivatives (in particular 1,3,5-tris(pyrrolidino)benzene derivatives)^[6] were extensively investigated in their protonated cyclohexadienylic form, X-ray diffraction studies on **1** and **2** or other similar compounds protonated on the nitrogen atom have not been yet reported in the literature.

The findings of this study extend the number of cases in which the protonation of 1,3,5-tris(dialkylamino)benzene derivatives occurs on nitrogen atom and since this is often the main process, we tried to crystallize the product derived from the reaction between **1** and **8** and the herein used acids **4H**, **5H** and **6H**.

We were able to obtain crystals suitable for X-ray diffraction analysis from the reaction between tris(dialkylamino)benzenes **1** and **8** and 4-nitro-2,1,3-benzoxadiazol-5-ol (**6H**).

In figure 4 are reported the structures determined by single crystal X-ray diffraction analysis of compounds **1** and two N–H salts named as **1H⁺** and **8H⁺** obtained by reaction of **6H** with **1** and **8**, respectively. In all the three structures the aromatic central ring is planar whereas the three piperidine substituents in **1**, the protonated and the two unprotonated piperidine rings in **1H⁺** and the protonated, unprotonated piperidine and morpholine rings in **8H⁺** adopt a chair conformation.

As a consequence of the protonation of the piperidinic N atom, the N(H)-C(aryl) bonds become longer (1.477(3) and 1.484(2) Å for compound **1H⁺** and **8H⁺**, respectively) than the other N-C(aryl) distances in **1H⁺**, **8H⁺** and **1** that fall in the range of 1.391(2)-1.418(2) Å.

The most striking feature in the solid state is the localization of the proton in both protonated derivatives **1H⁺** and **8H⁺** on the nitrogen atom of one of the

piperidine moiety. Interestingly, the twist angle between the protonated piperidine and the benzene ring in both **1H**⁺ and **8H**⁺ is larger than that between the unprotonated piperidine or morpholine substituents and the aromatic ring (for **1H**⁺ and **8H**⁺, respectively). In particular in compound **8H**⁺ the twist angles for the unprotonated morpholine or piperidine rings and the benzene ring (angles between atoms N1-C7-C8-O5-C10-C11 and C1-C2-C3-C4-C5-C6 and between N3-C12-C13-C14-C15-C16 and the aromatic ring) are 5.4(3) and 21.9(2)°, respectively while in compound **1H**⁺ the two unprotonated piperidine rings have similar twist angles of 11.9 and 22.3(1)°. A further comparison with the neutral **1** shows that also in this compound the piperidine substituents and the benzene ring are not coplanar presumably because of steric congestion and packing forces effects. The torsion angles are similar to those observed in **1H**⁺ and **8H**⁺ for the unprotonated piperidine substituents.

The benzofurazane anion is almost perpendicular to the benzene ring of the cationic component of **1H**⁺ and **8H**⁺ and approaches the protonated piperidine with the oxygen O1 and one oxygen of the nitro group. The O1–C23 distance in the anionic benzofurazane moiety in **1H**⁺ and **8H**⁺ is 1.255(4) and 1.250(3) Å, respectively, showing a double bond character and indicating an electron delocalization inside the furoxane ring.

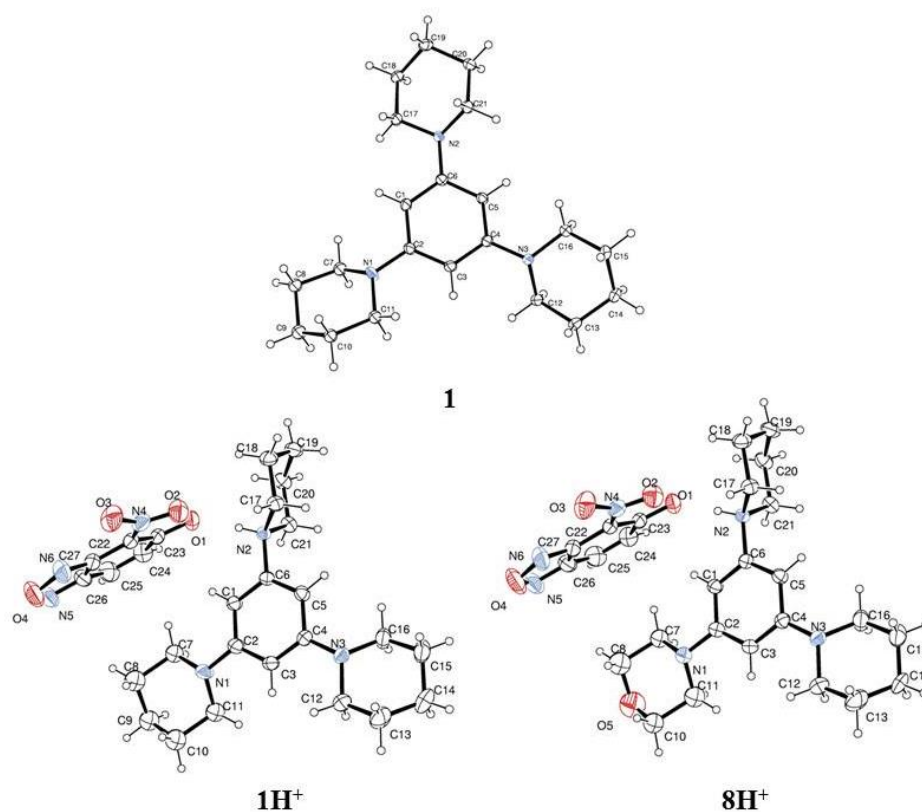
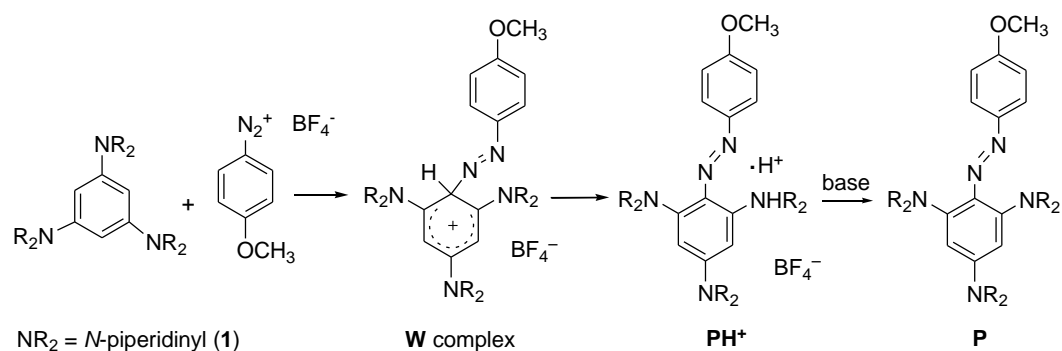


Figure 2. ORTEP of **1**, **1H⁺**, and **8H⁺**.

2.2 First X-ray structure of the Wheland complex in azo-coupling reaction

The azo-coupling reaction between compounds **1** and **2** (Figure 1) and a series of benzenediazonium tetrafluoroborate salts was previously described by us.^[9] The less reactive diazonium salt was that bearing an electron-donating group. This caused the slowing down of all processes including the return back^[11] and the proton departure. On the basis of this findings we realized that 4-methoxybenzenediazonium tetrafluoroborate might be a suitable candidate to obtain single crystals of a **W** complex on this aza-coupling reaction. We focused our attentions on the reaction between **1** and 4-methoxybenzenediazonium tetrafluoroborate as shown in Scheme 7.



Scheme 7. The reaction between tris(*N*-piperidinyl)benzene and 4-methoxybenzenediazonium tetrafluoroborate.

As previously described,^[9] this reaction shows NMR and UV/Vis spectroscopic evidence of the formation of the **W** complex. Its moderate stability in the common solvents suggested us to try to grow crystals suitable for an X-ray diffraction study of this **W** complex. After several attempts, the solid Wheland complex precipitated by using a mixture of CH₂Cl₂/*n*-hexane at low temperature (about -60°C). From this solution some crystals of **W** were obtained. Two different crystals were analyzed through X-Ray diffraction analysis at different temperatures. The first data collection was carried out at 223°K, whereas the second one at 100°K. In both cases the nature of compound **W** was the same but the lower temperature data set allowed to understand the disorder involving the N1, N2 atoms and the methoxyphenyl ring (see later) and therefore this discussion will comment the structural features of **W** based on the X-ray structure determination at 100 °K. The crystal structure of **W** is shown in Figure 3.

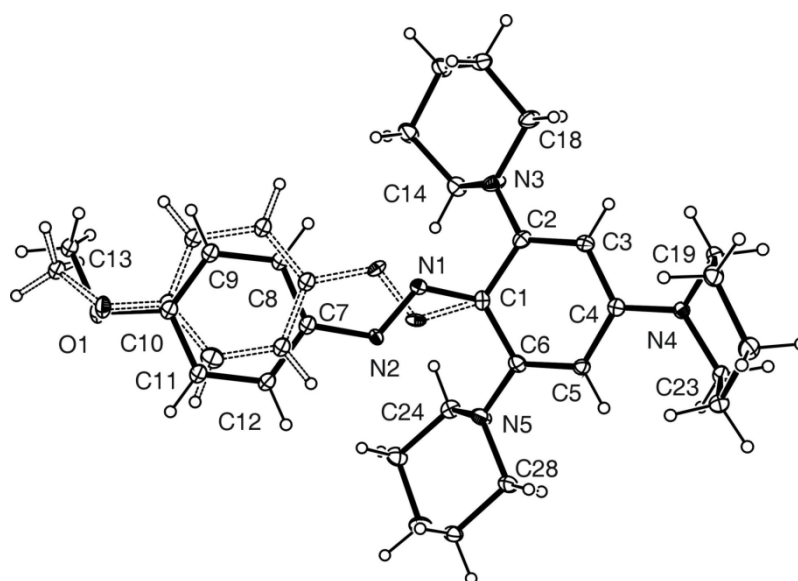


Figure 3. The crystal structure of **W** complex featured by the pedal motion.²⁷

The cation **W** consists of a tris(piperidine)substituted ring bearing a 4-methoxyphenylazo ligand. The tris(piperidine)substituted ring shows a significant loss of planarity (dihedral angle between the C2-C3-C4-C5 and C2-C1-C6 planes 23.3(2)° and the C1 carbon of **W** changes its hybridization from sp^2 to sp^3). The C2-C3 and C5-C6 bonds are the shortest ones (1.372 and 1.360(4) Å, respectively), the C3-C4 and C4-C5 bonds are at longer distance (1.422 and 1.425(4) Å, respectively) and the C1-C2 and C1-C6 bonds are the longest ones (1.470 and 1.461(4) Å, respectively). This bond lengths distribution evidences the importance of a quinoid structure in delocalizing the positive charge (Figure 4) and is similar to that found in the benzenium cation.^[28] The analogous tris(piperidine)substituted ring in the neutral compound **P** (Figure 5) is planar (maximum deviation from planarity 0.020(1) Å and the bond lengths fall in the range 1.383-1.418(2) Å.

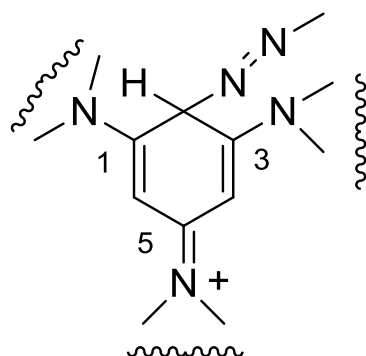


Figure 4. Representation of a quinoid resonance structure of complex **W**.

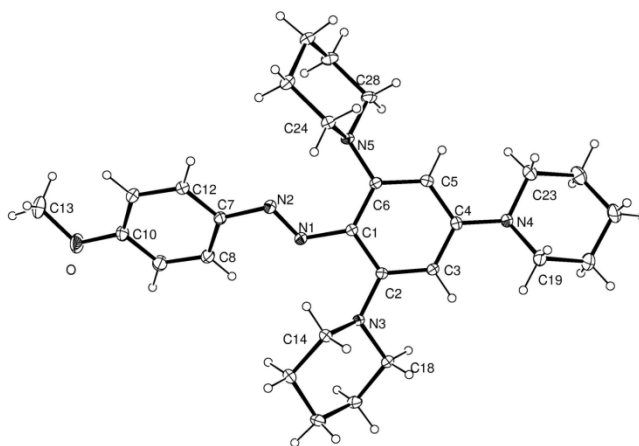


Figure 5. The crystal structure of compound **P**.

The piperidine substituents in **W** show that the N-C(phenyl) distances C2–N3, C4–N4 and C6–N5 are slightly shorter than the related N-C(phenyl) bonds in **P**, indicating the participation of the amino nitrogen atoms in supporting the positive charge of the σ complex **W**. These data, as well as the lengthening of the C1–C2 and C1–C6 bonds in **W** compared to the corresponding distances in the final product **P** (1.423 and 1.418(2) Å) are in agreement with those previously reported for the trispyrrolidinocyclohexadienylium cation.^[3]

Finally the 4-methoxyphenylazo group in **W** was found to be disordered over two sites with 70% and 30% occupancy factors respectively. This is a common feature in azobenzenes and stilbenes known as pedal motion.^[27] The

tris(piperidino)substituted benzene ring is not affected by this disorder because of the presence in the two *ortho* positions of the bulky piperidine substituents.

On the contrary, this type of disorder has not been observed in the 4-methoxyphenylazo group in **P** presumably because of the very low population of the minor component. The two substituted phenyl rings in **P** do not lie on the same plane and therefore there is no π delocalization through the azo group. The N1-N2 distance in **P** of 1.262(2) Å has the typical value of a double bond character whereas the equivalent N=N distance in **W** of 1.326(6) Å is longer than a normal double bond. This lengthening of the N=N bond in **W** is associated to a shortening of the C1-N1 distance of 1.324(5) Å which is indicative of some double bond character. It should be pointed out that the interactions involving the azo group in the cationic **W** are affected by dynamic disorder and therefore it is not possible to completely rule out the contemporary presence in the crystal in trace amounts of a cation in which there is a protonated nitrogen in place of the Wheland complex.

The Wheland complex **W** spontaneously (but slowly) produces a salt of the usual product of substitution which may be obtained quickly by using a base^[9] (NaOH, tertiary amines, *etc.*). The shift of the proton from the carbon atom produces a salt with a N-H bond. The ¹H NMR spectrum of **W** at -30 °C in CD₃CN shows the signal related to the sp³ carbon atom at $\delta = 6.42$ ppm^[9] which disappears and a signal at $\delta = 12.51$ grows, which may be attributed to N-H bond of the salt **PH**⁺. The fact that the chemical shifts of protons H-4 and H-6 of the salt **PH**⁺ are different^[9] ($\delta = 5.81$ ppm and 6.13 ppm in CDCl₃ at 20 °C) indicates an unsymmetric situation caused by the presence of the proton bound to an heterocyclic nitrogen in 1 (or 3) position. The presence of the proton in other positions (on the nitrogen atom of the heterocyclic moiety in 4 position or on nitrogen atoms of azo group) causes an equivalence of the C-4 and C-6 positions.

Probably, the nitrogen atoms in 1 or in 3 positions are preferred to the nitrogen atom in 4 position because of the proton sharing between the piperidine moiety and the two nitrogen atoms of the azo group.

The interaction between two nitrogen atoms may be considered a situation extremely favourable to the bonding of the proton to the nitrogen atom. This is supported by the fact that the return back of the proton on the carbon atom was not observed even when the final product **P** was dissolved in the presence of strong amount of HCl. In the same way, the decrease of the temperature of a solution of **PH**⁺ (obtained directly in the NMR probe) did not produced a return to the **W** complex.

Conclusions

The studies above mentioned are an extension of the previous work on the peculiar properties of tris(dialkylamino)benzenes, in particular the “proton dance” on these systems.

In the 2.1 chapter we analyzed the interaction of tris(dialkylamino)benzenes with the simplest electrophile, the proton. First of all it has to be noticed that this work reports for the first time, to the best of our knowledge, X-ray diffraction data of N-adducts between proton and tris(dialkylamino)benzene derivatives which showed that in the solid state the proton is localized on a nitrogen atom of piperidine ring. The obtained results, together with the previous work, help us to have a better understanding on these systems, but there are a lot of open questions. The first question is: from where arises the regioselectivity of the electrophiles on trisaminobenzenes? What parameters influence this regioselectivity?

Some of these parameters might be:

- The pKa values relative to aromatic C carbon atoms and to the nitrogen atoms of the amino moiety.
- The softness of the two reaction centres.
- The symmetry of the systems that may produce some degenerate structures with a clear gain of the resonance energy. Even if the symmetry is considerably lowered by changing the substrate from **1** to **8** (which presents only two

equivalent nitrogen atoms) the proton on **8** seems to be shared in solution by both nitrogen atoms of piperidine moiety which are more basic than the nitrogen atom of the morpholine moiety.

The second question is: why **DNBF** and proton are in a dynamic situation respect to the electron-rich center (the aromatic carbon and the nitrogen atom respectively). In other words, why **DNBF** and H^+ do not have a fixed position of attack by a σ bond?

The two questions involve a lot of parameters, and, up to now, we were not able to have completely convincing answers. However, we can try the hypothesis of a “generical symmetry” of the present systems in lowering the energy of these not usual situations.

Furthermore, up to now, we are not able to state if the proton is bonded as in a charge transfer complex or it is “dancing” from a nitrogen to another as depicted in Scheme 5. The dancing hypothesis seems to be more valid for the dynamic phenomenon observed for **DNBF** which is stopped by lowering the temperature. However, it cannot be excluded that both hypotheses might coexist in explaining the observed behaviours.

The studies described in chapter 2.2 show how the isolation, crystallization and investigation on **W** complex in aza-coupling reaction support our previous findings on this S_EAr reaction carried out in the absence of bases different from the starting tris(dialkylamino)benzene derivative. The reaction proceed through a two steps pathway. On the contrary to that reported in the literature, the first step is a fast step, while the spontaneous proton releasing process is in a slow step with the possibility of a relevant base catalysis towards to the re-aromatized substrate.^[10]

In conclusion, in the present case, the “proton dance” regards the hydrogen shift from a carbon atom to nitrogen atoms in the same molecule, without evidence of a return back, even if we reported evidence on the reversibility of the whole substitution process.^[11]

Some NMR data related to the products here described can be found in the Ph.D. thesis of Silvia Tozzi: “Caratterizzazione ed isolamento di intermedi delle reazioni di sostituzione elettrofila e nucleofila in serie aromatiche” which is freely available online at <http://amsdottorato.cib.unibo.it/>

References

- [1] L. Forlani, C. Boga *Targets in Heterocyclic Systems, Chemistry and Properties*, **2011**, 15, 372–401.
- [2] F. Effenberger; R. Niess, *Angew. Chem.* **1967**, 79, 1100, *Angew. Chem. Int. Ed. Engl.* **1967**, 6, 1067.
- [3] F. Effenberger; F. Reisinger, K.H. Schönwälder, P. Bäuerle, J.J. Stezowski, K.H. Jogun, K. Schöllkopf, and W.D. Stohrer, *J. Am. Chem. Soc.* **1987**, 109, 882–892.
- [4] F. Effenberger, *Acc. Chem. Res.* **1989**, 22, 27–35 and ref. therein.
- [5] a) W. Sachs; W. Knoche, S. Herrmann; *J. Chem. Soc. Perkin Trans. 2* **1991**, 701–710. b) S. Vogel W. Knoche, W. W. Schoeller, *J. Chem. Soc. Perkin Transaction 2*, **1986**, 769–772. c) W. Knoche; W. Schoeller; R. Schomaecker; S. Vogel. *J. Am. Chem. Soc.* **1988**, 110, 7484–7489. d) W. Knoche, W. Sachs; S. Vogel, *Bull. Soc. Chim. France* **1988**, 377–382.
- [6] a) R. Niess, K. Nagel, F. Effenberger, *Tetrahedron Lett.* **1968**, 40, 4265–4268; b) F. Effenberger, K. E. Mack, K. Nagel, R. Niess, *Chem. Ber.* **1977**, 110, 165–180; c) P. Fischer, K. E. Mack, E. Mossner, F. Effenberger, *Chem. Ber.* **1977**, 110, 181–188.
- [7] a) P. Menzel, F. Effenberger, *Angew.Chem. It. Ed.*, 1972, 11. 922. b) F. Effenberger, P. Menzel, *Angew.Chem. It. Ed.*, 1975, 14. 72.
- [8] C. Boga, E. Del Vecchio, L. Forlani, A. Mazzanti, P. E. Todesco, *Angew. Chem.* **2005**, 117, 3349–3353; *Angew Chem. Int. Ed. Engl.* **2005**, 44, 3285–3289.
- [9] C. Boga, E. Del Vecchio, L. Forlani, *Eur. J. Org. Chem* **2004**, 7, 1567–1571.
- [10] Boga, C.; Del Vecchio, E.; Forlani, L.; Tocke Dite Ngobo A.-L.; Tozzi, S. *J. Phys. Org. Chem.*, **2007**, 20, 201–205.
- [11] C. Boga, E. Del Vecchio, L. Forlani, S. Tozzi, *J. Org. Chem.*, **2007**, 72 (23), 8741–8747.
- [12] K. Schollkopf, J.J. Stazowski, F. Effenberger, *Organometallics*, **1985**, 4, 922–929.
- [13] D.T. Glatzhofer, M. A. Khan, *Acta Cryst.*, **1993**, C49, 2128–2133.
- [14] T. Yamaoka; H. Hosoya; S. Nagakura, *Tetrahedron* **1968**, 24, 6203–6213.
- [15] T. Yamaoka; H. Hosoya; S. Nagakura, *Tetrahedron* **1970**, 26, 4125–4130.
- [16] W. Knoche, W. Sachs; S. Vogel, *Bull. Soc. Chim. France* **1988**, 377–382.
- [17] W. Knoche; W. Schoeller; R. Schomaecker; S. Vogel. *J. Am. Chem. Soc.* **1988**, 110, 7484–7489.

-
- [18] W. Sachs; W. Knoche, S. Herrmann; *J. Chem. Soc. Perkin Trans. 2* **1991**, 701–710.
- [19] a) D. T. Glatzhofer; D. Allen; R. W. Taylor, *J. Org. Chem.* **1990**, *55*, 6229–6231; b) D.T. Glatzhofer, M. A. Khan, *Acta Cryst.*, **1993**, *C49*, 2128–2133.
- [20] C. Boga, E. Del Vecchio, L. Forlani, R. Goumont, F. Terrier, S. Tozzi, *Chem. Eur. J.* **2007**, *13*, 9600–9607.
- [21] L. Forlani, C. Boga, A. Mazzanti, N. Zanna, *Eur. J. Org. Chem.* **2012**, 1123–1129.
- [22] C. Boga, E. Del Vecchio, L. Forlani, A. Mazzanti, C. Menchen Lario, P. E. Todesco, S. Tozzi, *J. Org. Chem.* **2009**, *74*, 5568–5575.
- [23] a) H. Mayr, M. Patz, *Angew. Chem.* **1994**, *106*, 990–1010; *Angew. Chem., Int. Ed. Engl.* **1994**, *33*, 938–957; b) H. Mayr, B. Kempf, A. R. Ofial, *Acc. Chem. Res.* **2003**, *36*, 66–77; c) H. Mayr, M. Patz, M. F. Gotta, A. R. Ofial, *Pure Appl. Chem.* **1998**, *70*, 1993–2000; d) H. Mayr, T. Bug, M. F. Gotta, N. Hering, B. Irrgang, B. Janker, B. Kempf, R. Loos, A. R. Ofial, G. Remmenikov, N. Schimmel, *J. Am. Chem. Soc.* **2001**, *123*, 9500–9512.
- [24] a) L. Forlani, *Hydrogen Bonding and Complex Formation Involving Compounds with Amino, Nitroso and Nitro Groups* in *Amino, Nitroso, Nitro and Related Groups*, Patai's Chemistry of Functional Groups, (Ed S. Patai), John Wiley & Sons, Ltd, Chichester, UK.Ch.10, 2003; b) L. Forlani, *Hydrogen bonds of anilines* in *The Chemistry of Anilines, Part I Patai's Chemistry of Functional Groups*, (Ed. Z. Z. Rappoport), John Wiley & Sons, Ltd, Chichester, UK.Ch.8, 2007; c) R. Taylor, O. Kennard, W. Versichel *J. Am. Chem. Soc.* 1984, *106*, 244–248; d) M. T. Scerba, C. M. Leavitt, M. E. Diener, A. F. DeBlase, T. L. Guasco, M. A. Siegler, N. Bair, M. A. Johnson, T. Lectka *J. Org. Chem.* **2011**, *76*, 7975–7984.
- [25] a) J. A. Riddick, W. B. Bunger in *Organic Solvents* (Ed.: A. Weissberger) Wiley-Interscience, New York, **1970**; b) C. Reichardt, *Solvents and Solvent Effects in Organic Chemistry*, 3rd Edition, Wiley-VCH, Weinheim, **2003**.
- [26] J. F. Coetzee, G. R. Padmanabhan, *J. Am. Chem. Soc.* **1965**, *87*, 5005–5010.
- [27] a) J. Harada, K. Ogawa, *J. Am. Chem. Soc.*; **2001**, *123*, 10884–10888; b) J. Harada, K. Ogawa, *Chem. Soc. Rev.*; **2009**, *38*, 2244–2252).
- [28] C. R. Reed, K-C. Kim, E. S. Stoyanov, D. Stasko. F. S. Tham, L. J. Mueller, P. D. W. Boyd, *J. Am. Chem. Soc.* **2003**, *125*, 1796–1804.

Chapter 3

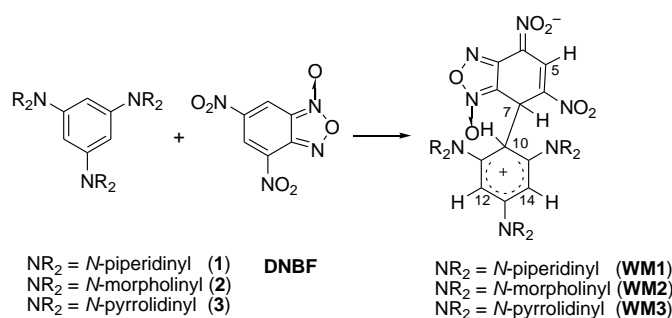
2,4-dipyrrolidine-1,3-thiazole as a new supernucleophile

Chemical reactions involving neutral carbon atoms of strongly activated nucleophilic and electrophilic molecules permit to observe particular behaviours of the simple nucleophile/electrophile coupling reaction. This is the case of superelectrophilic species such as 4,6-dinitrobenzofuroxan (**DNBF**), or supernucleophilic species such as 1,3,5-tris(*N,N*-dialkyl)aminobenzenes.

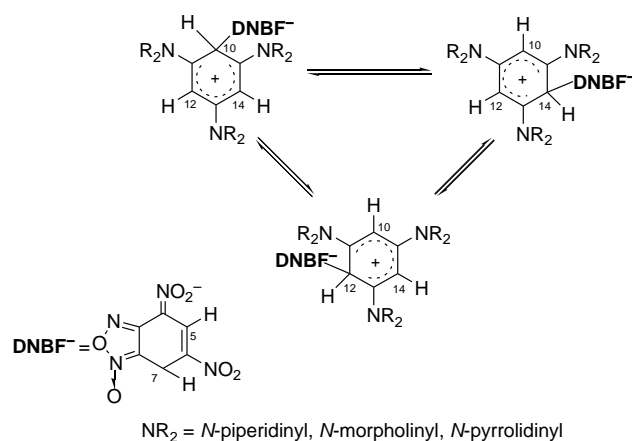
σ -Anionic complexes (Meisenheimer complexes)^[1] involving a number of strongly activated electrophilic substrates have been extensively described.^[2] σ -cationic complexes (Wheland complexes),^[3] intermediates of the electrophilic aromatic substitution reaction,^[4-7] have been less investigated^[8,9] due also to some experimental difficulties in their isolation or simple observation by spectroscopic methods. Recently, our interest has been devoted to Wheland complexes and we have been able to isolate some of them and to study their reactivity.^[10]

The reaction between superelectrophilic and supernucleophilic reagents afforded a new kind of σ -complex, zwitterionic in character, which was called by us Wheland-Meisenheimer complex (**WM**), as shown in Scheme 1.^[11]

Zwitterionic adducts **WM1-3** are moderately stable^[11] and showed, in variable temperature ¹H NMR experiments, a very peculiar and unexpected behaviour. The signals ascribed to H-10, H-12, and H-14, at low temperature are well separated, but, on raising the temperature, they undergo a broadening until to a coalescence situation. This reversible dynamic process was explained hypothesizing the existence of the Wheland-Meisenheimer complex in three homomeric structures rapidly exchanging, as depicted in Scheme 2.^[11]



Scheme 1. Formation of Wheland-Meisenheimer complexes (WM) from 1,3,5-tris(*N,N*-dialkyl)aminobenzenes and 4,6-dinitrobenzofuroxan (DNBF).



Scheme 2. Proposed explanation of the reversible dynamic process observed for WM1–3 in variable temperature ¹H NMR experiments,

Recently, Lenoir^[12] reported a theoretically calculated comparison between the formation of **WM** complex and the formation of donor/acceptor complex (such as π - π complex) in the reaction between **DNBF** and symmetrical triaminobenzenes: the π - π complex results thermodynamically more stable than the **WM** complex in the case of 1,3,5-triaminobenzene, while **WM** complex is thermodynamically more stable than the donor/acceptor π - π complex in the case of the reaction between **DNBF** and 1,3,5-tris(*N,N*-dialkyl)aminobenzenes.

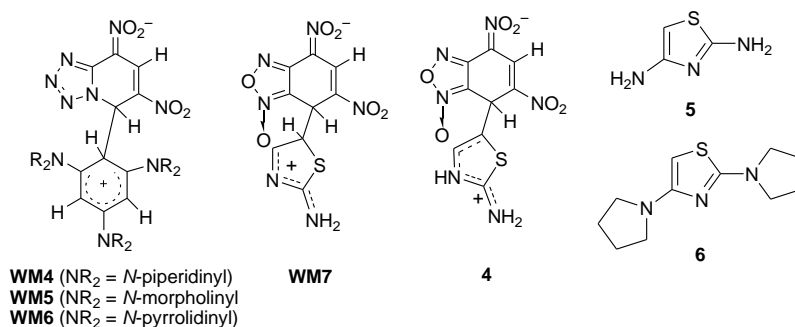
The high positive-charge stabilization effect of the supernucleophiles 1,3,5-tris(*N,N*-dialkylamino)benzenes is due to the strong donor ability of dialkylamino group, as reported by Effenberger.^[13]

Another superelectrophilic^[14] carbon reagent, 4,6-dinitrotetrazolo[1,5-a]pyridine (**DNTP**), which, within the electrophilic scale developed by Mayr,^[15] is a considerably more powerful electrophile than DNBF,^[16] reacts with 1,3,5-tris(*N,N*-dialkylamino)benzenes affording σ -complexes^[17] **WM4–6** (Scheme 3) that behave, in variable temperature ¹H NMR experiments, similarly to **WM1–3** complexes. In addition, some experiments strongly indicated that the formation of these complexes is a reversible process.

Thiazole ring is reported to show border-line properties^[18] emphasized by the presence of particular substituents. 2-Aminothiazole strongly reacts with electrophilic reagents, but nitrothiazoles afford moderately stable σ -anionic complexes (Meisenheimer complexes) with nucleophilic reagents.^[19]

Recently, a study on the nitrogen and carbon nucleophilicities of 2-aminothiazoles through coupling reaction with superelectrophilic **DNBF** was carried out.^[20] The investigation of the system **DNBF**/2-aminothiazole derivatives^[21] permitted to detect the σ -complex **WM7** but the very short life-time of this intermediate prompted us to turn our attention towards more nucleophilic thiazole substrates, such as 2,4-diaminothiazole (**5**) and its derivatives.

It is known that compound **5** is an electron-rich molecule able to complex electrophilic species, such as bromine^[22] but generally 2,4-diaminothiazole derivatives present further properties complicated by the tautomerism of both amino groups.



Scheme 3. Some example of stable WM complexes and nucleophilic thiazole derivatives.

In *N,N*-tetra(alkyl)2,4-diaminothiazole derivatives this complication does not exist and they can be promising candidates to behave as carbon supernucleophiles. Their high carbon nucleophilicity is confirmed also by a previous work of Gompper^[23] which discussed the formation of zwitterionic complexes between *N,N,N',N'*-tetramethyl-1,3-thiazole-2,4-diamine and 1,3,5-trinitrobenzene.

These considerations suggested us that the presence on the thiazole ring of two pyrrolidinyl groups in 2 and 4 position might enhance the nucleophilic power at 5 position of the thiazole ring thus giving a supernucleophile at the neutral carbon at least comparable with 1,3,5-tris(*N,N*-dialkylamino)benzenes. With this in mind, we prepared 2,4-dipyrrolidin-1-yl-1,3-thiazole^[24] (**6**, Scheme 3), and we studied its reactivity with the superelectrophiles **DNBF** and **DNTP**. We were able to obtain and crystallize in both cases ultrastable **WM** complexes thus gaining important information from their X-ray diffraction analysis. These are the first examples of Wheland-Meisenheimer complexes so stable to permit a study on their crystallographic structures. After that we decided to perform a theoretical study of these reactions by using the Density Functional Theory approach (DFT).

Besides the experimental work which will be discussed in chapter 3.1, hence, we reported a detailed theoretical study on the energetic, stabilities and properties of reactants and products reported in this study (chapter 3.2).

3.1 Synthesis and characterization of ultrastable W-M complexes

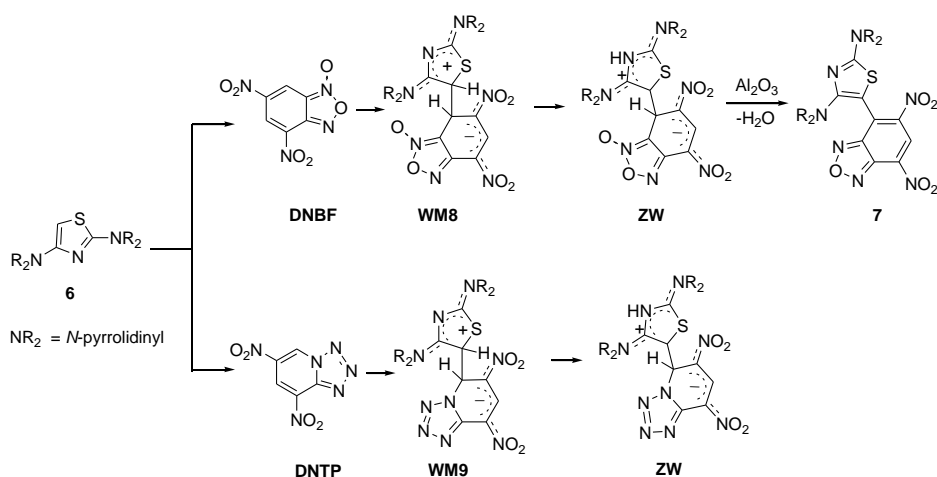
When 2,4-dipyrrolidin-1-yl-1,3-thiazole (**6**), dissolved in CH₃CN, was added (at 25 °C) to an equimolar amount of **DNBF** (or **DNTP**), immediately the solution color changed, and a solid precipitated. The ¹H NMR spectrum of the solid obtained from **6** and **DNBF** showed, in [D₆]DMSO and in the range of chemical shifts between 5 and 9 ppm, two doublets centered at 5.63 and 6.13 ppm (*J* = 2.7 Hz), respectively, and a singlet signal at 8.63 ppm, while the related ¹³C NMR signals (correlated through *g*-HSQC experiments) were at 35.6, 59.6 and 48

132.7 ppm, respectively. The presence of two doublets with the same coupling constant in the region of protons bound to an sp^3 carbon atom, the proton signal area, and the relative chemical shifts in the ^{13}C NMR spectrum confirmed the structure of the zwitterionic σ -complex **WM8** (Scheme 4). 1H NOE experiments permitted to assign the doublets at 5.63 ppm and 6.13 ppm to the proton bound to the sp^3 carbon of the **DNBF** and of the thiazole moiety, respectively, while the singlet at 8.63 ppm is related to the proton bound to the sp^2 carbon of **DNBF** moiety. The ESI-MS analysis was also in agreement with the structure **WM8**.

Also NMR spectral data of the solid obtained from **6** and **DNTP** agree with structure **WM9** (Scheme 4). In particular, in the range of chemical shifts between 5 and 9 ppm, in $[D_6]DMSO$, 1H NMR signals at 6.32 (br.s., 1 H), 7.23 (d, $^3J_{H,H} = 1.8$ Hz, 1 H), and 8.65 ppm (s, 1 H) were found, and the related ^{13}C NMR signals were at 61.9, 56.1 and 131.2 ppm).

Thanks to the stability of complexes **WM8** and **WM9** we were able to obtain crystals suitable for X-Ray diffraction analysis from the mixture CH_3CN/CH_2Cl_2 (1/1 by volume). Structures of **WM8** and **WM9** were confirmed by this technique. We emphasize that these are the first instances of detailed structural X-Ray diffraction analysis of a stable crystalline intermediate of the nucleophilic/electrophilic aromatic substitution reaction. Some details of the structure of **WM8** and **WM9** (Figure 1) are discussed below.

The X-Ray structure showed that the C1-C7 (for both complexes) distance is longer than a standard C-C distance (1.49 Å), being it 1.56 Å both for **WM8** and for the corresponding C1-C5 bond in **WM9**. This confirms the weakness of the bond, that can be the cause of the possibility, in **WM1–6** complexes, to observe the dynamic process indicated in Scheme 2. Obviously, this process cannot occur in the present case. The relative spatial situation of the substituents around the C1-C7 bond corresponds to a gauche relationship, the torsion angle H1-C1-C7-H7 for **WM8** being 66.7° (the corresponding angle for **WM9** is 71.7°).



Scheme 4. Reaction between the thiazole derivative **6** and DNBF or DNTP with formation of new Wheland-Meisenheimer complexes **WM8** and **WM9** and conversion of **WM8** to benzofurazane derivative **7**.

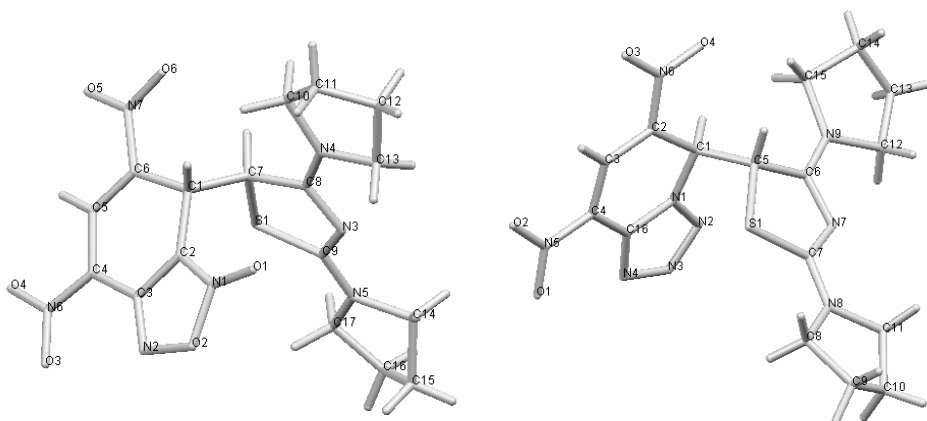


Figure 1. Graphic representation of crystalline structure of **WM8** and **WM9**.

An important point is conceiving the possible formation of different stereomeric forms that we can obtain by this reaction: being both reactive carbons of starting materials stereogenic centers we expected to obtain all the 4 possible σ -complexes and to observe two diastereomeric species in the NMR spectra, and all the four stereoisomers through X-Ray diffraction analysis. On the contrary, NMR spectroscopy data showed the presence of only one diastereomer, a crystal of which, when analyzed by X-Ray diffraction analysis, revealed the presence of the enantiomeric couple (*R,R*) and (*S,S*) for **WM8** and of the enantiomeric couple (*R,S*) and (*S,R*) for **WM9**. A single crystal of **WM8** (or **WM9**), after being

analyzed by X-Ray diffraction, was dissolved in CD₃CN and his ¹H NMR spectrum showed the same signals observed in the NMR spectrum of the solution from which the crystal was precipitated.

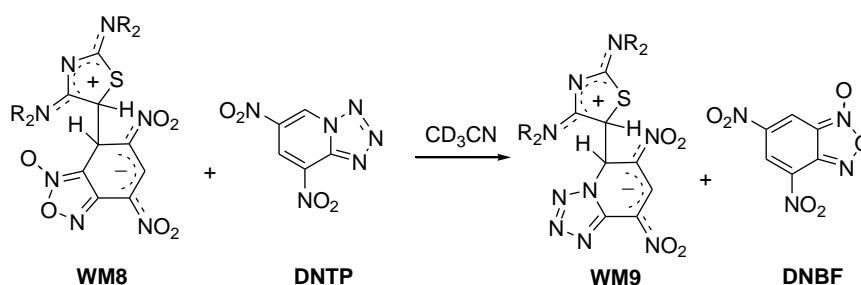
This diastereoselectivity can be explained considering the spatial conformation of the complexes in the solid phase: as shown in Figure 1 the furoxanic ring (as well as the tetrazole ring of **DNTP** of **WM9**) of **DNBF** is facing the thiazole ring and the medium distance between the two rings is near the Van der Waals radii for both enantiomeric forms; an approach between the two reagents that might be responsible for the observed stereoselection.

From crystallographic data it is possible to note as C9-N5 and C8-N4 (1.30 and 1.31 Å respectively for **WM8**) and the corresponding C7-N8 and C6-N9 (1.31Å for **WM9**) exocyclic bonds are slightly shorter (or equal for **WM9**) than C9-N3 and C8-N3 (1.34 and 1.31 Å, respectively for **WM8**) and C7-N7 and C6-N7 (1.33 Å) for **WM9** endocyclic bonds of the thiazole ring. One can deduce that C-N exocyclic bonds are more in π character than the C-N endocyclic bonds, in agreement to the strong electron-donating effect of the two amino groups bound to the thiazole ring. The thiazole ring and the furoxanic ring are face to face, and the observed configuration agrees with the presence of an internal donor/acceptor interaction between the positively charged thiazole moiety and the negatively charged benzofuroxan or tetrazolopyridine moiety of **WM8** or **WM9**, respectively. For instance, S1-C2, S1-C5, and S1-C3 distances are 3.144, 3.714 and 3.690 Å, respectively for complex **WM8**, and for **WM9** complex S1-N1, S1-C16, and S1-C3 are 3.04, 3.513 and 3.687 respectively. Packing of molecules does not show donor-acceptor intermolecular interactions. This structural situation is an indication that the two moieties are prone to a donor-acceptor interaction which may be conceived also between starting reagents.

Even if it is reasonable that the first evolution of **WM8** may be the shift of the proton from the C7 of the thiazole ring to a more basic centre, probably the N3 atom (and the corresponding shift of the proton bound to the C5 of the thiazole ring to the N7 atom **WM9**) we were not able (in both cases) to have evidence on the presence of the zwitterionic σ -complex **ZW**. Interestingly, we observed, in the

reaction mixture containing the **WM8** complex, the slow formation of the final C-C coupling product **7** which may be obtained, in almost quantitative yields, by adding Al_2O_3 to the reaction mixture in CH_2Cl_2 . It has to be noted that this is the first example of observed evolution of **WM** complexes to neutral products, probably favoured by the possibility, for **WM8**, to lose water.

Finally, when **DNTP** is added to a solution in CD_3CN of **WM8**, **WM9** complex is formed in a slow process (about 2 weeks to rise quantitative conversion), as depicted in Scheme 5 to confirm our previous conclusion on the reversibility of the formation of the **WM** complexes.



Scheme 5. Exchange of the electrophilic partner from **WM8** to **WM9**.

3.2 A theoretical study on the structure, energetic and properties of the W-M complexes

As described in the introduction, to better understand the peculiar behavior of these reagents and products we decided to carry out a theoretical study. The first step was to compare calculated *vs.* experimental structures and in particular to optimize all the intermediates compounds leading to the obtained **WM**'s. In a second step we performed a benchmark by using MP2 and a variety of DFT functionals for evaluating the energies of all molecules in the reaction's pathways; this has a twofold interest: first of all the performance of the different functionals can be assessed, secondly the profile of this peculiar reaction can be characterized in terms of activation energy. Finally, we investigated the electronic properties

(frontier orbitals, electrostatic potential, etc...) of all reagents and products in order to provide more insight into their peculiar reactivity.

All calculations were carried out with the Gaussian 09 program package (Rev. A.02).^[25]

The initial guess geometry of the compounds **WM8** and **WM9** were taken from the X-Ray coordinates.^[26] All geometries were fully optimized using ultrafine grid at the B3LYP/6-31G(d) level of theory, which is known to produce reliable geometries and frequencies of the stationary points.

Intrinsic Reaction Coordinate (IRC) calculation followed by geometry optimizations were used to characterize the reaction path, and in particular to find reactant complexes (π - π complexes) and products connected to the transition state.

Frequencies were calculated at the same level of theory as the geometry optimization to verify the nature of the stationary points and to obtain zero-point vibrational corrections. As suggested in previous works, the zero point correction was scaled by 0.977 to better reproduce experimental results.^[27]

Different exchange correlation functionals (listed in table 1) were tested as well as MP2 for the evaluation of the energies of the compounds along the reaction's pathways by single-point energy calculations performed using fairly large basis set such as 6-311+G(d,p).

The basis set superposition error (BSSE) corrections (using the Boys-Bernardi counterpoise correction scheme) were applied using the automated procedure available in the Gaussian 09 software package.^[28]

Solvent (acetonitrile) effects were introduced in the single point energy calculations by the universal solvation model SMD^[29] using the geometries optimized in the gas phase.

Binding energies were calculated as the differences between the energy of the complexes and the sum of the energies of the isolated reagents.

Partial atomic charges are obtained by using different methods implemented in Gaussian 09 namely Chelp^[30], ChelpG^[31], Hirshfeld^[32-34], Merz-Singh-Kollman (**MK**)^[35,36] and NBO.^[37]

Table 1. List of functionals used in the present study.

Method	Type	X^a	Reference(s)
B3LYP	Hybrid GGA	20	38, 39, 40, 41
B97-D	GGA + D	0	42
B97-1	Hybrid GGA	21	43
B97-2	Hybrid GGA	21	44
BMK	Hybrid meta-GGA	42	45
CAM-B3LYP	Range-separated-hybrid	19/65	46
HCTH	GGA	0	43
LC- ω PBE	Range-separated-hybrid	0/100	47, 48
M05	Hybrid meta-GGA	28	49
M05-2X	Hybrid meta-GGA	56	50
M06	Hybrid meta-GGA	27	51
M06-HF	Hybrid meta-GGA	100	52
M06-L	Meta-GGA	0	53
M06-2X	Hybrid meta-GGA	54	51
MP2	WFT ^b		54
mPW1PW91 ^c	Hybrid GGA	25	55
mPWPW91 ^d	GGA	0	55
OLYP	GGA	0	56
PBE0 ^e	Hybrid GGA	25	57
τ -HCTH	Meta-GGA	0	58
τ -HCTHhyb	Hybrid meta-GGA	15	58
TPSSh	Hybrid meta-GGA	10	59
VSXC ^f	Meta-GGA	0	60
ω B97X	Range-separated-hybrid	15.77/10	61
ω B97X-D	Range-separated-hybrid	22.2/100	62
X3LYP	Hybrid GGA	21.8	63

^aPercentage of Hartree-Fock exchange in each functional; where two values are present, the first mean the percentage of Hartree-Fock exchange at short range, while the second at long range.

^bWFT stands for Wave Function Theory based methods. ^cAlso called mPW1PW, mPW0, and mPW25. ^dAlso called mPWPW. ^eAlso called PBE1PBE. ^fAlso called VS98.

3.2.1 Theoretical structures

The X-ray structures of **WM8** and **WM9** are compared with their counterparts optimized in gas phase and no great conformational discrepancies are observed among them as can be seen in Figure 2. The overlay similarity is really high (0.97% for both structures), demonstrating that the standard method used for optimization B3LYP/6-31G(d) is accurate in predicting also these particular structures, which we are able to compare for the first time with experimental results thanks to their unexpected stability. Moreover, the high value of the overlay similarity also implies that the crystal packing only induces slightly distortion structure of the equilibrium geometry. This fact can be due to the high rigidity of the conjugated structure.

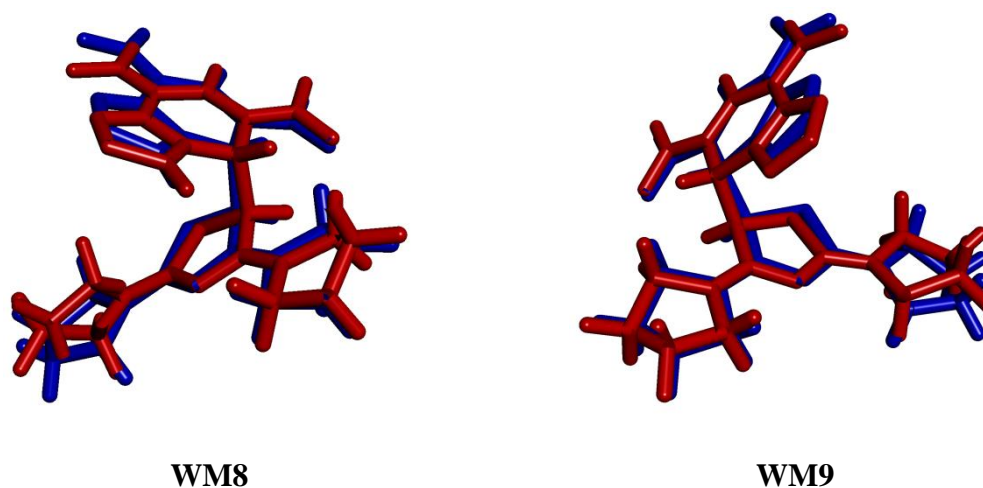


Figure 2. Atom-by-atom superimposition of the structure calculated (red) over the X-ray structure (blue) for the titled compounds. The overlay similarity is 0.97 for both structures.

To be sure that the two optimized structures are in a global and not in a local minimum because of the choice of starting guess, a search for a lowest energy structure was performed using the scan method implemented in Gaussian 09 at AM1 level of theory as a function of the selected rotational degree of freedom between the new C-C bonds formed. This search did not found any

lower-lying structure, confirming that the structures previously shown are indeed the lowest energy conformers.

Once the transition states geometry preceding the formation of WMs complexes have been optimized and the nature of these stationary points has been verified (one imaginary frequency), we performed an Intrinsic Reaction Coordinate (IRC) scan at B3LYP/6-31G(d) level of theory to establish their connection with the initial and final species. A π - π complex was found to be, as usually supposed for these kinds of reactions, an intermediate preceding the formation of the WM complex for both reactions. In Figure 3 the optimized structures of all species involved in both reactions are shown.

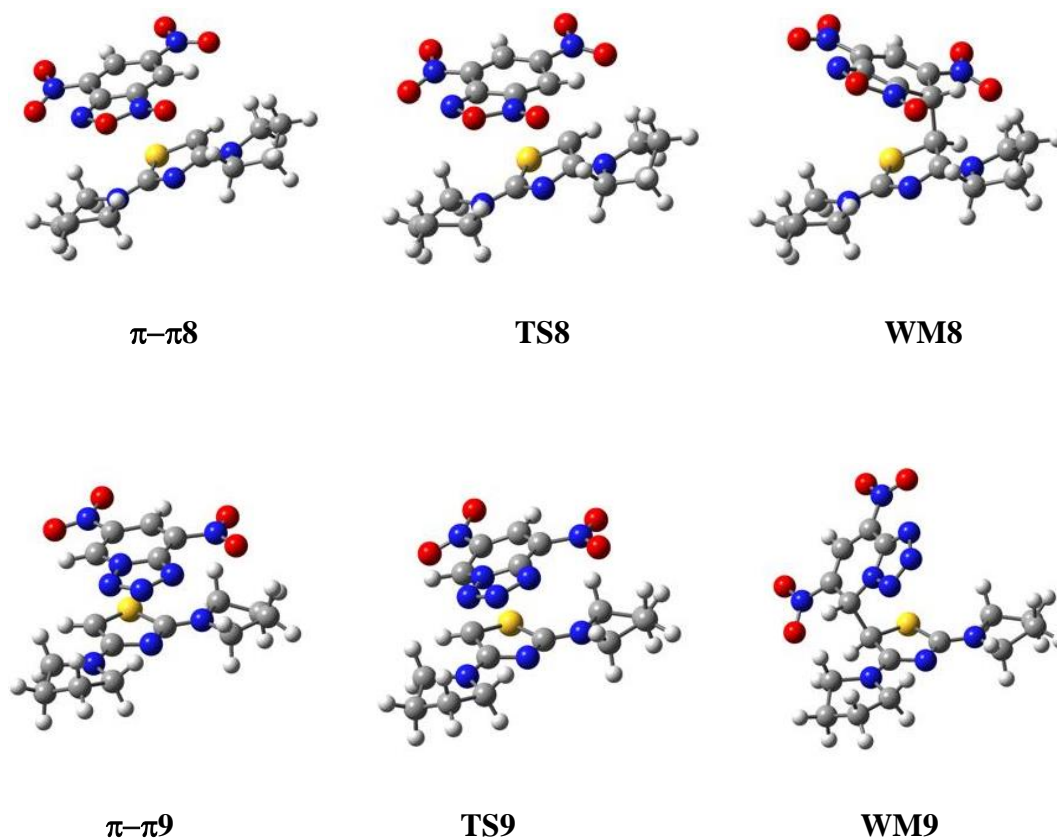


Figure 3. Optimized structures at B3LYP/6-31G(d) level of theory of WMs and the compounds preceding their formation.

The distance between the two carbon atoms involved in the formation of the new bond is reported in Table 2. The theoretical distance of the new bonds formed in the WMs show a good agreement with the experimental one. The distance of the aromatic rings of the two moieties (**DNBF-DPT** and **DNTP-DPT**) in the π - π complexes is about 3 Å, typical for such kind of complexes.^[64] An interesting substantial difference for the two reactions is that in the π - π complex between **DNTP** and **DPT** the thiazole ring is directly facing to the six member ring of the tetrazolepyridine while in the π - π complex between **DNBF** and **DPT** the six member rings of the benzofuroxane is facing to the sulphur atom of the thiazole ring (Figure 4). This can result in a better overlapping between the reactant's orbitals in the π - π 9, whose interaction can be governed by charge transfer between the aromatic rings, while for π - π 8 the dominant interaction could be an n- π between sulphur atom and benzofuroxane aromatic ring.

Table 2. Selected bond lengths of the titles optimized structure (Å). In parenthesis the experimental values.

	DNBF + DPT	DNTP + DPT
π - π	3.02	3.05
TS	2.34	2.34
WM	1.60 (1.57)	1.58 (1.56)

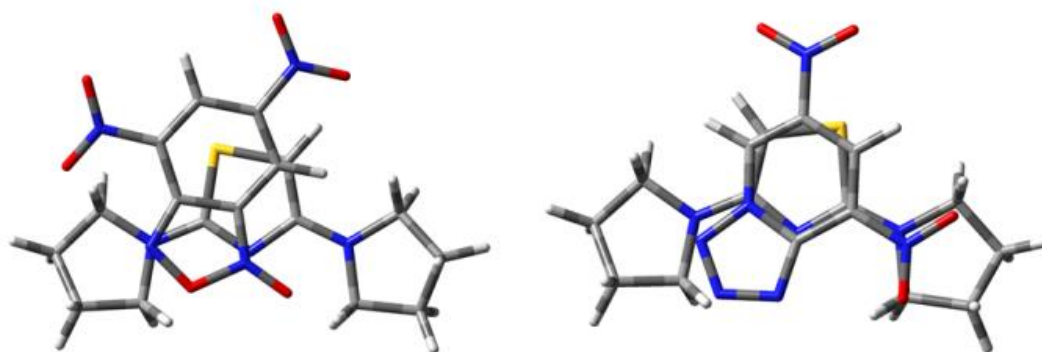


Figure 4. Pictures of π - π 8 and π - π 9 complexes.

3.2.2 Energetic along reaction's pathways and functional benchmark.

To assess the performance of the most common used DFT exchange correlation functionals, we performed single point energy calculation with all methods listed in Table 1 on the stationary points structures along the pathways for the reaction between **DNBF** and **DPT** (previously optimized with B3LYP/6-31G(d) in gas phase) with the fairly large basis set 6-311+G(d,p). The data collected in Table 3 (which are not corrected for both ZPVE and BSSE) show, as expected, a large variance among them. First of all is necessary to remember that energy of **TS8** can be in some cases lower than that of π - π **8** because its energy is calculated by using large basis set on a geometry optimized at a different level of theory, and is not due to a bad evaluation of the transition state, whose nature is confirmed by the number of imaginary frequency. The feature common to all the functionals tested is the high binding energy of **WM8** complex, with the only exception found in VSXC functional which show a strong overstabilization of the π - π **8** and **TS8** complexes with respect to the final product. We can also note that, in addition to some different values of relative energies for the same structure, there is a substantial divergence in the evaluation of the barrier height. In fact, MP2, together with B97-D, BMK, M06-HF, M05-2X, M06-2X, mPW1PW91, PBE0, τ -HCTHhyb and TPSSh indicate a barrierless reaction, while for the other functionals the activation energy exist. Going more in deep and trying to find if there is a systematical improvement for example by passing from GGA to the usually most accurate Hybrid-metaGGA, we can observe that a simple explanation is not possible. The addition of high percentage of Hartree-Fock exchange for hybrid functionals or the inclusion of long-range/dispersion correction terms not always brings significant changes towards an univocal result or trend. Anyway, the level of theory usually advised for the determination of barrier heights, since they are considered to be the most accurate (such as M06-2X and BMK) follow the same energy trend of the wave function based method MP2.

As the recent benchmarks for this kind of reactions show that M06-2X overcome in accuracy both MP2 and BMK,^[65] we decided to further carry on our study by using this functional.

Table 3. Relative energies (Kcal/mol) at various computational levels of the three structures along the DNBF-DPT reaction's pathways.

	π - π 8	TS8	WM8
B3LYP	-8,7	-7,1	-20,3
B97-D	-25,1	-25,9	-31,9
B97-1	-12,8	-12,3	-26,7
B97-2	-8,2	-6,9	-21,5
BMK	-11,9	-13,2	-35,7
CAM-B3LYP	-8,5	-7,1	-26,6
HCTH	-9,7	-4,5	-11,7
LC- ω PBE	-7,4	-5,5	-31,2
M05	-13,1	-10,1	-25,1
M06	-20,1	-19,4	-34,4
M06-HF	-20,3	-25,2	-49,8
M06-L	-23,0	-21,4	-29,7
M05-2X	-17,3	-20,1	-39,1
M06-2X	-18,3	-19,6	-37,8
MP2	-27,4	-27,8	-37,8
mPW1PW91	-10,0	-10,4	-27,1
mPWPW91	-12,5	-12,3	-22,6
OLYP	-2,5	1,6	-7,8
PBE0	-11,9	-12,5	-29,1
τ -HCTH	-10,4	-7,8	-16,4
τ -HCTHhyb	-12,5	-12,6	-26,2
TPSSH	-11,6	-11,7	-23,8
VSXC	-63,1	-62,9	-56,9
ω B97X	-13,3	-10,4	-32,4
ω B97X-D	-19,1	-18,2	-36,6
X3LYP	-10,0	-8,6	-22,3

In Table 4 we reported the relative energies computed in both solvent and gas phase at M06-2X/6-311+G(d,p)//B3LYP/6-31G(d) all corrected for zero-point vibrational energy (BSSE corrected energies in parenthesis). Without taking into account the BSSE correction, the reaction between **DNBF** and **DPT** appears to be barrierless in both solvent and gas phase, while the reaction between **DNTP** and **DPT** show the transition state to be slightly higher in energy respect to the π - π complex, resulting in a very low activation energy (about 2 Kcal/mol). If we take into account the effect of BSSE we observe for both reactions that the energetic gap between TS and π - π complex becomes relevant especially in solvent phase, which can be easily explained by the fact that the orbitals' overlap on the two reactant becomes more pronounced for transition state.

Indeed, the difference in energy between TS and π - π complex is in solvent phase 6.0 and 12.3 Kcal/mol for **DNBF+DPT** and **DNTP+DPT** respectively. As discussed previously, the explanation can arise from a better overlap of the reactants' aromatic rings in π - π complex, lowering its binding energy and raising the gap with **TS9**. During the experimental characterization we had no evidence on the formation of such kind of stacking complexes by NMR spectroscopy. The only noteworthy behaviour was the changes in colour observed during the reaction of **DNTP+DPT**. After the addition of a solution of **DNTP** (light yellow) to a solution of **DPT** (colourless) we observed a rapid change in colour of the mixture which became intense red, lasting for a few second before turning into orange. For the reaction between **DNBF** and **DNTP** we had not observed such behaviour; the explanation of this phenomena, which is supported by the present theoretical investigation, can be ascribed to the formation of a stacking complex dominated by charge transfer interaction (which usually favour bathochromic shift) between **DNTP** and **DPT**.

To give a more scientific support to our hypothesis we followed the reactions by using UV-Visible spectroscopy. While for the reaction of **DNBF+DPT** we observed a change in the absorption maximum during the reaction which corresponds to the value of the final product, for the reaction of **DNTP+DPT** we observed a bathochromic shift followed by a rapid shifting of the absorption maximum towards that of the final product. These data are again coherent with the hypothesis of the formation of a stacking complex dominated by charge transfer interaction for the reaction of **DNTP+DPT**.

The low barrier height and the high binding energy of the final **WM** complexes, confirm the fast rate of these reactions and the unprecedented stability of these compounds. Since the next steps of these reactions were not deeply studied experimentally and are complicated to investigate from a theoretical point of view because they include basic catalysis favoured by a solid reagent, we will not tackle the mechanistic study of the second part of the reaction in the present study.

Table 4. Relative energies (Kcal/mol) calculated at M06-2X/6-311+G(d,p)//B3LYP/6-31G(d); BSSE corrected values in parenthesis.

	DNBF+DPT (Gas)	DNBF+DPT (Sol)	DNTP+DPT (Gas)	DNTP+DPT (Sol)
$\pi-\pi$	-17.5 (-13.8)	-9.8 (-6.1)	-21.7 (-17.8)	-12.9 (-8.9)
TS	-18.2 (-13.9)	-14.0 (0.1)	-20.1 (-15.4)	-14.2 (3.4)
WM	-34.4 (-29.6)	-40.4 (-21.6)	-32.3 (-27.6)	-39.6 (-20.7)

3.2.3 Electronic properties

The simplest way to explore the special reactivity of our reagents and understand the nature of their interactions, is to analyse some important electronic properties such as the Electrostatic Surface Potential (ESP), the frontier orbitals and the charge distribution.

Figure 5 shows ESP and HOMO-LUMO distribution for the 3 reagents discussed in this study. Both the highest occupied molecular orbital (HOMO) and the lowest-lying unoccupied molecular orbital (LUMO) are well distributed over the molecules, indicating that the HOMO-LUMO orbitals are mostly the π -type orbitals and are perpendicularly oriented to each other. The only exception is the LUMO of **DPT** which is distributed all over the thiazole aromatic ring, through a bonding, nodeless pattern. The HOMO-LUMO analysis allow us to understand that the formation of the final products happens by the interaction of the HOMO of **DPT** and the LUMO of both electrophilic partners, but the regioselectivity is well understandable by the ESP analysis. In fact, the most electron-poor region in **DNBF** and **DNTP** is localized on the carbon atoms which are effectively involved in the new bonds formation, while in **DPT** the most electron-rich region is localized in the exocyclic nitrogen atom and the carbon atom that effectively reacts. The regioselectivity toward the latter can therefore be explained also by a steric effect which could become important in the case of attack to the exocyclic nitrogen by the two bulky electrophiles **DNBF** and **DNTP**.

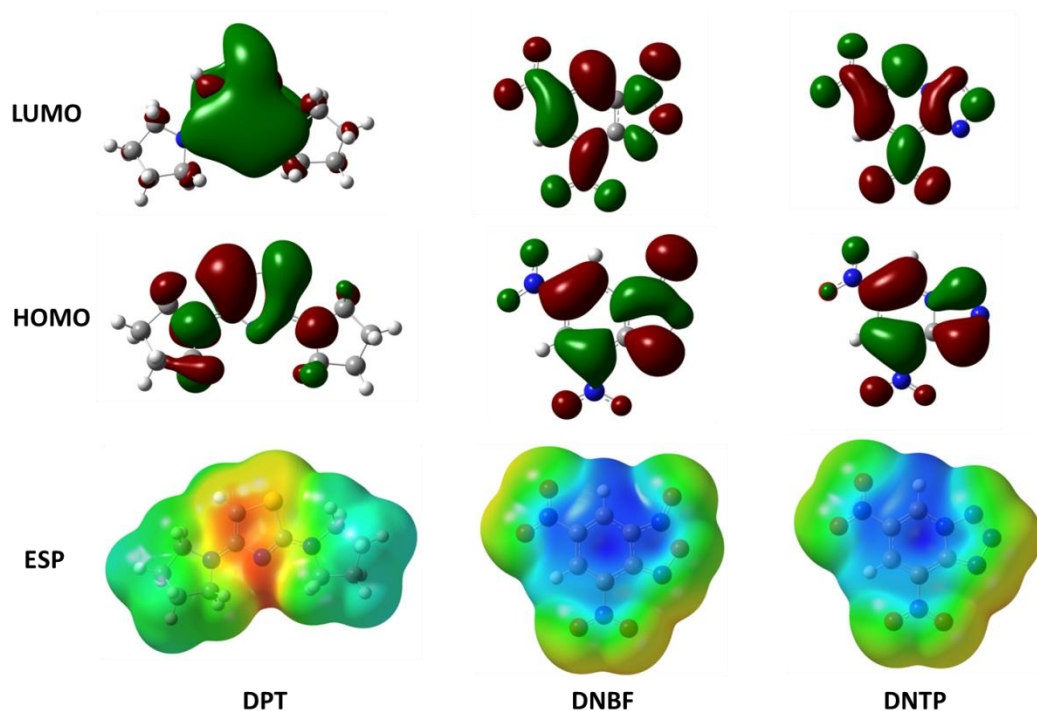


Figure 5. Electrostatic surface potential (ESP) and frontier orbitals of reagents **DPT**, **DNBF** and **DNTP**. ESP is mapped on the electron-density surface where red corresponds to electron-rich and blue corresponds to electron-poor regions.

In Figure 6 we reported the frontier orbital of π - π , **TS** and **WM** for both reactions. As expected, in the π - π complexes the HOMO is mainly localized on **DPT** moiety while LUMO in **DNBF** and **DNTP** moieties. In **TSs**, the orbitals are localized as in π - π complexes, but with a more balanced distribution across the other moieties. For the final **WM** complexes, since HOMO and LUMO are mainly localized on the electrophilic **DNBF** and **DNTP** moieties, we also represent the HOMO-1 and LUMO+1, which are mainly spread over the **DPT** moiety.

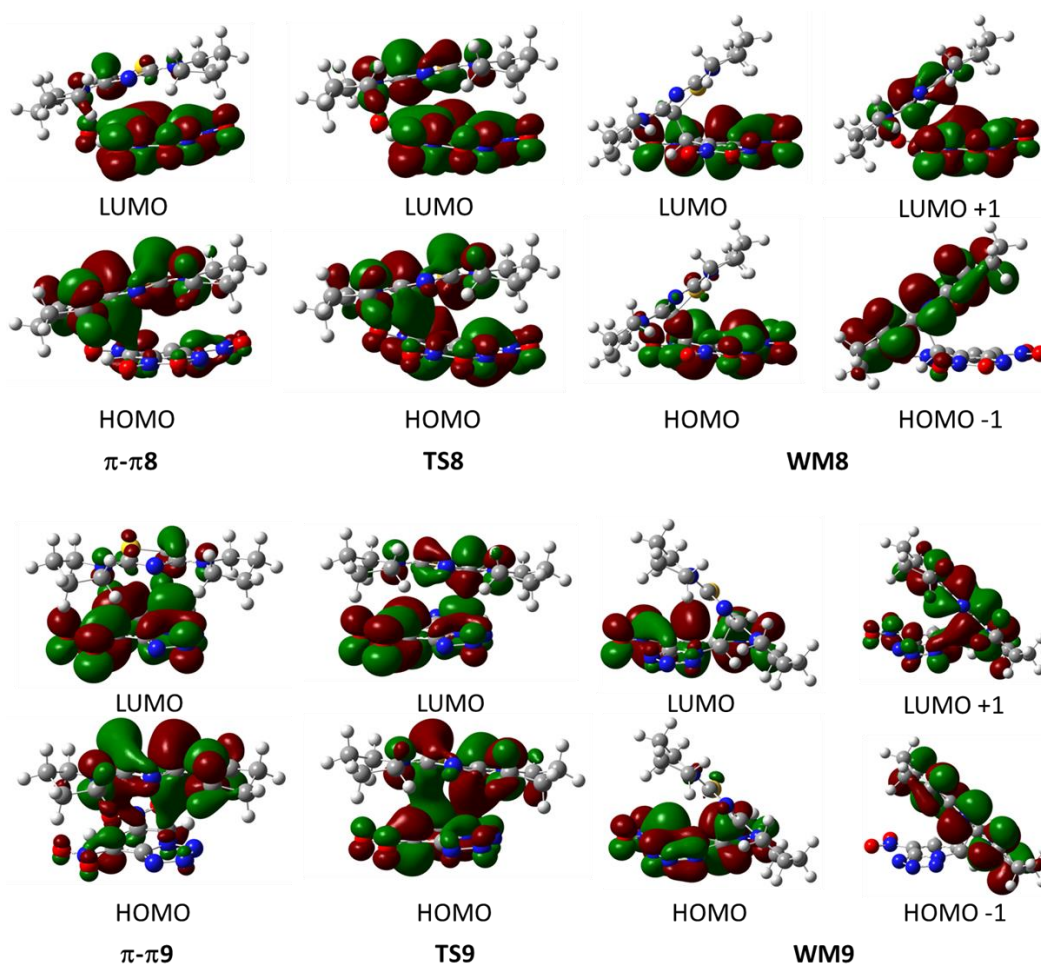


Figure 6. Frontier orbitals of all intermediates along the reaction's pathway for DNBF+DPT and DNTP+DPT.

The HOMO-LUMO gaps reported in table 5 show its increase by passing from the π - π complexes to the WMs, for which the extremely high values can explain their exceptional stability.

Table 5. HOMO-LUMO gap (eV) of titled compounds in gas phase (solvent in parenthesis).

	DNBF+DPT	DNTP+DPT
π - π	2.95 (2.92)	3.56 (3.50)
TS	4.02 (3.96)	4.63 (4.50)
WM	5.10 (5.22)	5.08 (5.21)

Since there are a lot of controversy about the validity of the methods used for population analysis, we decided to test all the ones included in Gaussian 09 (Rev. A.02) software package, except the Mulliken population which is known to produce unrealistic results. As reported in Table 6, all the methods tested show only a very little discrepancy on the results obtained, indicating a clear and general trend. The analysis of the charge distribution on the different moiety reveal interesting indication about the charge delocalization. In the π - π complexes the charge on **DPT** moiety is about 0.15, a value which is not so high, but that cannot exclude a charge transfer interaction. In both TS the charge on **DPT** moiety increase until to reach the unitary positive charge in WMs, which creates an electrostatic interaction that probably also contribute to the enhancement of the stability of these complexes.

Table 6. Charge distribution on the DPT moiety of titled compounds obtained by using different methods (the charges on DNBF and DNTP moieties possess the same values with opposite sign).

	π - π 8	TS8	WM8	π - π 9	TS9	WM9
CHELP	0.16	0.80	0.84	0.15	0.56	0.92
CHELPG	0.16	0.61	0.88	0.15	0.54	1.04
HIRSHFELD	0.11	0.51	0.82	0.09	0.44	0.84
MK	0.15	0.62	0.99	0.15	0.57	1.15
NBO	0.15	0.58	0.96	0.15	0.55	0.96

Besides the charge analysis, also the dipole moment calculated for all the structures (Table 7) show an increasing zwitterionic character by passing from π - π complexes to WM's complexes, confirming the previous underlined trend.

Table 7. Dipole moment in gas phase in Debye (solution in parenthesis).

	DNBF+DPT	DNTP+DPT
π - π	4.89 (8.42)	3.49 (4.35)
TS	9.68 (12.90)	7.48 (10.14)
WM	16.68 (20.39)	17.82 (21.60)

Conclusion

In conclusion, the reaction between 2,4-dipyrrolidin-1-yl-1,3-thiazole and 4,6-dinitrobenzofuroxan or 4,6-dinitro-tetrazolopyridine quantitatively produces a covalent complex which is contemporaneously a Wheland and a Meisenheimer intermediate of the two main reactions on aromatic substrates: the nucleophilic and electrophilic substitution reaction. The reaction occurs with high diastereoselectivity and this is explained by considering the particular approach of the two partners. The particular stability at room temperature of these complexes permitted to obtain single crystals suitable for X-Ray diffraction analysis which confirmed their structure and revealed some interesting details useful to explain the behaviour of **WM** complexes. Furthermore, exchange of the electrophilic partner from **WM8** to **WM9** has been also observed thus to confirming also in present case our previous conclusion on the reversibility of the formation of the **WM** complexes. Finally, the complex obtained by using **DNBF** as electrophilic partner easily eliminates water with re-aromatization of both rings affording an unusual substitution product which is a furazane derivative.

The computational study was carried out to deeper investigate the reactivity of the supernucleophile **DPT** and superelectrophiles **DNBF** and **DNTP**.

The analysis of the reaction's pathways show the presence of π - π complexes and transition states along the reaction coordinates. Both reactions showed a low activation energy and an high binding energy for the **WM** complexes, which justify their great stability. The electrostatic surface potentials and frontier orbitals analysis allow us to explain the high reactivity and regioselectivity of the reagents. At last, the charge distribution and the dipole moment confirmed the large zwitterionic character of the **WM** complexes.

Furthermore our benchmark of the most used exchange correlation functionals showed that there is no negligible discrepancy in the results obtained, warning about exploring energetics by using common functionals, but confirming a good choice of B3LYP and M06-2X functionals for geometry and barrier height, respectively.

Part of this chapter is reproduced with permission from “European Journal of Organic Chemistry” by John Wiley and Sons. Further experimental data, included characterization data of the related products here described, can be found in the paper “L. Forlani, C. Boga, A. Mazzanti, N. Zanna, *Eur. J. Org. Chem.*, **2012**, 1123-1129” fully available at <http://onlinelibrary.wiley.com/>.

References

- [1] J. Meisenheimer, *Just. Lieb. Ann. Chem.* **1902**, 323, 205–246.
- [2] F. Terrier, *Nucleophilic Aromatic Displacement* (Ed. H. Feuer), Wiley-VCH, New York, **1991**.
- [3] G. W. Wheland, *J. Am. Chem. Soc.* **1942**, 64, 900–908.
- [4] R. Taylor, *Electrophilic Aromatic Substitution* John Wiley & Sons, New York, **1990**.
- [5] S. M. Hubig, J. K. Kochi, *J. Am. Chem. Soc.* **2000**, 122, 8279–8288 and ref. therein.
- [6] K. J. Szabò, A.-B. Hörnfeldt, S. Gronowitz, *J. Am. Chem. Soc.* **1992**, 114, 6827–6834.
- [7] M. Aschi, M. Attinà, F. Cacace, *J. Am. Chem. Soc.* **1995** 117, 12832–12839.
- [8] G. A. Olah, R. H. Schlosberg, R. D. Porter, Y. K. Mo, D. P. Kelly, G. D. Mateescu, *J. Am. Chem. Soc.* **1972**, 94, 2034–2043.
- [9] R. Rathore, J. Hecht, J. K. Kochi, *J. Am. Chem. Soc.* **1998**, 120, 13278–13279.
- [10] C. Boga, E. Del Vecchio, L. Forlani, *Eur. J. Org. Chem.* **2004**, 1567–1671.
- [11] C. Boga, E. Del Vecchio, L. Forlani, A. Mazzanti, P. E. Todesco, *Angew. Chem. Int. Ed.* **2005**, 44, 3285–3289.
- [12] P. Jin, F. Li, K. Riley, D. Lenoir, P. v. R. Schleyer, Z. Chen, *J. Org. Chem.* **2010**, 75, 3761–3765
- [13] a) F. Effenberger, P. Fischer, W. W. Schoeller, W.-D. Stohrer, *Tetrahedron* **1978**, 34, 2409–2417; b) F. Effenberger, *Acc. Chem. Res.* **1989**, 22, 27–35.
- [14] E. Buncel, F. Terrier, *Org. Biomol. Chem.* **2010**, 8, 2285–2308.
- [15] a) H. Mayr, M. Patz, *Angew. Chem., Int. Ed. Engl.* **1994**, 33, 938–957; b) Mayr, B. Kempf, A. R. Ofial, *Acc. Chem. Res.* **2003**, 36, 66–77.
- [16] a) T. Boubaker, R. Goumont, E. Jan, F. Terrier, *Org. Biomol. Chem.* **2003**, 1, 2764–2770; b) F. Terrier, S. Lakhdar, T. Boubaker, R. Goumont, *J. Org. Chem.* **2005**, 70, 6242–6253; c) S. Lakhdar, R. Goumont, F. Terrier, T. Boubaker, J. M. Dust, E. Buncel, *Org. Biomol. Chem.* **2007**, 5, 1744–1751.
- [17] C. Boga, E. Del Vecchio, L. Forlani, A. Mazzanti, C. Menchen Lario, P. E. Todesco, S. Tozzi, *J. Org. Chem.* **2009**, 74, 5568–5575.
- [18] J. V. Metzger, *Thiazole and its derivatives* J. Wiley & Sons, New York, **1979**).

-
- [19] a) L. Forlani, P. E. Todesco, *J. Chem. Res. (S)*, **1992**, 44–55; b) L. Forlani, A. Ferrara, A. Lugli, P. E. Todesco, *J. Chem. Soc. Perkin Trans.2*, **1994**, 1703–1707.
- [20] L. Forlani, A. L. Tocke, E. Del Vecchio, S. Lakhdar, R. Goumont, F. Terrier, *J. Org. Chem.* **2006**, *71*, 5527–5537.
- [21] C. Boga, E. Del Vecchio, L. Forlani, R. Goumont, F. Terrier, S. Tozzi, *Chemistry. A Eur. J.* **2007**, *13*, 9600–9607.
- [22] L. Forlani, *L. Synthesis* **1980**, 487–489.
- [23] R. Gompper, P. Krich, J. Schelble, *Tetrahedron Lett.* **1983**, *24*, 3563–3566.
- [24] R. Flaig, H. Hartmann, *Heterocycles*, **1997**, *45*, 875–888.
- [25] Gaussian 09, Revision B.01, Frisch, M. J.; Trucks, G. W.; Schlegel, H. B.; Scuseria, G. E.; Robb, M. A.; Cheeseman, J. R.; Scalmani, G.; Barone, V.; Mennucci, B.; Petersson, G. A.; Nakatsuji, H.; Caricato, M.; Li, X.; Hratchian, H. P.; Izmaylov, A. F.; Bloino, J.; Zheng, G.; Sonnenberg, J. L.; Hada, M.; Ehara, M.; Toyota, K.; Fukuda, R.; Hasegawa, J.; Ishida, M.; Nakajima, T.; Honda, Y.; Kitao, O.; Nakai, H.; Vreven, T.; Montgomery, Jr., J. A.; Peralta, J. E.; Ogliaro, F.; Bearpark, M.; Heyd, J. J.; Brothers, E.; Kudin, K. N.; Staroverov, V. N.; Kobayashi, R.; Normand, J.; Raghavachari, K.; Rendell, A.; Burant, J. C.; Iyengar, S. S.; Tomasi, J.; Cossi, M.; Rega, N.; Millam, J. M.; Klene, M.; Knox, J. E.; Cross, J. B.; Bakken, V.; Adamo, C.; Jaramillo, J.; Gomperts, R.; Stratmann, R. E.; Yazyev, O.; Austin, A. J.; Cammi, R.; Pomelli, C.; Ochterski, J. W.; Martin, R. L.; Morokuma, K.; Zakrzewski, V. G.; Voth, G. A.; Salvador, P.; Dannenberg, J. J.; Dapprich, S.; Daniels, A. D.; Farkas, Ö.; Foresman, J. B.; Ortiz, J. V.; Cioslowski, J.; Fox, D. J. Gaussian, Inc., Wallingford CT, 2009.
- [26] L. Forlani, C. Boga, A. Mazzanti, N. Zanna, *Eur. J. Org. Chem.*, **2012**, 1123–1129.
- [27] Alecu, I. M.; Zheng, J.; Zhao, Y.; Truhlar, D. G. *J. Chem. Theory Comput.* **2010**, 2872–2887.
- [28] Boys, S. F.; Bernardi, F. *Mol. Phys.* **1970**, *19*, 533.
- [29] Marenich, A. V.; Cramer, C. J.; Truhlar D. G. *J. Phys. Chem. B*, **2009**, *113*, 6378–6396.
- [30] Chirlian, L. E.; Francl, M. M. *J. Comp. Chem.*, **1987**, *8*, 894–905.
- [31] C. M. Breneman, C. M.; Wiberg, K. B. *J. Comp. Chem.*, **1990**, *11*, 361–373.
- [32] Hirshfeld, F. L. *Theor. Chem. Acc.*, **1977**, *44*, 129–138.
- [33] Ritchie, J. P. *J. Am. Chem. Soc.*, **1985**, *107*, 1829–1837.
- [34] Ritchie, J. P.; Bachrach, S. M. *J. Comp. Chem.*, **1987**, *8*, 499–509.
- [35] Singh, U. C.; Kollman, P. A. *J. Comp. Chem.*, **1984**, *5*, 129–145.
- [36] Besler, B. H.; Merz Jr. K. M.; Kollman, P. A. *J. Comp. Chem.*, **1990**, *11*, 431–439.
- [37] NBO Version 3.1, E. D. Glendening, A. E. Reed, J. E. Carpenter, and F. Weinhold.
- [38] Lee, C.; Yang, W.; Parr, R. G. *Phys. Rev. B* **1988**, *37*, 785.
- [39] Becke, A. D. *Phys. Rev. A* **1988**, *38*, 3098.
- [40] Becke, A. D. *J. Chem. Phys.* **1993**, *98*, 5648.

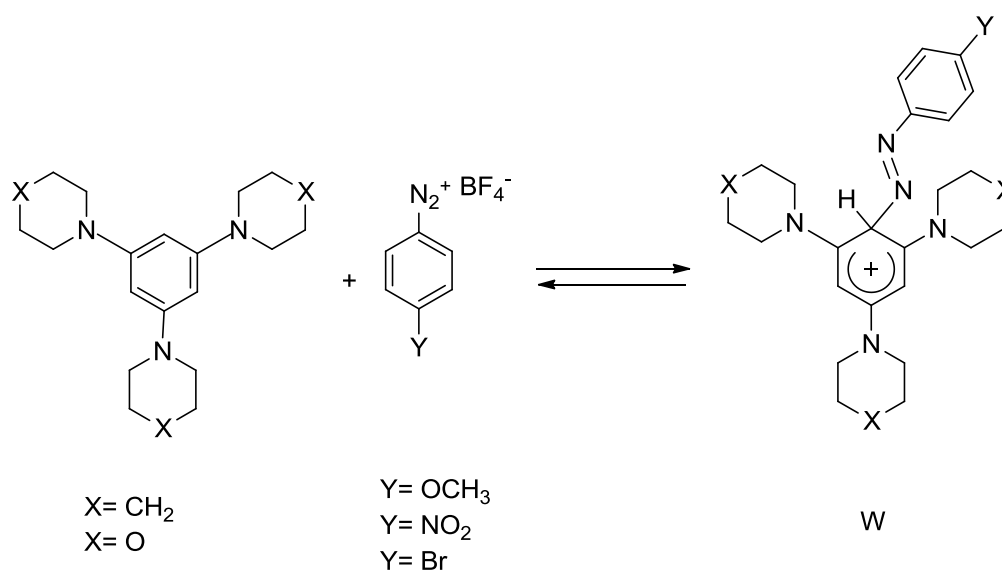
- [41] Stephens, P. J.; Devlin, F. J.; Chabalowski, C. F.; Frisch, M. J. *J. Phys. Chem.* **1994**, 98, 11623.
- [42] Grimme, S. *J. Comput. Chem.* **2006**, 27, 1787.
- [43] Hamprecht, F. A.; Cohen, A. J.; Tozer, D. J.; Handy, N. C. *J. Chem. Phys.* **1998**, 109, 6264.
- [44] Wilson, P. J.; Bradley, T. J.; Tozer, D. J. *J. Chem. Phys.* **2001**, 115, 9233.
- [45] Boese, A. D.; Martin, J. M. L. *J. Chem. Phys.* **2004**, 121, 3405.
- [46] Yanai, T.; Tew, D. P.; Handy, N. C. *Chem. Phys. Lett.* **2004**, 393, 51.
- [47] Vydrov, O. A.; Heyd, J.; Krukav, A. V.; Scuseria, G. E. *J. Chem. Phys.* **2006**, 125, 074106.
- [48] Vydrov, O. A.; Scuseria, G. E. *J. Chem. Phys.* **2006**, 125, 234109.
- [49] Zhao, Y.; Schultz, N. E.; Truhlar, D. G. *J. Chem. Phys.* **2005**, 123, 161103.
- [50] Zhao, Y.; Schultz, N.; Truhlar, D. G. *J. Chem. Theory Comput.* **2006**, 2, 364.
- [51] Zhao, Y.; Truhlar, D. G. *Theor. Chem. Acc.* **2008**, 120, 215.
- [52] Zhao, Y.; Truhlar, D. G. *J. Phys. Chem. A* **2006**, 110, 13126.
- [53] Zhao, Y.; Truhlar, D. G. *J. Chem. Phys.* **2006**, 125, 194101.
- [54] Møller, C.; Plesset, M. S. *Phys. Rev.* **1934**, 46, 618.
- [55] Adamo, C.; Barone, V. *J. Chem. Phys.* **1998**, 108, 664.
- [56] Handy, N. C.; Tozer, D. *J. Mol. Phys.* **1998**, 94, 707.
- [57] Adamo, C.; Barone, V. *J. Chem. Phys.* **1999**, 110, 6158.
- [58] Boese, A. D.; Handy, N. C. *J. Chem. Phys.* **2002**, 116, 9559.
- [59] Staroverov, V. N.; Scuseria, G. E.; Tao, J.; Perdew, J. P. *J. Chem. Phys.* **2003**, 119, 12129.
- [60] Van Voorhis, T.; Scuseria, G. E. *J. Chem. Phys.* **1998**, 109, 400.
- [61] Chai, J.-D.; Head-Gordon, M. *J. Chem. Phys.* **2008**, 128, 084106.
- [62] Chai, J.-D.; Head-Gordon, M. *Phys. Chem. Chem. Phys.* **2008**, 10, 6615.
- [63] Xu, X.; Goddard, W. A. *Proc. Natl. Acad. Sci. U.S.A.* **2004**, 101, 2673.
- [64] Foster, R. *Organic Charge Transfer Complexes*; Academic Press: New York, **1969**.
- [65] Zheng, J.; Zhao, Y.; Truhlar, D. G. *J. Chem. Theory Comput.* **2009**, 5, 808–821.

Chapter 4

Solid state fluorescence in protonated azobenzenes

In previous work of my research group interesting mechanistic information have been obtained by using diazonium salts derivatives as electrophilic substrates.

For example the reaction of tris(dialkylamino)benzenes with diazonium salts allow to isolate Wheland intermediates (Scheme 1) and to study separately the two steps of the reaction thus collecting important information such as the reversibility of the whole reaction and the departure of the proton as the rate determining step.^[1,2]



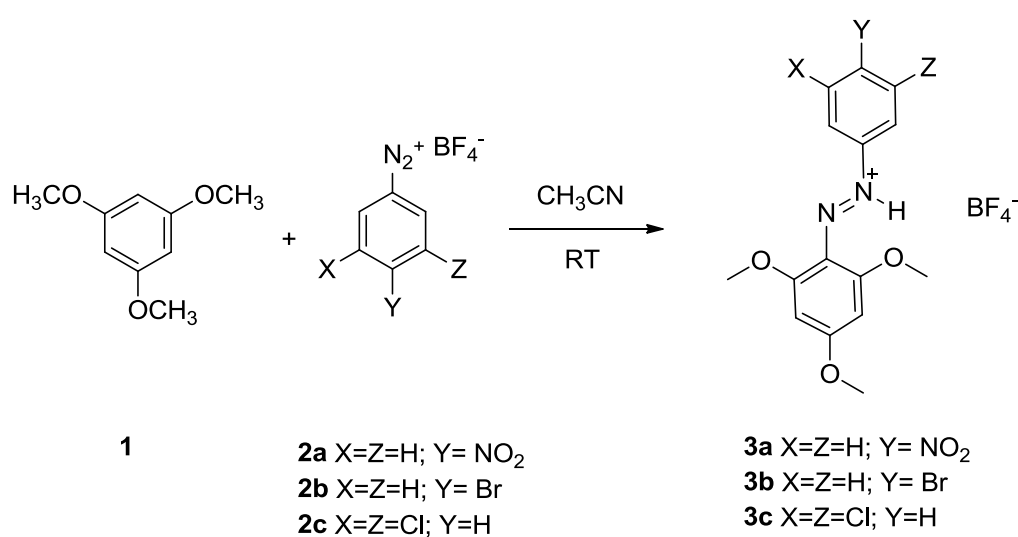
Scheme 1. Reaction between tris(dialkylamino)benzenes and *p*-substituted benzenediazonium salts.

After that, we decided to continue this mechanistic study by changing the nucleophilic partner to compare the reactivity with tris(dialkylamino)benzenes. The most interesting candidate was found to be 1,3,5-trimethoxybenzene because

of its symmetry and the electron-donating effect of methoxy substituents which are comparable with tris(dialkylamino)benzenes.

4.1 Coupling reaction of 1,3,5-trimethoxybenzene and diazonium salt derivatives

The reactions showed in Scheme 2 were carried out in acetonitrile at room temperature and gave, in high yields, the monosubstituted coupling products in saline form (tetrafluoroborate salts), which are easily recovered by simple filtration since they are poorly soluble in the reaction medium. All these products were fully characterized by standard $^1\text{H-NMR}$, $^{13}\text{C-NMR}$ and mass analyses.



Scheme 2. Reaction between 1,3,5-trimethoxybenzene and benzenediazonium salt derivatives.

In this case we did not detect the formation of Wheland intermediates, but we were surprised because of the formation of the inner salt on compounds **3**. In fact, it is known that the nitrogen atoms of the azo moiety are poorly basic. A possible explanation could be the formation of an intramolecular hydrogen bond

between the proton and the oxygen atom of the methoxy moiety. To confirm this hypothesis we crystallized the compound **3a** and performed X-ray diffraction analysis on it.

The obtained structural data confirmed our hypothesis, showing that also intermolecular hydrogen bonds are present (Figure 1).

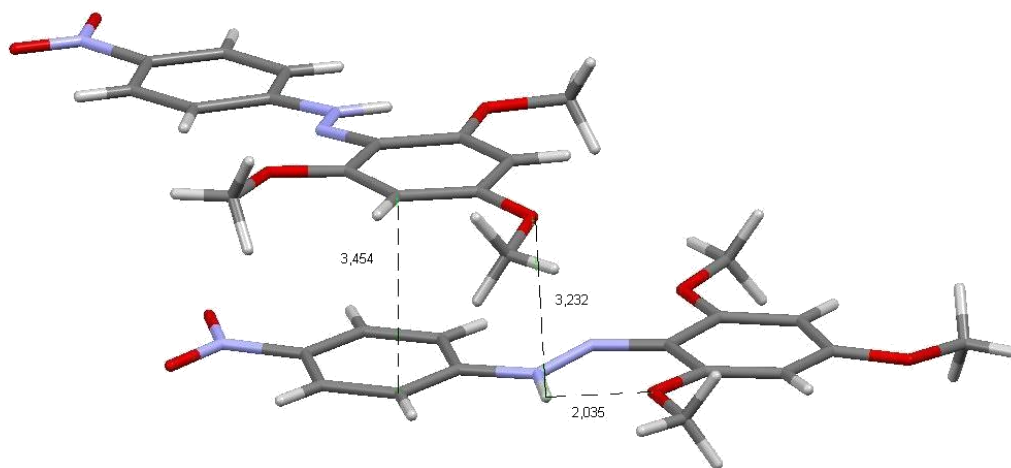


Figure 1. X-ray diffraction structure of compound 3a showing inter/intramolecular hydrogen bonding.

The crystallographic analysis provided also interesting information on the nature of the packing in the solid state. As shown in Figure 2 the molecules of **3a** are parallel-aligned (top) and a strong overlap between the electron-rich trimethoxy substituted rings and the electron-poor nitro substituted rings (bottom) is present.

This closely packed structure could be hence due to the non-covalent interactions, which include intra/intermolecular hydrogen bonding and π - π stacking interaction.

During this work we observed an interesting property: the solid state fluorescence of compounds **3** (Figure 3). We decide to better investigate this property that is unusual, especially for azobenzene derivatives.

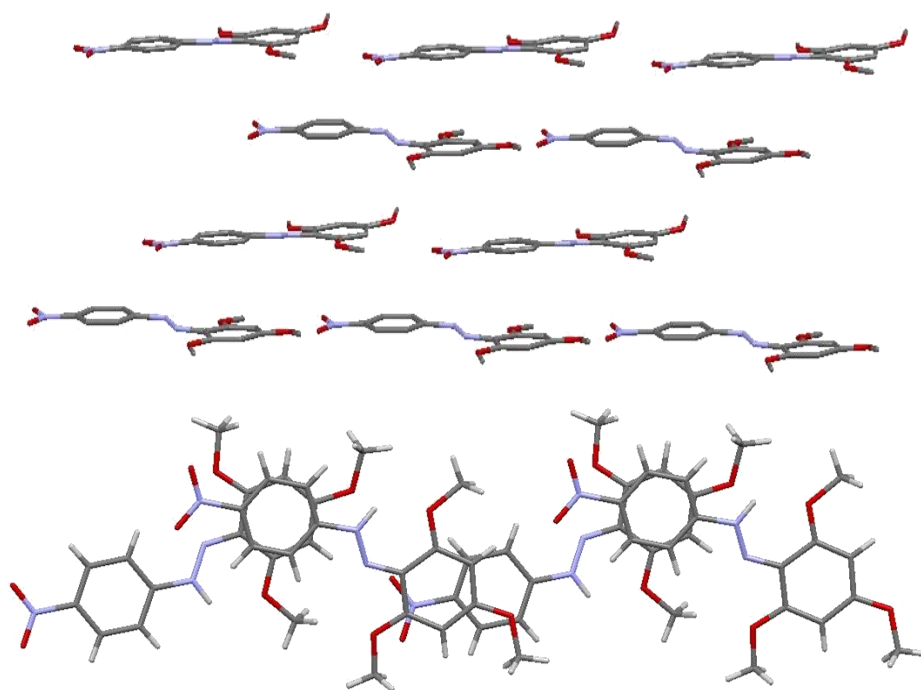


Figure 2. Crystal packing of compound 3b.

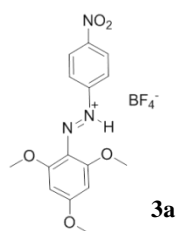
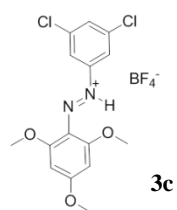
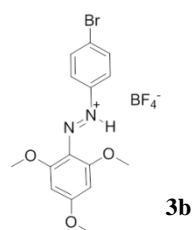
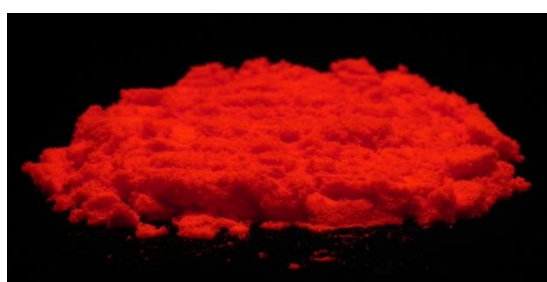
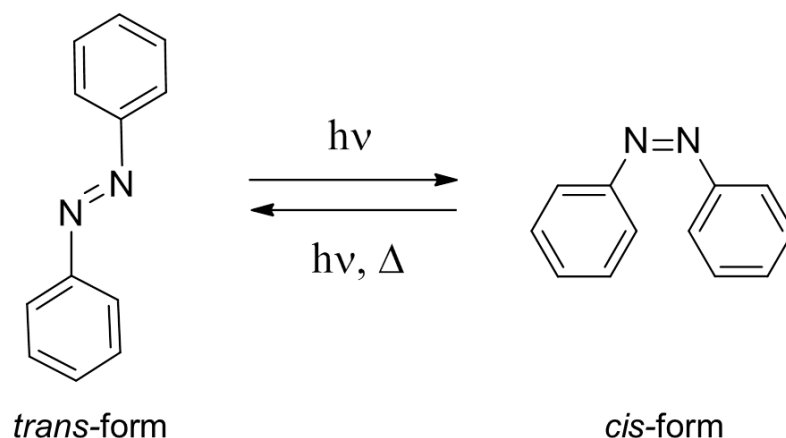


Figure 3. Solid state fluorescence of compounds 3a-c under 365nm UV lamp.

4.2 Fluorescence of azobenzene derivatives

Since the discovery of azobenzene derivatives in the mid-1800s,^[3,4] they became an important class of synthetic coloring agents in the dye industry.

Azobenzene derivatives were also used as acid-base indicators^[5,6], metal ion indicators^[6,7] and, in the last decade, their photochromic properties due to the reversible *trans-cis* conformational change upon photoexcitation (Scheme 3) have been utilized as light triggered switch in a variety of polymers,^[8-10] surface-modified materials,^[12-14] protein probes^[15-18] and molecular machines^[19-21]. The *cis-trans* photoisomerization process (Scheme 3) is so efficient in photoexcited states that inhibits their fluorescence emission that is slower and not competitive. In fact, azobenzenes are known to be not fluorescent since the fluorescence quantum yield in solution at room temperature for the unsubstituted azobenzene is about 10^{-5} .^[22]



Scheme 3. *Trans-cis* photoisomerization in azobenzene derivatives.

However there are some exceptions, such as azobenzenes in rigid matrix at low temperature^[23], self-assembled aggregates^[24-27], ortho-metalated azobenzenes^[28-31], hydroxy-substituted^[32, 33] and protonated azobenzenes^[34], for which the quantum yield is still low (less than 10^{-3}).

Recently Yoshino *et al.* reported the synthesis of the most intense fluorescent azobenzene derivatives by utilizing the intramolecular B-N interaction (Figure 4).^[35,37]

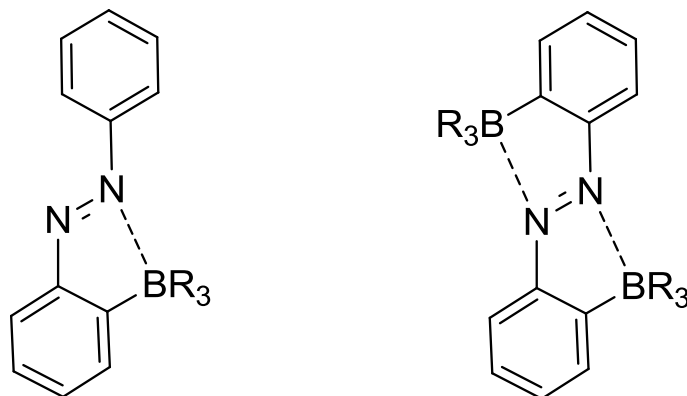


Figure 4. Fluorescent azo-boryl derivatives.

Rau reported a detailed analysis of the spectroscopic properties of azobenzenes,^[38] especially their fluorescent behaviors. It is well known that the fluorescence of azo-compounds is higher if the *cis-trans* photoisomerization is blocked and if there is an inversion of the $\pi-\pi^*$ and $n-\pi^*$ transitions which can occur by coordination of one nitrogen atom of the azo-moiety for example by simple protonation.

We start our investigation by recording the UV-visible spectra of compounds **3a-c** in acetonitrile. During the measurement we discovered that, if the solvent is not perfectly anhydrous, there is a shift of the absorption maximum upon dilution (Figure 5).

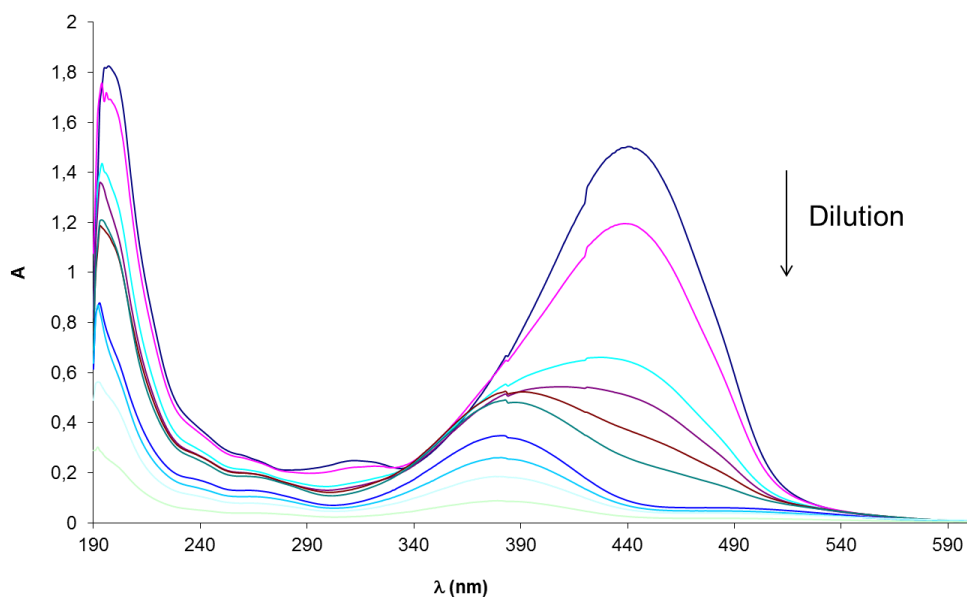


Figure 5. UV-vis spectrum of 3a in acetonitrile after dilution.

Hence we recorded the spectrum of 2 mL of a 4×10^{-5} M solution of **3a** after addition of subsequent aliquots of 10 μ L of water. The spectrum reported in Figure 6 show that water addition shifts the absorption maximum.

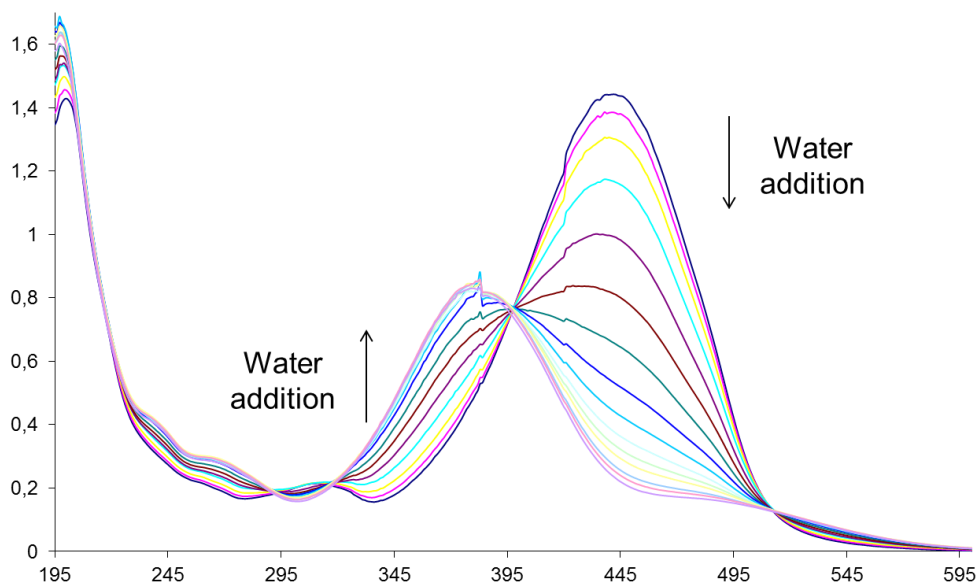
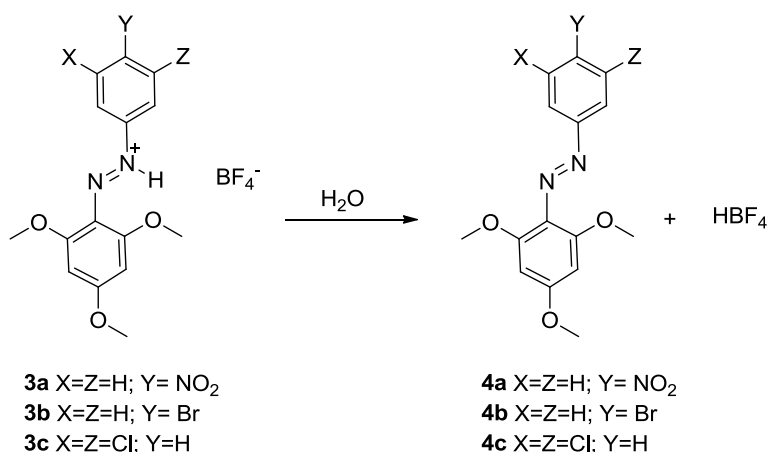


Figure 5. UV-vis spectrum of 3a in acetonitrile after water addition.

The observed peak at 380 nm was found to belong to compound **4a** (the non-saline form of compound **3a**, Scheme 4 and Figure 6), which has been separated and fully characterized by NMR and MS analyses. The same behavior occurs also with compounds **3b** and **3c**. This indicates that water acts as a scavenger for the proton, probably interacting through H-bond.



Scheme 4. Formation of **4** by water addition to compounds **3**.

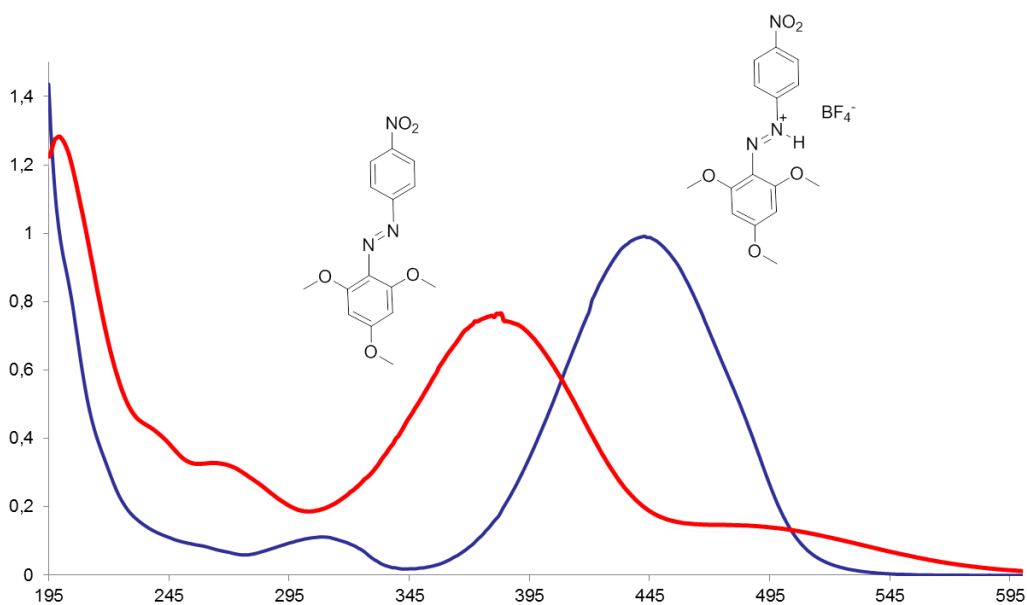


Figure 6. UV-vis spectrum of **3a** and the related non-saline form **4a**.

It is interesting to note that compounds **4** do not show fluorescence emission in both solution and solid state. This behavior is in accordance with the literature data.

Since this work is still in progress (not all the measures of fluorescence quantum yield were done) we reported the preliminary results, hypothesizing on the fluorescence behavior of compounds **3** and **4**.

As aforementioned, among all compounds synthesized, only **3** in solid state show fluorescence emission under 254nm and 365nm UV lamp.

The data reported in Table 1 show the solid state quantum yield in solid state for compounds **3a-c**.

Table 1. Solid state fluorescence quantum yield of compounds 3a-c (excitation 440nm).

	3a	3b	3c
Solid state quantum yield	0,3%	0,9%	0,2%

The solid state quantum yields of compounds **3a-c** are not high but, from a visual point of view, the fluorescence emission appears to be higher than in solution and also with respect to compounds **4a-c**. Pending for the complete quantum yield characterization for all compounds, we investigate on the reason of this behavior by performing experimental and theoretical structural analysis.

4.3 Experimental and theoretical structures of azobenzene derivatives

For comparison, we decided to perform X-ray crystallographic analyses on the protonated and unprotonated species with the same substituents. We were able to obtain suitable crystals for X-ray diffraction analyses of compounds **3b** and **4b**.

The results of X-ray diffraction analysis of **3b** depicted in Figure 7 shown that, as in the case of compound **3a**, the molecules are protonated at the nitrogen atom of the azo-moiety and the two aromatic rings are coplanar.

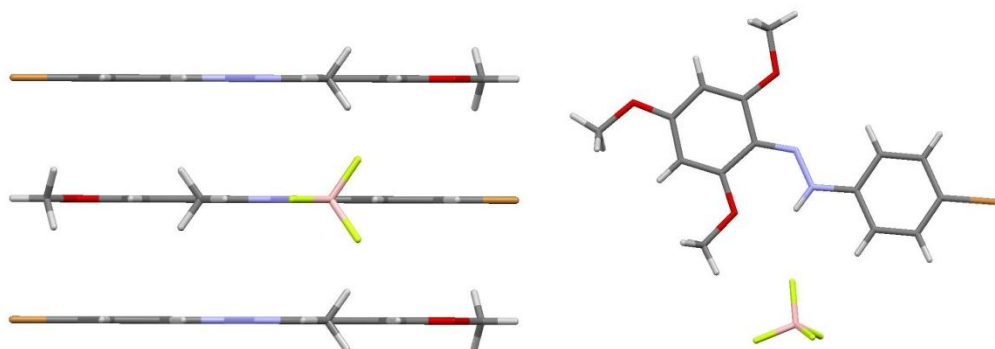


Figure 7. X-ray diffraction structure of compound **3b** (left: side view; right: molecular structure).

The packing in the crystal show an head-to-tail arrangement but, in the top view (Figure 8), it can be noted that there is no superposition of the bromine-substituted and the methoxy-substituted rings as in the case of compound **3a**.

The 3-fold higher quantum yield of **3b** respect to **3a** (see Table 1) could be due to charge transfer interaction that produce a fluorescence quenching in **3a**.

The densely packed crystalline molecular structure of **3b** can imply that *trans-cis* photoisomerization process through the rotation or inversion around the N=N double bond of azobenzene could be effectively blocked.

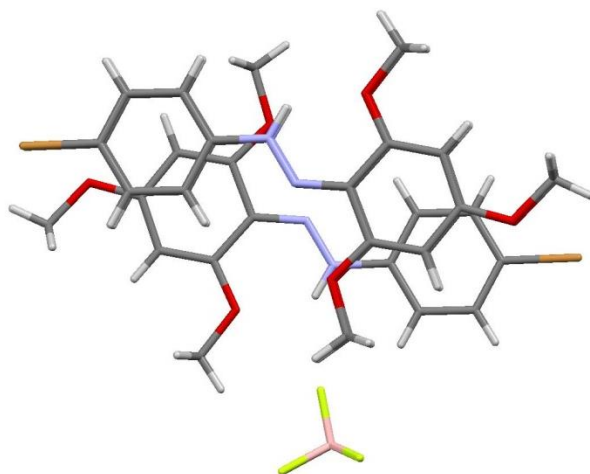


Figure 8. Packing in **3b** crystal.

The crystal structure of **4b** depicted in Figure 9 show that the two aromatic ring are not coplanar, being 38° the C6-C1-N1-N2 dihedral angle.

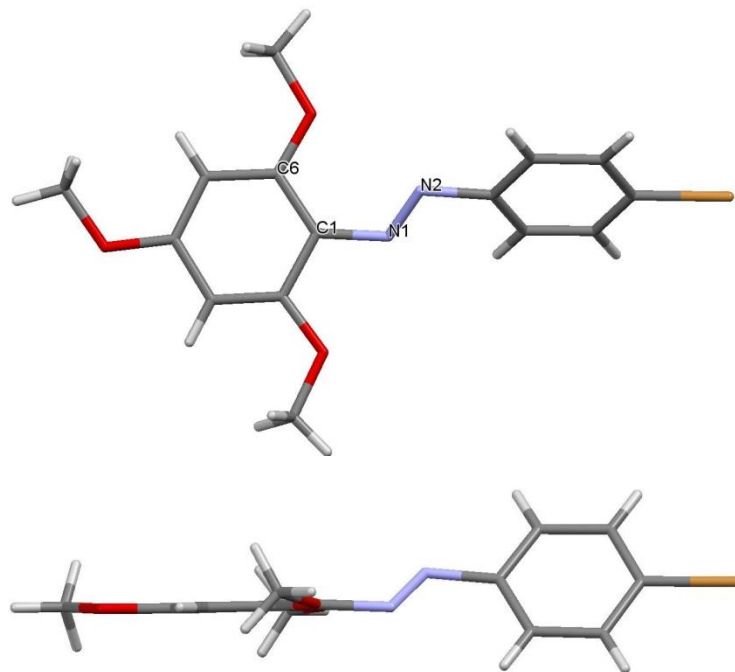


Figure 9. X-ray diffraction structure of compound **4b**.

The simplest explanation could be the repulsion between the lone pair of electrons among nitrogen and oxygen atoms.

This non-coplanar structure explains the less restricted packing shown in Figure 10. This could imply an higher degree of freedom in the vibration of the molecules inside the crystal which could produce non-radiative decay.

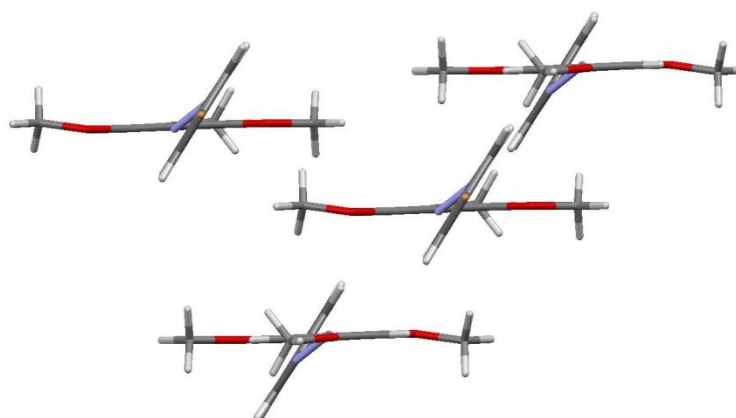


Figure 10. Packing in **4b** crystal.

The theoretical structures of **3b** and **4b** (optimized at MP2/6-31G(d)^[39] level of theory and including solvation effect with PCM formalism^[40] in acetonitrile with Gaussian 09 software package^[41] are in agreement with experimental structures.

To investigate on the rotational energy which could become important in the non-radiative decay, we perform a scan analysis on the energy by varying the dihedral angle at the same level of theory used for optimization.

The dihedral angle scan of **3b** (Figure 11) show an energy maximum when the dihedral reach an angle of about 90°. The rotational activation energy for this rotation is about 20 Kcal/mol.

The dihedral angle scan of **4b** (Figure 12) show instead two energy maxima, one at about 95 degrees and the other one at about 180°. The rotational activation energy is about 2 Kcal/mol for the barrier at 95°. These results indicate that in solution the unprotonated azobenzenes are free to rotate, while the 20 Kcal/mol of activation energy could be enough to hinder the rotation in **3b**, hence the non-radiative decay.

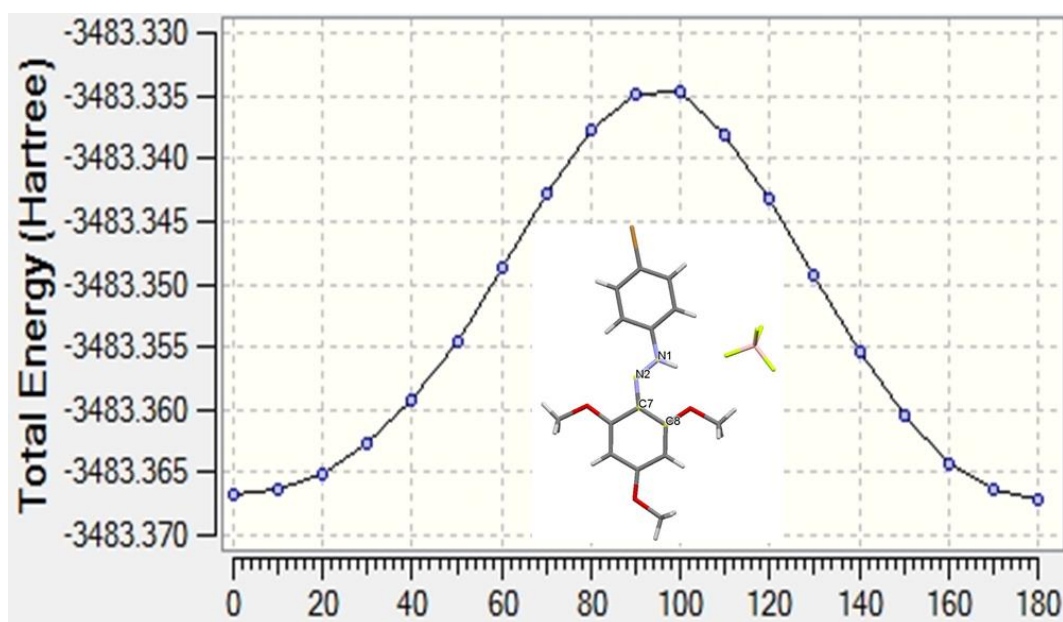


Figure 11. **3b** energy vs C6-C7-N2-N1 dihedral angle.

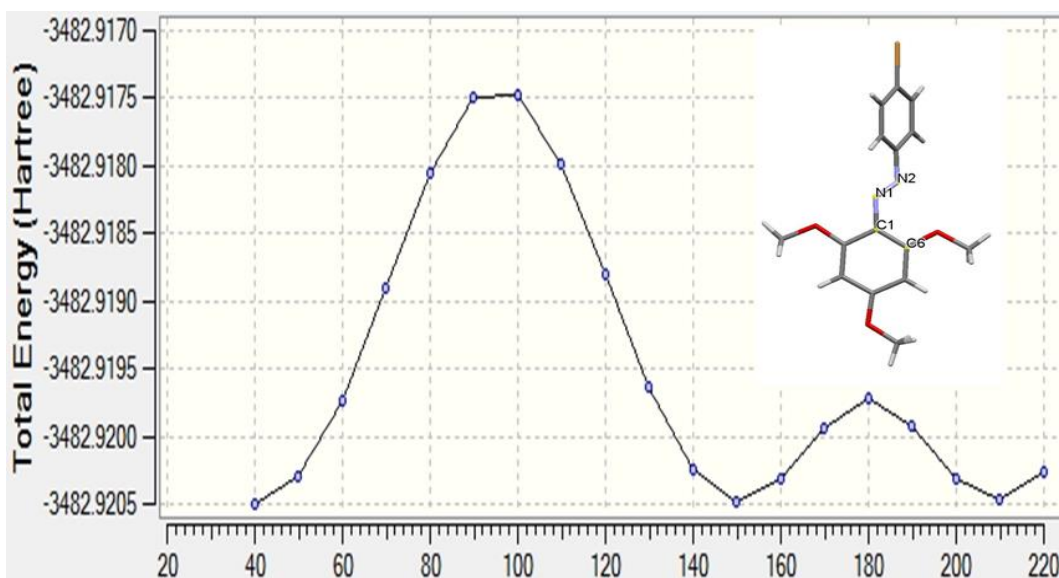


Figure 12. **4b** energy vs C6-C1-N1-N2 dihedral angle.

Since this work is still in progress it is not possible to clearly elucidate the mechanisms involved in the fluorescence of protonated azo derivatives **3**.

However, on the basis of these preliminary results, we could however formulate some hypotheses on the fluorescence mechanism. As well described in a recent review by Hong *et al.*,^[42] the solid state fluorescence which is usually defined as Aggregation Induced Emission (AIE), can be explained principally by different mechanistic pathways, such as conformational planarization, J-aggregates formation and Restriction of Intermolecular Rotation.

In our case, we observed a conformational planarization for protonated compounds **3**, in agreement with the fluorescence emission observed for **3a-c** and not observed for the unprotonated **4a-c**.

The J-aggregates are usually fluorescent and their formation is characteristic of molecules which possess donor (D) and acceptor (A) functional groups and hence experience D–A or push–pull interactions. The J-aggregates are characterized by antiparallel displacement of the donor and acceptor groups. The X-ray structural analysis of compounds **3a-c** revealed this kind of behavior which could be a reason for their fluorescence.

Finally, the X-ray diffraction analysis in **3b** and **4b** crystals showed a more dense packing state for the first, while the theoretical analyses showed an higher activation energy for the rotation in **3b** respect to **4b**. This could explain an higher fluorescence and a more difficult non-radiative decay of the excited states in compounds **3** because of the restriction of intramolecular rotations, especially in the solid state.

Conclusion

This work lead us to understand the importance of hydrogen bonding interactions which are the main responsible for the isolation of the saline derivatives **3** and their structural properties, also due to inter/intermolecular hydrogen bonds.

All the possible fluorescence mechanistic pathways for our compounds are here only hypothesized, and have to be experimentally confirmed since this work is still in progress. We hope to be able to rationalize these behaviors to enable an easy design of new azo-based fluorescent compounds.

References

- [1] C. Boga, E. Del Vecchio, L. Forlani, *Eur. J. Org. Chem* **2004**, 7, 1567–1571.
- [2] C. Boga, E. Del Vecchio, L. Forlani, S. Tozzi, *J. Org. Chem.*, **2007**, 72 (23), 8741–8747.
- [3] A. Noble, *Justus Liebigs Ann. Chem.*, **1856**, 98, 253–256.
- [4] J. Griffiths, *Chem. Soc. Rev.*, **1972**, 1, 481–493
- [5] H. Wenker, *Ind. Eng. Chem., Anal. Ed.*, **1935**, 7, 40–41.
- [6] D. Escudero, S. Trupp, B. Bussemer, G. J. Mohr and L. Gonzalez, *J. Chem. Theory Comput.*, **2011**, 7, 1062–1072.
- [7] Y.-W. Shi, X.-Q. Liu, P. Shi and X.-Y. Zhang, *Arch. Biochem. Biophys.*, **2010**, 494, 1–6.
- [8] M. E. Long and P. J. Trotter, *Appl. Spectrosc.*, **1981**, 35, 289–292.
- [9] C.-U. Bang, A. Shishido and T. Ikeda, *Macromol. Rapid Commun.*, **2007**, 28, 1040–1044.
- [10] F. Puntoriero, P. Ceroni, V. Balzani, G. Bergamini and F. Voegtle, *J. Am. Chem. Soc.*, **2007**, 129, 10714–10719.

-
- [11] R. M. Parker, J. C. Gates, H. L. Rogers, P. G. R. Smith and M. C. Grossel, *J. Mater. Chem.*, **2010**, 20, 9118–9125.
- [12] V. Ferri, M. Elbing, G. Pace, M. D. Dickey, M. Zharnikov, P. Samori, M. Mayor and M. A. Rampi, *Angew. Chem. Int. Ed.*, **2008**, 47, 3407–3409.
- [13] Y. Wen, W. Yi, L. Meng, M. Feng, G. Jiang, W. Yuan, Y. Zhang, H. Gao, L. Jiang and Y. Song, *J. Phys. Chem. B*, **2005**, 109, 14465–14468.
- [14] K. Kakiage, M. Yamamura, E. Ido, T. Kyomen, M. Unno and M. Hanaya, *Appl. Organomet. Chem.*, **2010**, 25, 98–104.
- [15] M.R. Banghart, A. Mourrot, D. L. Fortin, J. Z. Yao, R.H. Kramer and D. Trauner, *Angew. Chem. Int. Ed.*, **2009**, 48, 9097–9101.
- [16] Y. Kim, J. A. Phillips, H. Liu, H. Kang and W. Tan, *Proc. Natl. Acad. Sci. U. S. A.*, **2009**, 106, 6489–6494.
- [17] J. Wang, H.-B. Liu and C.-S. Ha, *Tetrahedron*, **2009**, 65, 9686–9689.
- [18] M. Banghart, K. Borges, E. Isacoff, D. Trauner and R.H. Kramer, *Nat. Neurosci.*, **2004**, 7, 1381–1386
- [19] Y. Norikane and N. Tamaoki, *Org. Lett.*, **2004**, 6, 2595–2598.
- [20] H. Murakami, A. Kawabuchi, K. Kotoo, M. Kunitake and N. Nakashima, *J. Am. Chem. Soc.*, **1997**, 119, 7605–7606.
- [21] T. Muraoka, K. Kinbara and T. Aida, *Nature*, **2006**, 440, 512–515.
- [22] T. Fujino, S. Yu. Arzhantsev, T. Tahara, *J. Phys. Chem. A*, **2001**, 105, 8123 – 8129.
- [23] M. Nepras̆, S. Lun̆a'k, Jr., R. Hrdina and J. Fabian, *Chem. Phys. Lett.*, **1989**, 159, 366 – 370.
- [24] M. Shimomura and T. Kunitake, *J. Am. Chem. Soc.*, **1987**, 109, 5175 – 5183.
- [25] M. Han and M. Hara, *J. Am. Chem. Soc.*, **2005**, 127, 10951 – 10955.
- [26] M. R. Han and M. Hara, *New J. Chem.*, **2006**, 30, 223 – 227.
- [27] M. Han, D. Ishikawa, E. Muto, *Journal of Luminescence*, **2009**, 129, 1163–1168.
- [28] Y. Wakatsuki, H. Yamazaki, P. A. Grutsch, M. Santhanam and C. Kotal, *J. Am. Chem. Soc.*, **1985**, 107, 8153 – 8159.
- [29] M. Ghedini, D. Pucci, G. Calogero and F. Barigelletti, *Chem. Phys. Lett.*, **1997**, 267, 341 – 344.
- [30] M. Ghedini, D. Pucci, A. Crispini, I. Aiello, F. Barigelletti, A. Gessi and O. Francescangeli, *Appl. Organomet. Chem.*, **1999**, 13, 565 – 581.
- [31] I. Aiello, M. Ghedini and M. La Deda, *J. Lumin.*, **2002**, 96, 249 – 259.
- [32] G. Gabor, Y. Frei, D. Gegiou, M. Kaganowitch and E. Fischer, *Isr. J. Chem.*, 1967, 5, 193 – 212.
- [33] H. Rau, *Ber. Bunsenges. Phys. Chem.*, **1968**, 72, 637 – 643.
- [34] H. Rau, *Ber. Bunsenges. Phys. Chem.*, **1967**, 71, 48 – 53.

- [35] J. Yoshino, N. Kano, T. Kawashima, *Chemical communications (Cambridge, England)* **2007**, 559–61.
- [36] J. Yoshino, A. Furuta, T. Kambe, H. Itoi, N. Kano, T. Kawashima, Y. Ito, M. Asashima, *Chemistry (Weinheim an der Bergstrasse, Germany)* **2010**, *16*, 5026–35.
- [37] N. Kano, A. Furuta, T. Kambe, J. Yoshino, Y. Shibata, T. Kawashima, N. Mizorogi, S. Nagase, *European Journal of Inorganic Chemistry*, **2012**, 1584–1587.]
- [38] H. Rau, *Angew. Chem. Int. Ed.* **1973**, *12*, 224–235.
- [39] C. Møller, M.S. Plesset, *Phys. Rev.* 1934, *46*, 618.
- [40] J. Tomasi, B. Mennucci, and R. Cammi, *Chem. Rev.*, **105** (2005) 2999–3093.
- [41] Gaussian 09, Revision B.01, Frisch, M. J.; Trucks, G. W.; Schlegel, H. B.; Scuseria, G. E.; Robb, M. A.; Cheeseman, J. R.; Scalmani, G.; Barone, V.; Mennucci, B.; Petersson, G. A.; Nakatsuji, H.; Caricato, M.; Li, X.; Hratchian, H. P.; Izmaylov, A. F.; Bloino, J.; Zheng, G.; Sonnenberg, J. L.; Hada, M.; Ehara, M.; Toyota, K.; Fukuda, R.; Hasegawa, J.; Ishida, M.; Nakajima, T.; Honda, Y.; Kitao, O.; Nakai, H.; Vreven, T.; Montgomery, Jr., J. A.; Peralta, J. E.; Ogliaro, F.; Bearpark, M.; Heyd, J. J.; Brothers, E.; Kudin, K. N.; Staroverov, V. N.; Kobayashi, R.; Normand, J.; Raghavachari, K.; Rendell, A.; Burant, J. C.; Iyengar, S. S.; Tomasi, J.; Cossi, M.; Rega, N.; Millam, J. M.; Klene, M.; Knox, J. E.; Cross, J. B.; Bakken, V.; Adamo, C.; Jaramillo, J.; Gomperts, R.; Stratmann, R. E.; Yazyev, O.; Austin, A. J.; Cammi, R.; Pomelli, C.; Ochterski, J. W.; Martin, R. L.; Morokuma, K.; Zakrzewski, V. G.; Voth, G. A.; Salvador, P.; Dannenberg, J. J.; Dapprich, S.; Daniels, A. D.; Farkas, Ö.; Foresman, J. B.; Ortiz, J. V.; Cioslowski, J.; Fox, D. J. Gaussian, Inc., Wallingford CT, 2009.
- [42] Y. Hong, W. Y. Lam, B. Zhong, *Chem. Comm.*, **2009**, 4332–4353.

Chapter 5

Multiple applications for a new class of azobenzene derivatives

The chemical properties of 1,3-thiazole derivatives are of great interest because of the unusual behavior of these pentatomic heterocycles (Figure 1).

The presence of a sulphur atom in pentatomic ring lead to an electron-rich system (similar to thiophene). On the contrary, the nitrogen atom acts as an electron-withdrawing group. In the case of thiazole, the presence of both sulphur and nitrogen atom lead to a system for which the net character of electrophile or nucleophile is not well defined.^[1]

By adding one amino-group in the position 2, the system becomes strongly nucleophilic (Figure 1).

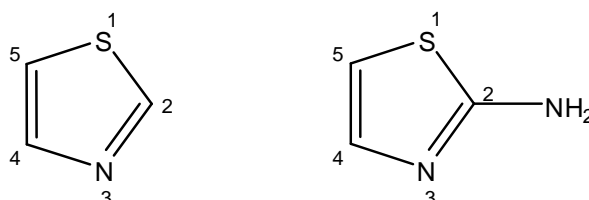


Figure 1. Structures of 1,3-thiazole and 2-amino-1,3-thiazole (left and right respectively).

2-amino-1,3-thiazole derivatives are important building blocks for many drugs, for example for treating hyperthyroidism and for their antibacterial activity.

The endocyclic nitrogen is a basic centre and the addition of an amino group in the 2 position enhances the basicity of the molecule.^[1]

An interesting feature comes from the possibility of 2-aminothiazole to react with two different tautomeric forms (Figure 2).

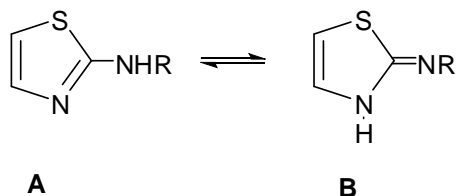


Figure 2. Tautomeric forms in 2-aminothiazole derivatives.

The tautomeric form **A** is the most stable, while form **B** prevails when an electron-withdrawing group is bonded to the exocyclic nitrogen.^[2,3]

The 2-amino-1,3-thiazole derivatives show another interesting feature: they can act as tridentate nucleophiles as shown in Figure 3.

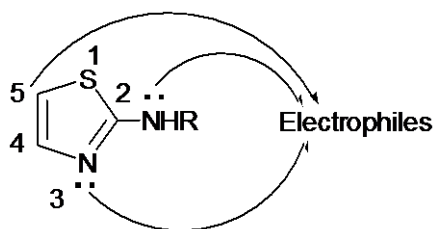
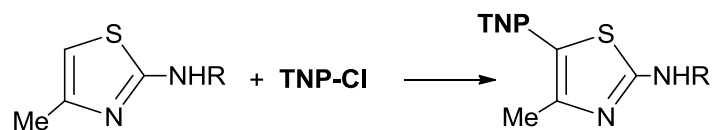
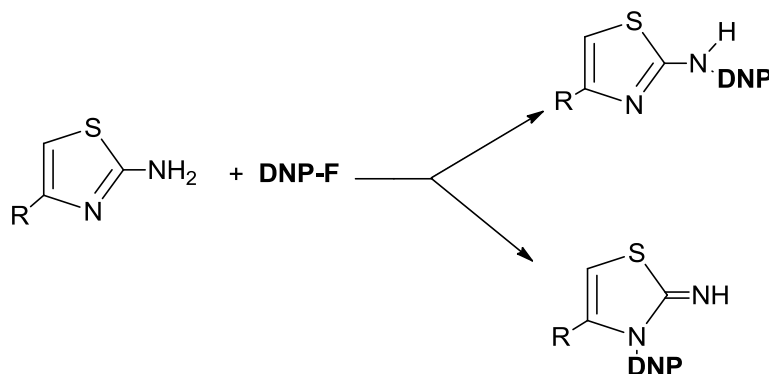


Figure 3. Nucleophilic centers in 2-aminothiazole derivatives.

The regioselectivity of the attack depends on the electrophile. For example in the reaction with picryl chloride the attack occurs in the 5 position,^[4] while the reaction with 2,4-dinitro-fluorobenzene lead to the formation of adducts on both the exo and endocyclic nitrogen^[5] (Scheme 1).



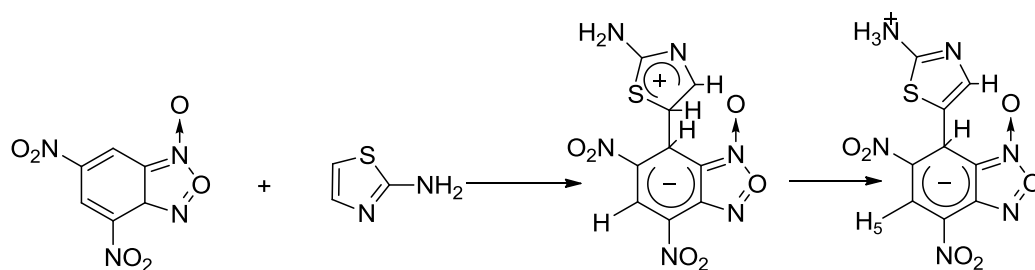
R = phenyl **TNP-Cl** = 2-chloro-1,3,5-trinitrobenzene



R = H, Me; **DNP-F** = 1-fluoro-2,4-dinitrobenzene

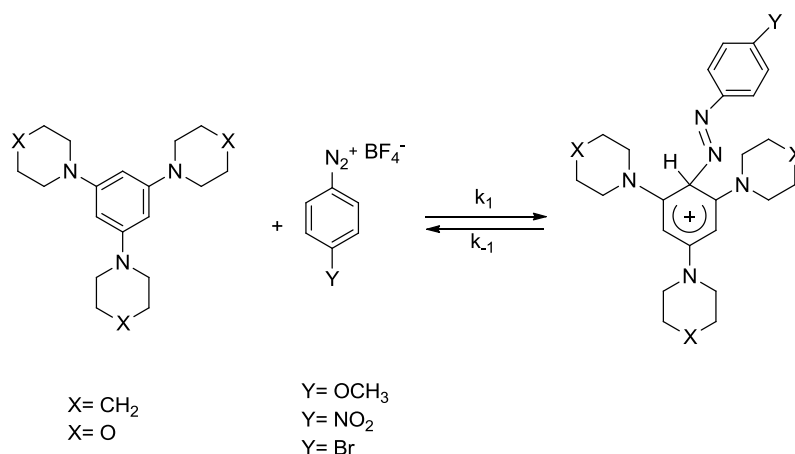
Scheme 1. Reactivity of different 2-aminothiazole derivatives.

Some of these peculiar behaviors of 2-aminothiazole derivatives were studied from a long time in my research group. Recently it has been possible to isolate a Wheland-Meisenheimer complex in the reaction between 2-aminothiazole and 2,4-dinitrobenzofuroxane (**DNBF**) by using NMR spectroscopy (Scheme 2).^[6]



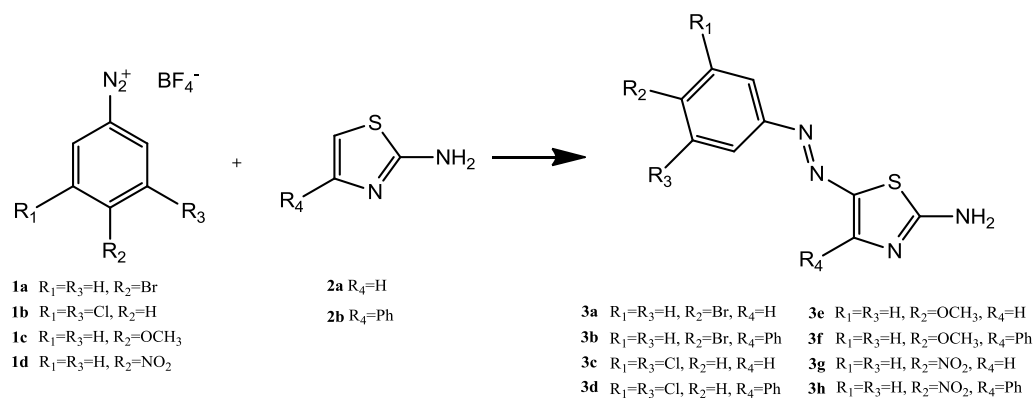
Scheme 2. Formation of the WM complex in the reaction between 2-aminothiazole and DNBF.

Since previous studies with tris(dialkylamino)benzenes as nucleophile and diazonium salts allowed the isolation of Wheland intermediates (Scheme 3),^[7,8] with the aforementioned behavior of 2-aminothiazole in mind, we decided to test its reactivity toward diazonium salts.



Scheme 3. Formation of the Wheland complex in the reaction between tris(dialkylamino)benzenes and diazonium salts.

Even though the reactions (showed in Scheme 4) were carried out at low temperature and followed by NMR spectroscopy, we were not able to identify the intermediates of these reactions. However, we discovered, sometimes accidentally, interesting feature of the related substitution products. In this chapter all these properties are reported, focusing the attention on the careful observation that makes possible to discover the multiple applications of these new compounds.



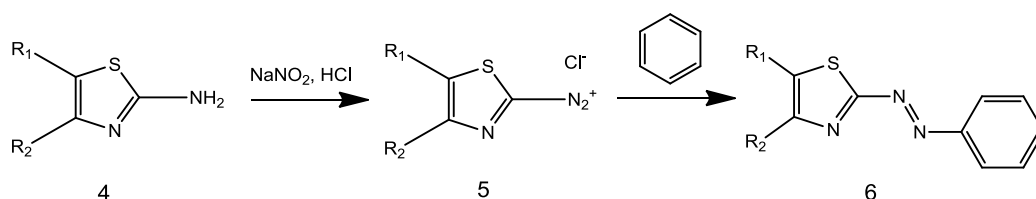
Scheme 4. Reaction between 2-aminothiazole derivatives and different diazonium salts.

5.1 The textile-dyeing property

Azo-based compounds are well known for their intense color and thanks to this property they were used for a long time in the dye industry.

During our literature research on the thiazole derivatives containing the azo moiety, we discovered that the diazotization reactions on 2-aminothiazole and the subsequent coupling with aromatic compounds, lead to the formation of strongly colored compounds which are used in the textile dyeing industry.^[1]

The difference between these azo-derivatives and **2a-h** is the position of the azo moiety. Comparing the two structures (products **3** in Scheme 4 and 5) it is easy to observe that in our case the product **3** contains a free amino functionality that could improve the anchoring to the fibers by enhancing the electrostatic interactions that are responsible of their adsorption.



Scheme 5. Diazotization of 2-aminothiazole and subsequent coupling with aromatic compounds (here generalized as benzene).

The low solubility in water of these compounds suggested us to apply them as disperse dyes.

Disperse dyes are compounds insoluble in water but “soluble” in the fibers. The fiber is soaked in a suspension of the finely ground dye in water, so the dye can migrate inside the fiber where it becomes adsorbed. Usually a dyeing temperature of 130 °C is required and a pressurized dyebath is used. The very small particle size gives a large surface area and favours the dissolution to allow uptake by the fiber. Disperse dyes are usually used to dye cellulose acetate, nylon, triacetate, polyester and acrylic fibers.

In spite of this, we preferred to try the first dyeing test on the most easily available fibers, such as pure cotton and wool, and to use very mild dyeing conditions (20-60°C, atmospheric pressure).

Our preliminary dyeing test was made using only four of all the products we obtained (**3e-h**).

We first added 500 mg of the dye to 25 mL water and made it very finely grinded by using an ultrasounds generator.

Subsequently, we added 2 wires of cotton or wool of about 15 cm in length to this suspension, continuously stirring the mixture at room temperature (Figure 4, on the left). After about 20 minutes the solution appeared to be more clear and the fibers became coloured (Figure 4, on the right).

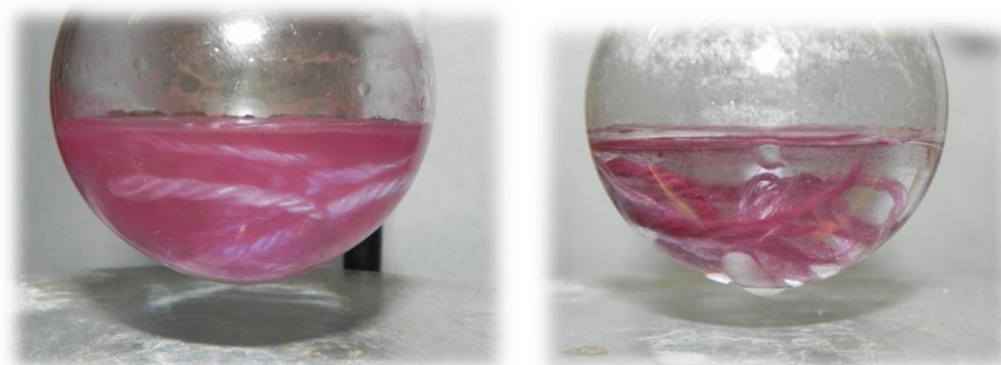


Figure 4. The fiber just added to the stirred solution (left) and after 20 minutes (right).

The wires were then pulled out from the solution and abundantly rinsed with fresh water; after this the dye seemed to be very well anchored to both fibers.

We were surprised from this unexpected result; in fact, as just discussed previously, disperse dyes are good only for dyeing synthetic fibers, but in this case this is not truth.

It is also noteworthy that usually the compounds that well colour the cotton, are not good for wool, and *vice-versa*; on the contrary, our tested products can dye both wool and cotton.

The results, as can be seen in Figure 5, are very good. Just changing the concentration of the dye, we are able to obtain many different colour shades.



Figure 5. The fiber of wool (top) and cotton (bottom) coloured with compounds 3e-h.

The colour of the cotton fibers results to be a little more light with respect to that of wool, but with a better brightness. The better way to achieve a more intense fiber colour is to add to the solution a little amount of NaCl that, enhancing the ionic strength of the solution, help the dye transfer into the fibers. In our test, the temperature rising (60 °C) give the same results only for cotton.

This new dyes are very promising. Their simple preparation (short reaction times, mild conditions, facile recovery, high yields) and their interesting dyeing features (good color brightness, mild dyeing conditions, application to different fibers) can be attractive for a future developments and industrial production.

Obviously, more accurate tests must be done such as washfastness, lighfastness and specific allergenic tests.

5.2 The pH indicator property

Some of the most known pH indicators are based on azo-derivatives. However, we discovered this property on our compounds accidentally, just by washing with a KOH solution a flask containing traces of compounds **3h**; we observed a change in colour from red to blue.

Then we tested the change in colour of all compounds **3a-h** at different pH values (1, 7 and 13).

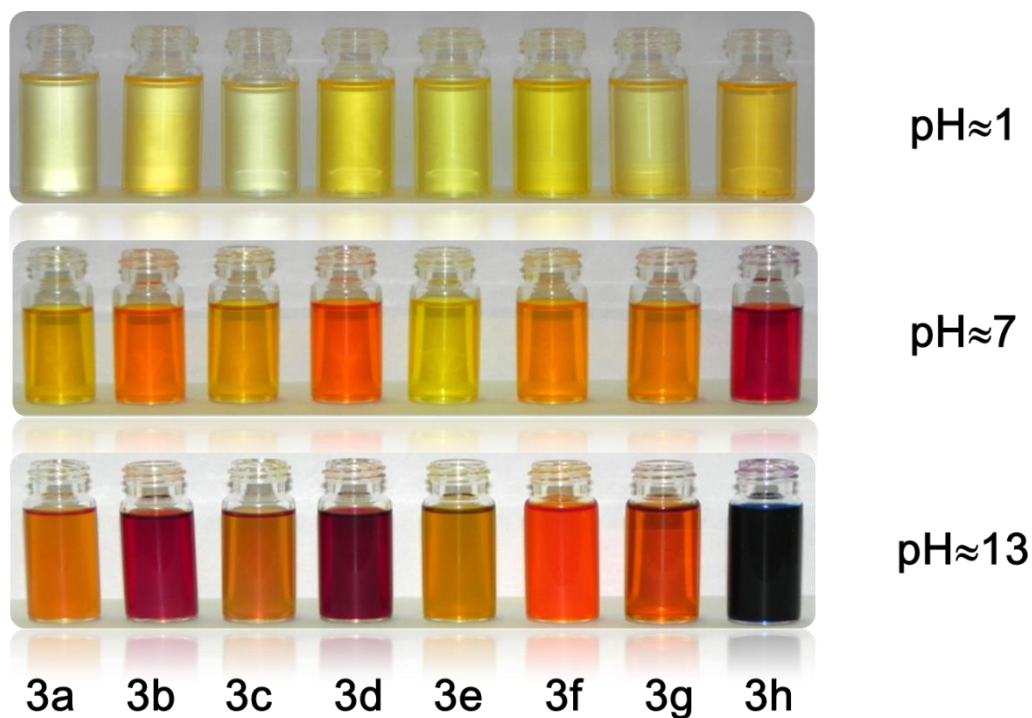


Figure 6. Compounds 3a-h at different pH.

As shown in Figure 6 the most intense variation of colour occurs for compounds **3b**, **3d** and **3h**. The common feature for these compounds is the presence of a phenyl substituent on the 4 position of the thiazole ring moiety, which probably influence the conjugation of the system.

However, the most striking feature is the change in colour at basic pH: in fact, there are not strong acidic protons in these molecules. By using NMR and mass spectroscopy techniques we discovered that a mild base such as cesium carbonate is able to remove the N-H proton on the 2-aminothiazole moiety, modifying the conjugation of the system and allowing the colour change.

5.3 Formation of fluorescent nanoparticles

An interesting feature involving one of these compounds comes from the observation of the solid that is formed by evaporating different solvents (acetone, acetonitrile, THF) from a solution of **3h**. As depicted in Figure 7, we observed the formation of green microcrystals with opalescent behaviour. In fact the solution of **3h** in all the solvents above mentioned appeared to be red coloured, while in the solid state a brilliant green colour was observed; another interesting feature is that the colour of this solid turns into red under intense light. This behaviour was better seen when the solid was analysed by optical microscope (see Figure 7), which showed the green/red change in colour and let us size these microwires, which are about 40 μm in diameter.

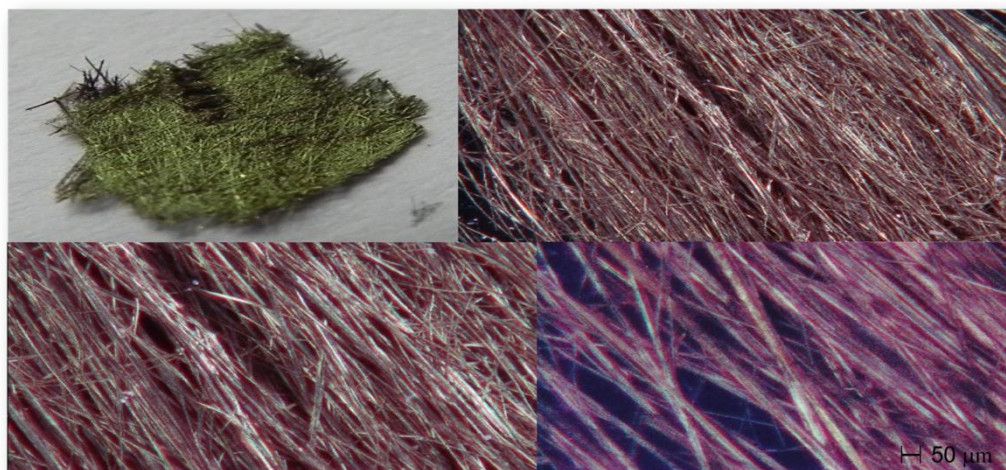


Figure 7. Formation of 3e microwires by simple solvent evaporation.

To better investigate the structural properties of these microaggregates we tried to crystallize them by using different techniques.

The most unexpected results occur by using the solvent/non solvent technique. In fact, after addition of some drops of water to a tetrahydrofuran solution of **3h**, the solution became cloudy and showed an intense green fluorescence under ambient light.

We discovered that the fluorescence is given by the formation of nanoparticles (since in solution there is no emission). By utilizing with compounds **3a-h** this techniques, usually called reprecipitation method, we observed for all the formation of fluorescent nanoparticles (Figure 8). Then we decided to start a deeper investigation on this behaviour, since fluorescent organic nanoparticles find application in optoelectronic^[9,10,11] and bioimaging.^[12]

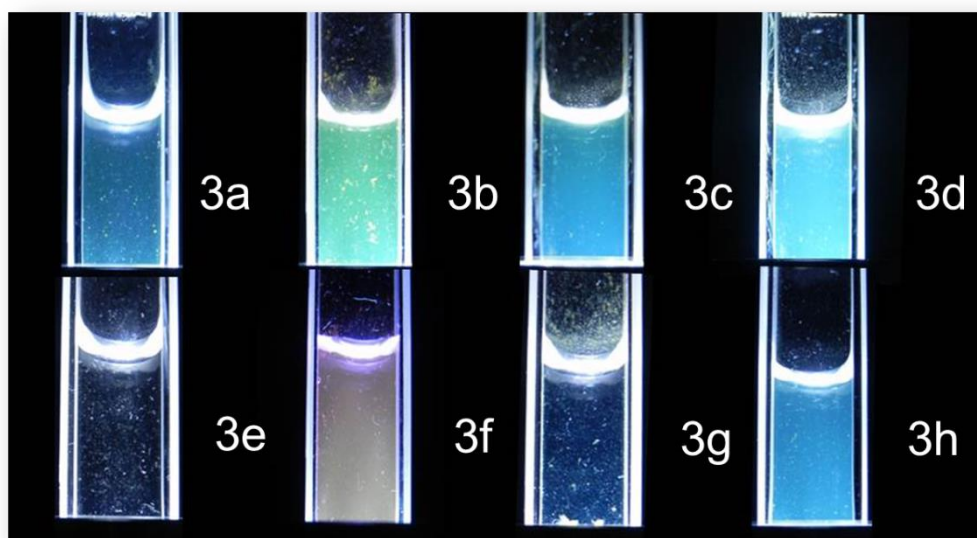


Figure 8. Fluorescent organic nanoparticle of compounds 3a-h.

5.3.1 Preparation of fluorescent nanoparticles

The common way to prepare organic nanoparticles is called “reprecipitation method”.^[13,14] A concentrated solution of the sample in an organic solvent is rapidly injected into a vigorously stirred large amount of water in which solvent is fully miscible. The abrupt modification of the medium induces the agglomeration of the compound which can form nano/micro-sized crystals or aggregates. In our case we added 40 μL of a 2.0×10^{-3} M solution of compounds **3** in THF to 1.96 mL of water, obtaining a nominal final concentration of 2.0×10^{-5} M. For all compounds **3**, just after mixing, the suspension become progressively cloudy,

showing a blue to green fluorescence simply under sunlight. The aggregation's evolution was monitored by using UV-Visible spectroscopy

The sample were then analysed by Dynamic Light Scattering and fluorescence spectroscopy.

Because this work is still in progress and for the sake of clarity, here we present the analyses carried out on compound **3b**, which is at this moment the well characterized.

5.3.2 UV-Visible analyses

The UV-Visible analyses is an useful tool to monitor the evolution process of the nanoparticle formation.

For a comparison we reported the UV-Vis spectrum of compound **3b** in THF at the same nominal concentration of the nanoparticles' solution (2.0×10^{-5} M).

As shown in Figure 9, just after mixing the solution, there is a bathochromic shift of the absorption maximum from 465 nm to 473nm. With time the absorption maximum progressively shifts toward the red region and its intensity decrease. However the change with time in is not pronounced but becomes important after some days: this means that the particles tend to continue the aggregation process, which is anyway slow.

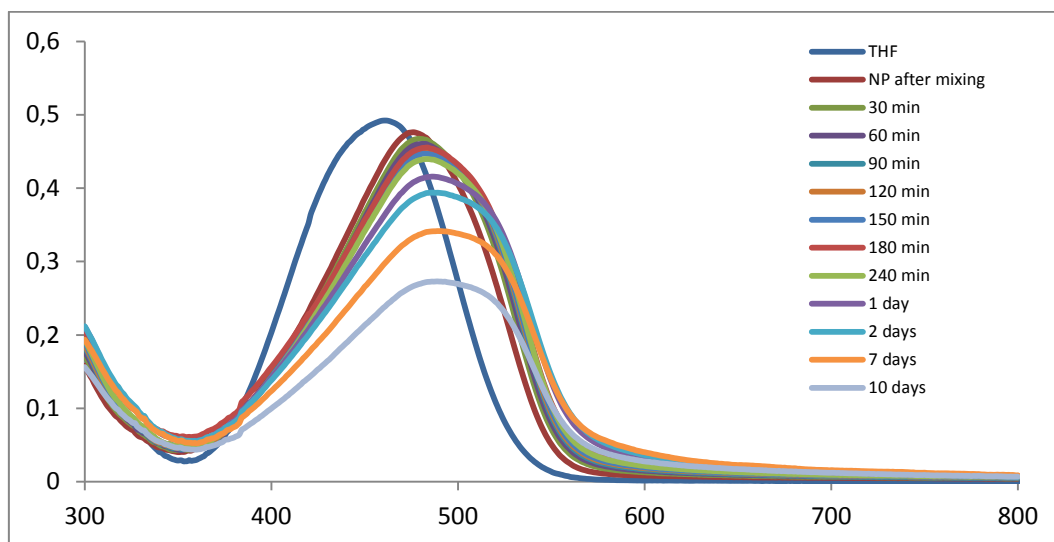


Figure 9. Evolution of the UV-Vis absorption spectrum during the reprecipitation process of compound **3b**.

5.3.3 Size measurement

Among the methods for determination of the nanoparticles' size, Dynamic Light Scattering (**DLS**) is one of the most used. When light hit small particles, the light is scattered in all directions. The time-dependent fluctuations of the scattering intensity, elaborated by using appropriate equations, give as result the dimension of the particles.

In Figure 10 is shown the result of the **DLS** measurement of **3b** nanoparticles after 1 hour from their preparation.

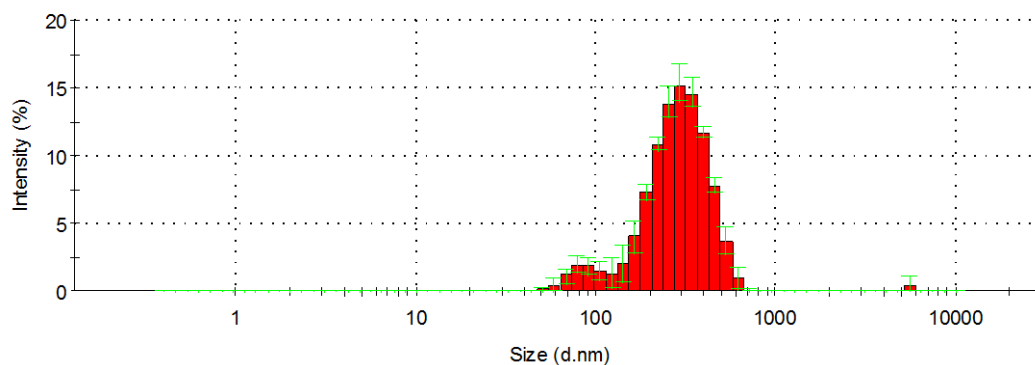


Figure 10. DLS result of the size distribution for **3b** nanoparticles.

The mean size (diameter) of the particles is about 314 ± 14 nm with a good distribution, also if the entire mixture is mainly formed by particles of about 54 and 300 nm as depicted in Figure 10.

To confirm these data and obtain most accurate results, we planned, in the future, to analyze our particles by using also microscopy techniques such as SEM or TEM.

5.3.4 Fluorescence analyses

The fluorescence analyses of **3b** nanoparticles showed interesting results.

In Figure 11 emission and excitation fluorescence spectra for **3b** in THF solution, solid state and nanoparticles water dispersed are reported.

As in the case of UV-Visible analyses, for a better comparison we recorded the spectra of **3b** in THF solution and the aqueous nanoparticles (1 hour after their preparation) at the same nominal concentration (2.0×10^{-5} M) using the same instrumental parameters (excitation wavelength = 467 nm; emission wavelength = 610 nm; emission and excitation slit = 2 nm). We decided also to compare the nanoparticles emission with the one in solid state.

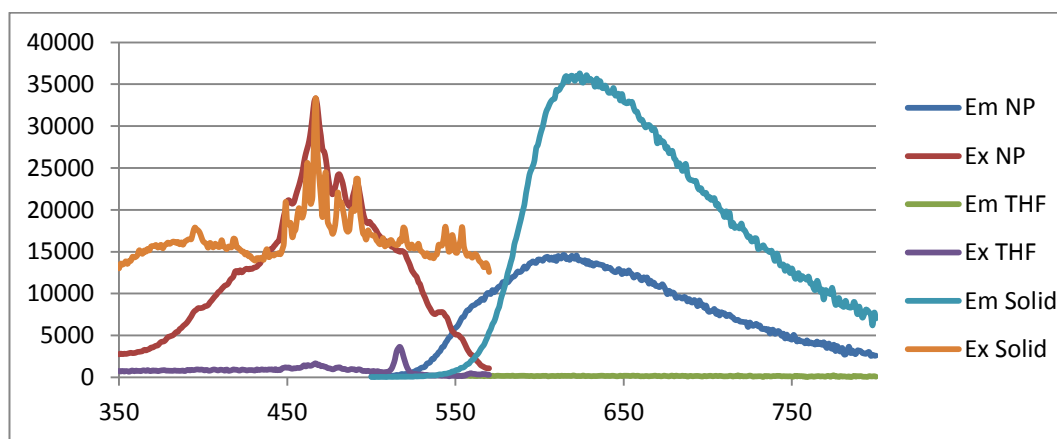


Figure 11. Emission and excitation fluorescence spectra for 3b in THF solution, solid state and nanoparticles water dispersed.

As depicted in Figure 11 one can see that **3b** in THF solution (green line) practically do not show fluorescence emission, while the nanoparticles fluorescence is 58 fold higher than THF solution.

The solid state emission maximum is 10 nm red shifted respect to that of the nanoparticles which is slightly broader but with the emission covering also the green region.

Conclusion

This work, which is still in progress, shows how many applications can be found for a simple class of compounds.

Probably, the most interesting feature is the fluorescent nanoparticles formation, not only for the possible applications in various field of materials chemistry, but also because it opens a new research field for azo-derivatives, which are usually considered not fluorescent. This study is still in progress and a more accurate characterization with other techniques such as SEM and TEM to evaluate the shape of the particles, powder X-ray diffraction analyses to understand if the aggregates are crystalline or amorphous are necessary. Finally, it could be interesting to test the nanoparticles for the use as probes in bioimaging.

Some of the properties here described were discovered serendipitously, but a careful observation and a basic knowledge in different field of chemistry were also important. This means that sometimes we have to not look only at the goal of our research, but it is also important understand the potential behaviours of the substances we work with.

References

- [1] Jacques V. Metzger, *Thiazole And Its Derivatives, Part Two*, **1979**.
- [2] L. Forlani, in *Targets in Heterocyclic Systems*, O. A. Attanasi and D. Spinelli Eds., Italian Society of Chemistry, Roma, 1, **1997**, 75.
- [3] L. Forlani, G. Breviglieri, P. De Maria, *J. Chem. Soc. Perkin Transaction 2*, **1979**, 163-165

- [4] L. Forlani, L. P. Battaglia, A. Bonamartini Corradi and P. Sgarabotto, *J. Cryst. and Spectrosc. Res.*, **1992**, 22, 705.
- [5] L. Forlani, P. De Maria, E. Foresti, and G. Pradella, *J. Org. Chem.*, **1981**, 46, 1156.
- [6] C. Boga, E. Del Vecchio, L. Forlani, R. Goumont, F. Terrier, S. Tozzi, *Chemistry. A Eur. J.* **2007**, 13, 9600–9607.
- [7] C. Boga, E. Del Vecchio, L. Forlani and S. Tozzi, *J. Org. Chem.*, **2007**, 72, 8741-8747.
- [8] C. Boga, E. Del Vecchio, L. Forlani, *Eur. J. Org. Chem.*, **2004**, 1567-1571.
- [9] Hagfeldt, A.; Grätzel, M. *Chem. Rev.* **1995**, 95, 49-68.
- [10] Schlamp, M. C.; Peng, X.; Alivisatos, A. P. *J. Appl. Phys.* **1997**, 82, 5837-5842.
- [11] (a) Wohltjen, H.; Snow, A. W. *Anal. Chem.* **1998**, 70, 2856-2859. (b) Shipway, A. N.; Katz, E.; Willner, I. *ChemPhysChem* **2000**, 1, 18-52.
- [12] (a) Bruchez, M.; Moronne, M.; Gin, P.; Weiss, S.; Alivisatos, A. P. *Science* **1998**, 2013-2016. (b) Michalet, X.; Pinaud, F.; Lacoste, T. D.; Dahan, M.; Bruchez, M. P.; Alivisatos, A. P.; Weiss, S. *Single Mol.* **2001**, 2, 261-276.
- [13] H. Kasai, H. S. Nalwa, H. Oikawa, S. Okada, H. Matsuda, N. Minami, A. Kakuda, K. Ono, A. Mukoh, H. Nakanishi, *Jpn. J. Appl. Phys.* **1992**, 31, 1132.
- [14] H. Nakanishi, H. Oikawa, *Single Organic Nanoparticles* (Eds: H. Masuhara, H. Nakanishi, K. Sasaki), Springer, Berlin, **2003**, Ch.2, p. 17.

Chapter 6

Phospha Michael-type reaction of bidentate nucleophile

The Michael addition is one of the most useful methods in synthetic organic chemistry for the formation of C–C bonds.^[1] However, the importance of this conjugate addition in organic synthesis is not limited to the formation of C–C bonds. In fact, a wide number of variants both in the nucleophilic part and in the electrophilic one permits to obtain a series of carbon-heteroatom bonds, as carbon-sulfur, carbon-nitrogen, carbon-oxygen, or carbon-phosphorus through the so-called sulfa-,^[2] aza-,^[3] oxa-,^[4] or phospha-^[5] Michael reaction, respectively. This latter is one of the most important tools for the formation of the P–C bond, one bond of great interest in synthetical, applied, and biological chemistry.

Among the non-classical Michael electrophilic partners, 1,2-diaza-1,3-dienes (DDs) represent a class of compounds with a good reactivity as Michael acceptors owing to the electron-withdrawing effect of the azo group in the heterodiene system.^[6,7]

The regioselective nucleophilic attack at the terminal carbon atom in the 4-position of the heterodiene system of DDs occurs with a variety of carbon- and hetero-nucleophiles such as oxygen, nitrogen-, sulfur-, selenium- and phosphorus nucleophiles giving the corresponding hydrazones.^[6] Previously, the phospha Michael reaction on DDs has been studied using triphenylphosphine,^[8] trialkylphosphines,^[9] trialkyl phosphites,^[10] dialkylphenylphosphonites,^[11] phosphoramidites, phosphorodiamidites, and tris(dimethylamino)phosphines.^[12]

All these reactions occur under very mild conditions and involve, as key step, the spontaneous formation of ylidic intermediates. The good results obtained suggested us to explore the reactivity of DDs also with diphosphine derivatives in

order to obtain diylides, a class of compounds useful in various fields of chemistry^[13,14] but, to the best of our knowledge, rarely reported so far.

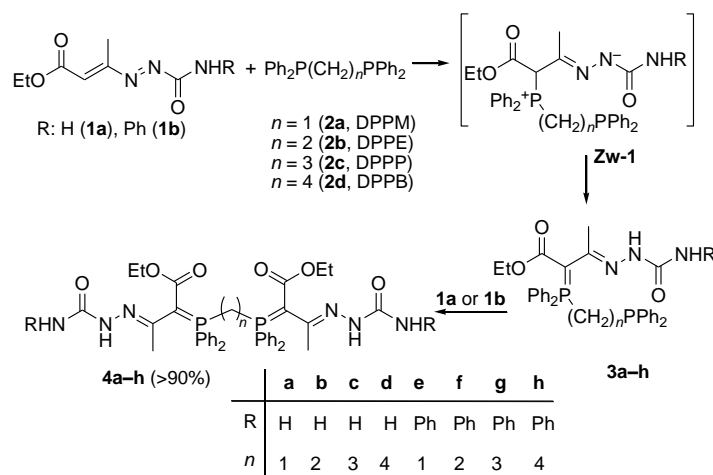
In particular, we have investigated the reaction in neutral conditions between a series of methylene-bridged diphosphines and DDs and the obtained results showed the efficiency of our approach as a route to a new class of symmetrical diylidic compounds. In addition, we extended the investigation using methylene-bridged phosphinoamine derivatives with the same DDs.

6.1 Brief summary of used reagents

The reactivity of DDs **1a,b** was studied towards bis(diphenyl)phosphines, namely bis(diphenylphosphino) methane (DPPM, **2a**), bis(diphenylphosphino) ethane (DPPE, **2b**), bis(diphenylphosphino)propane (DPPP, **2c**) and bis(diphenylphosphino)butane (DPPB, **2d**) (Scheme 1), and diphenylphosphino amines such as 2-(diphenylphosphino)ethanamine (**5a**) and 3-(diphenylphosphino) propan-1-amine (**5b**) (Scheme 3). The related results have been separately discussed in the following sub-headings.

6.2 Reactions between 1,2-diaza-1,3-dienes (DDs) and bis(diphenyl) phosphines

The reactions between DDs **1a,b** and bis(diphenyl)phosphines **2a-d** (Scheme 1) were carried out at room temperature in ethyl acetate or in chloroform; the disappearance of the typical red colour of the starting DD indicated the completion of the reaction which was monitored also through ¹H and ³¹P NMR spectroscopy.



Scheme 1. Reaction between DDs **1a** and **1b** and bis(diphenyl)phosphines **2a–d**.

The reactions were carried out in different relative molar ratio of the reagents, and the results treated separately.

6.2.1 Reactions carried out with equimolar amount of DDs and diphosphines

The reaction between equimolar amount of compound **1a** and DPPM (**2a**) in ethyl acetate gave, after a few minutes, formation of a white solid. After filtration, this solid was analyzed and resulted to be pure compound **3a**, recovered in about 50% yield. When **1b** was reacted with **2a** in ethyl acetate, no solid was formed. In both cases, a mixture of starting reagent **2a**, of monoyleide (**3a** or **3e**) and diylide (**4a** or **4e**) was found in the solution. The reactions of DDs **1a** and **1b** with **2a** were carried out also in CDCl_3 directly in the NMR spectroscopy tube and monitored through ^1H and ^{31}P NMR spectroscopy: in these cases, no precipitate was formed and the corresponding mono-adducts **3a,e** were formed in nearly quantitative yield.

From the reactions between equimolar amount of **1a,b** and the diphosphines **2b–d** in ethyl acetate, a white solid precipitated but in these cases the spectral data agreed with the structure of the corresponding diadduct **4**. When the reactions between DDs **1a,b** and phosphines **2b–d** were carried out in deuteriochloroform, no precipitate was formed and monoyleides **3b–d** and **3f–h**

were obtained in higher yield, even if in mixture with the corresponding diadducts **4**.

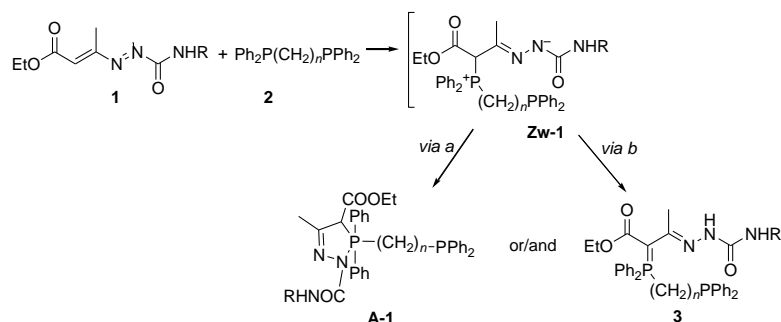
These data indicate that the solubility in ethyl acetate of **3a** is lower than that of all others mono-ylides, being it, in the same experimental conditions, the sole mono-adduct recovered by precipitation from the reaction mixture. On the other hand, the poor solubility in ethyl acetate showed by diadducts **4b–h** (see below) causes their precipitation from the solution thus increasing the conversion to the bis-adduct. Attempts to isolate derivatives **3b–h** by column chromatography from reactions carried out in chloroform failed and for this reason **3b–h** have been characterized by ^1H and ^{31}P NMR carrying out the reaction directly in NMR spectroscopy tube.

6.2.2 Reactions carried out with DDs and diphosphines in a 2/1 relative molar ratio

The reaction between **1a,b** and **2a–d** in 2:1 relative molar ratio in ethyl acetate gave, after about 15 min, compounds **4a–h** in almost quantitative yield and their low solubility permitted to obtain them from the reaction mixture by filtration. Products **4a–d** were recovered by filtration in almost double yield with respect to **4e–h**, and this suggests that the presence of the NPh end group of the DDs moiety increases the solubility of these diylides. Compound **4a** was obtained also by addition of DD **1a** to an equimolar amount of pure **3a**, obtained as described in the above section.

The ylidic structure of Michael-like mono- and bis-adducts is supported by their IR, ^1H , ^{13}C , ^{31}P NMR and mass spectral data. Below are reported some remarks from both the structural and mechanistic point of view.

Probably, zwitterionic forms as **Zw-1** (Scheme 1) are firstly formed by phospho-Michael addition of one phosphorus atom of **2** on one molecule of DD. To gain information on the involved intermediates, we carried out the reaction between equimolar amount of **1a** and **3a** directly in the NMR spectroscopy tube in CD_2Cl_2 at $-70\text{ }^\circ\text{C}$ but in our experimental conditions no evidence of species **Zw-1** have been obtained.



Scheme 2. Simplified possible reaction pathways for the first attack of diphosphanes to DDs.

Probably, the intermediate **Zw-1** is immediately converted into more stable neutral structures. In principle, from **Zw-1** two different can be obtained (Scheme 2): **A-1**, derived from an internal nucleophilic attack of the nitrogen on the phosphorus of phosphonium salt through the pathway *a*, and **3** derived from an 1,4-hydrogen shift (*via b*) favoured by the great acidity of the hydrogen atom bound to the carbon in α -position both to the phosphorus and to the ester group.

A-1 is a cyclic pentacoordinated phosphorus species, more stable than an acyclic one of about 10^6 fold,^[15] but the absence, in the ^1H NMR spectrum, also when recorded at $-70\text{ }^\circ\text{C}$, of the signal belonging to the proton in α position to the carboxy group, together with ^{31}P NMR chemical shifts of the reaction products (that fall far from the range typical of pentacoordinate phosphorus species^[16]) permitted to exclude **A-1** in favour of the ylidic structure **3**. In particular, ^{31}P NMR spectrum of compound **3a** shows, in CDCl_3 at $25\text{ }^\circ\text{C}$, a couple of doublets at $\delta=19.8\text{ ppm}$ ($J_{\text{PP}}=61.8\text{ Hz}$) and $\delta=-27.3\text{ ppm}$ ($J_{\text{PP}}=61.8\text{ Hz}$), indicative of a $\text{P}_{\text{IV}}\text{CP}_{\text{III}}$ sequence (the first signal belongs to a tetracoordinate phosphorus atom while the second one is due to a tricoordinated phosphorus atom, with a δ value very close to that of starting phosphine **2a**). In the case of formation of an **A-1**-like species, ^{31}P NMR signal of the corresponding pentacoordinate phosphorus atom should be expected at negative δ values.

Analogous considerations can be made about the diadducts obtained between diphosphines **2a-d** and two molecules of DD. Also in these cases, many

intermediates might be expected. However, the presence of a single signal in the ^{31}P NMR spectrum (δ values around +20 ppm in CDCl_3 at 25 °C) indicates the presence of the bis-ylide **4**, confirmed also by ^1H and ^{13}C NMR. Consequently, intermediates **Zw**-like are probably very short life-time species.

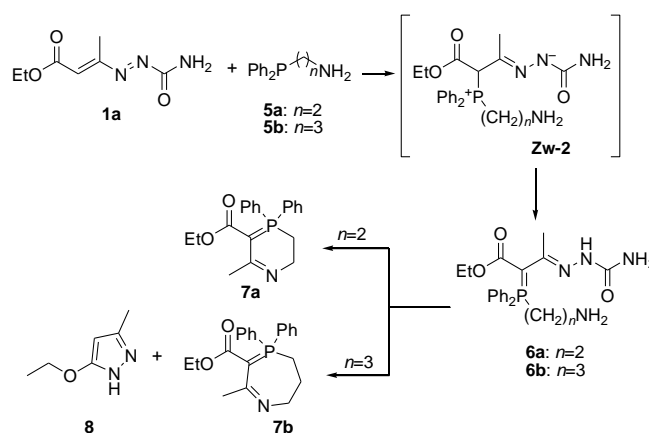
Finally, during the NMR monitoring of the reaction decourse between **1a** and **2a** in CD_2Cl_2 in variable temperature NMR conditions we observed, at -70 °C, a little amount of **2a** ($\delta_{\text{P}} = -23.5$ ppm) and two couple of doublets, at +22.8 and -28.8 ppm ($J_{\text{P-P}} \sim 62$ Hz) and +20.3 and -27.4 ppm ($J_{\text{P-P}} \sim 61$ Hz) indicating the presence of two species. The corresponding ^1H NMR spectrum recorded at the same temperature confirmed the presence of two compounds in 65/35 relative ratio. On raising the temperature, both ^{31}P and ^1H NMR spectra do not changed until -50 °C. Above -50 °C the signals showed line broadening and the coalescence was reached at -35 °C. A further increase of the temperature caused a gradual sharpening of the signals until a final averaged situation, which spectra agreed with those of product **3a**. The dynamic process is reversible and, based on the Eyring equation,^[17] the data permitted to calculate an activation energy of the process of $\Delta G^\ddagger = (11.2 \pm 0.2)$ Kcal mol $^{-1}$ a value in agreement^[18] with that of a rotational constraint due, in this case, to the bulky groups present on compound **3a** that make the molecule quite rigid.

6.3 Reactions between 1,2-diaza-1,3-dienes 1a,b and diphenylphosphino amines 5a,b

Since it is known that DDs react with amines to give aza-Michael-like addition,^[23] from the reaction between phosphoamino derivatives **5a,b** and 1,2-diaza-1,3-diene **1a** (Scheme 3) beside the phospho-, also an aza-Michael-like addition might occur or even a tandem phospho-aza Michael^[24] double addition.

When the reactions between equimolar amount of **1a** and **5a,b** were carried out at room temperature in ethyl acetate (or in chloroform), the only products obtained were compounds **6a,b** (Scheme 3), whose structure was ascertained by ^1H , ^{13}C , ^{31}P and g-HSQC NMR analyses. Compound **6a**, kept in

CDCl₃ solution, after 1 day was quantitatively converted into a new stable product with spectral data in agreement with those of structure **7a**. When the reaction between **1a** and **5a** in 2/1 relative molar ratio was carried out in CDCl₃, the ¹H NMR spectrum of the crude reaction mixture showed only the presence of compound **6a** and of starting DD thus suggesting that the expected aza-Michael addition between **6a** and **1a** does not occur in our experimental conditions: also in this case, with time, the formation of cyclic compound **7a** was observed.



Scheme 3. Reaction between aminophosphanes **5a** and **5b** and DD **1a**.

The cyclization of **6b** to cyclic seven-membered compound **7b** resulted less selective with respect to that observed for **6a**. In fact, compound **6b**, kept in chloroformic solution, was slowly converted into a mixture of products: among them, we were able to identify and isolate compound **7b** and pyrazole derivative **8**. The structure of **8** was ascertained by comparison of its spectral properties with those of an authentic sample.^[8]

New heterocycles 1-aza-2,3-dihydro-4-phosphinine (**7a**) and 1-aza-5,6-dihydro-4-phosphepine (**7b**) resulted to be stable and their spontaneous formation from precursors **6a** and **6b** can be due to an internal nucleophilic attack of the amino nitrogen atom of **6** to the imino carbon atom^[23] with displacement of a molecule of semicarbazide through a pathway analogous to that recently reported.^[24]

It is interesting to note that the behaviour of the ylidic adducts **6a,b** is different from that observed for ylides **3**, derived from the reaction of diphosphines **2a–d**. In fact, while adducts **3** undergo addition of a second molecule of DD giving diadducts **4**, in the case of ylides **6a,b** obtained from DD **1a** and aminophosphines **5a,b**, the intramolecular attack by the amino nitrogen atom to give new heterocyclic species is preferred over the aza-Michael addition of this amino group with a second molecule of **1a,b**.

Conclusions

In conclusion, the reaction between 1,2-diaza-1,3-dienes and bidentate nucleophiles gave in high yield and under mild conditions new phospho-Michael adducts. In particular, the use of a series of methylene-bridged bis(diphenylphosphino) derivatives gave access to new ylides and symmetrical diylides while diphenylphosphinoamino derivatives produced ylidic intermediates that spontaneously were converted to new six- and seven-membered heterocycles.

Part of this chapter is reproduced with permission from “European Journal of Organic Chemistry” by John Wiley and Sons. Further experimental data, included characterization data of the related products here described, can be found in the paper “Forlani L., Attanasi O. A., Boga C., De Crescentini L., Del Vecchio E., Favi G., Mantellini F., Tozzi S., Zanna N., *Eur. J. Org. Chem*, **2012**, 4357-4366” fully available at <http://onlinelibrary.wiley.com/>.

References

- [1] a) M. B. Smith, J. March, *March's Advanced Organic Chemistry*, 6th Edition, J. Wiley & Sons; Hoboken, N.J., **2007**, p.1105 and ref. cit. therein; b) P. Perlmutter in *Conjugate Addition Reactions in Organic Synthesis*, Pergamon Press; Oxford, U.K., 1992; c) S. Paganelli, A. Schionato, C. Boga, A. Fava, *J. Mol. Catal.* **1991**, *66*, 7–21, and ref. cit. therein.
- [2] D. Enders, K. Lüttgen, A. A. Narine, *Synthesis* **2007**, 959–980 and ref. cit. therein.

-
- [3] For a recent review on aza-Michael reaction see: D. Enders, C. Wang, J. X. Liebich, *Chem. Eur. J.* **2009**, *15*, 11058–11076.
- [4] C. F. Nising, S. Bräse, *Chem. Soc. Rev.* **2008**, *37*, 1218–1228.
- [5] a) D. Enders, A. Saint-Dizier, M.-I Lannou, A. Lenzen, *Eur. J. Org. Chem.* **2006**, 29–49; b) R. Engel in *Synthesis of Carbon–Phosphorus Bonds*, CRC Press; Boca Raton, FL, **1988**.
- [6] For recent reviews see: (a) O. A. Attanasi, L. De Crescentini, P. Filippone, F. Mantellini, S. Santeusano, *ARKIVOC* **2002**, *XI*, 274–292; (b) O. A. Attanasi, L. De Crescentini, G. Favi, P. Filippone, F. Mantellini, F. R. Perrulli, S. Santeusano, *Eur. J. Org. Chem.* **2009**, 3109–3127.
- [7] T. Kanzian, S. Nicolini, L. De Crescentini, O. A. Attanasi, A. Ofial, H. Mayr, *Chem. Eur. J.* **2010**, *16*, 12008–12016.
- [8] O. A. Attanasi, P. Filippone, A. Mei, *Tetrahedron*, **1992**, *48*, 1707–1714.
- [9] O. A. Attanasi, P. Filippone, S. Giovagnoli, *Org. Prep. Proced. Int.* **1994**, *26*, 321–326.
- [10] O. A. Attanasi, G. Baccolini, C. Boga, L. De Crescentini, P. Filippone, F. Mantellini, *J. Org. Chem.* **2005**, *70*, 4033–4037.
- [11] O. A. Attanasi, G. Baccolini, C. Boga, L. De Crescentini, P. Filippone, F. Mantellini, *Tetrahedron* **2008**, *64*, 6724–6732.
- [12] O. A. Attanasi, G. Baccolini, C. Boga, L. De Crescentini, G. Giorgi, F. Mantellini, S. Nicolini, *Eur. J. Org. Chem.* **2008**, 5965–5979.
- [13] a) O. I. Kolodiazny, in *Phosphorus Ylides, Chemistry and application in Organic Synthesis*, Wiley–VCH; Weinheim, **1999**; b) G. Pohnert, W. Boland, *Eur. J. Org. Chem.* **2000**, 1821–1826.
- [14] a) D. E. Berry, J. Browning, K. R. Dixon, R. W. Hilts, *Can. J. Chem.* **1988**, *66*, 1272–1282; b) A. Spannenberg, W. Baumann, U. Rosenthal, *Organometallics* **2000**, *19*, 3991–3993; c) L. R. Falvello, M. E. Margalejo, R. Navarro, E. P. Urriolabeitia, *Inorg. Chim. Acta* **2003**, *347*, 75–85; d) Y. Canac, C. Lepetit, M. Abdalilah, C. Duhayon, R. Chauvin, *J. Am. Chem. Soc.* **2008**, *130*, 8406–8413.
- [16] F. H. Westheimer, *Acc. Chem. Res.* **1968**, *1*, 70–78.
- [16] a) R. R. Holmes, in *Pentacoordinated Phosphorus Structure and Spectroscopy*, ACS Monograph 175, American Chemical Society: Washington, DC, **1980**, Vols. I and II; b) L. D. Quin, A. J. Williams, *Practical Interpretation of P-31 NMR Spectra and Computer Assisted Structure Verification*. Advanced Chemistry Development, Inc.: Toronto, **2004**, Chapt. 12, pp.83–85; c) E. Fluck, G. Heckmann, Empirical Methods for Interpreting Chemical Shifts of Phosphorus Compounds, in ‘*Phosphorus-31 NMR Spectroscopy in Stereochemical Analysis Organic Compounds and Metal Complexes*’, J. G. Verkade, and L. D. Quin, Eds., VCH Publishers, Deerfield Beach, FL, **1987**, Chapter 2; d) G. Baccolini, C. Boga, R. A. Buscaroli, *Eur. J. Org. Chem.* **2001**, 3421–3424; e) G. Baccolini, C. Boga, M. Mazzacurati, F.

- Sangirardi, *Org. Lett.* **2006**, *8*, 1677–1680; f) G. Baccolini, C. Boga, M. Mazzacurati, *Eur. J. Org. Chem.* **2007**, 4529–4534.
- [[17]a) H. S. Gutowsky, C. H. Holm, *J. Chem. Phys.* **1956**, *25*, 1228–1234; b) H. Eyring, *Chem. Rev.* **1935**, *17*, 65–77.
- [18] L. Lunazzi, A. Mazzanti, A. Muñoz Álvarez, *J. Org. Chem.* **2000**, *65*, 3200–3206.
- [23] J. Vicario, D. Aparicio, F. Palacios, *J. Org. Chem.* **2009**, *74*, 452–455.
- [24] O. A. Attanasi, S. Bartoccini, G. Giorgi, F. Mantellini, F. R. Perrulli, S. Santeusano, *Tetrahedron* **2010**, *66*, 5121–5129.

Chapter 7

Interaction between gliadins and coumarin: a joint theoretical and experimental study

Gliadins represent the alcohol soluble fraction of gluten, the wheat storage protein. They are a family of prolamines, heterogeneous polypeptides of molecular weight ranging from 30 to 55 kDa. Gliadins are monomeric and disulphide-bonded proteins formed by a non-repetitive domain rich in α -helix structures and by heterogeneous repetitive domains rich in β -reverse turns.^[1] The repetitive domains consist of short repeated sequences, with high content of proline and glutamine. They are classified according to their structure into α -, β -, γ -, and ω -type.^[2]

Unfortunately, gliadins may be strong food allergens. They cause IgE-mediated allergies, such as asthma, atopic dermatitis, urticaria, angioedema, food allergy and anaphylaxis,^[3,4] or may aggravate coeliac disease, a genetically-determined gluten-dependent disease.^[5] Because gluten plays a significant role in the human diet, many research efforts have been aimed at exploring the mechanisms of its allergenicity. Attempts to modify gluten proteins have appeared useful since they may considerably decrease allergen immunoreactivity.

In a previous study it has been reported that several anthocyanins and anthocyanidins interact with gliadins in conditions similar to those of the stomach.^[6] Anthocyanidins are flavylum salts, the pigments of the vascular plants. They are present in vegetables and flowers and give them brilliant red to violet colours. Anthocyanidins are powerful antioxidant molecules, with noteworthy biological activity, even if they do not have a long-lasting stability in solution.^[7]

The complexes formed between anthocyanidins and gliadins appeared quite “stronger” than those between anthocyanins and gliadins.^[6] Among all the tested

molecules, cyanidin (**Cya**, Figure. 1) was found to show the highest affinity for the gliadins. The previous studies on the interaction between anthocyanidins and gliadins were carried out by using several spectroscopic techniques, such as Nuclear Magnetic Resonance Spectroscopy (NMR), UV-Visible spectroscopy and Infrared spectroscopy. The analysis of the results was complicated due to the different forms in which anthocyanidins could be present in solution, so it seemed important to carry out further studies by using a molecular model. Coumarin was chosen as a model because has a benzocondensed structure similar to that of **Cya**.

In this study the interaction of the gliadins with a coumarin derivative was investigated in order to obtain further information about the conformational changes of gliadins. With this aim, 3-ethoxycarbonylcoumarin (**3-EcC**, Figure. 1) has been synthesized.

Coumarins constitute a group of natural compounds derived from 5,6-benzo-2-pyrone contained in more than 700 species of plants. Their name derives from the French word *coumarou*, the popular name of the tonka tree (*Coumarouna odorata*) from which coumarin was extracted for the first time.^[8]

Many studies have been focused on a large number of beneficial effects of coumarins including anti-inflammatory,^[9] antitumor,^[10] antioxidant,^[11] antiviral, and antimicrobial activities,^[12] even if some coumarin derivatives present a moderate toxicity. Unfortunately, some coumarins are not soluble in water and this could affect their bioavailability.^[13]

3-EcC and **Cya** have a similar structure, although **Cya** is a cationic species, instead **3-EcC** is neutral and does not have a phenyl moiety (ring **B**, Figure 1). Moreover, this coumarin is present in a sole form. The differences between the two types of molecules permit us to investigate the influence of the charge, the steric hindrance and other structural features in the formation of a complex with the gliadins (**Glia**). Furthermore, differently from **Cya**, **3-EcC** is stable also in neutral conditions, allowing to investigate the structural changes of **Glia** in different conditions of pH (7 and 2.5).

With the aim to better understand the nature of the interaction between the gliadins (**Glia**) and these ligands, Raman, IR and NMR spectroscopies were

employed. The obtained results have been summarized in order to compare the effect of the two different types of ligand in the interaction with the gliadins (**Glia**).

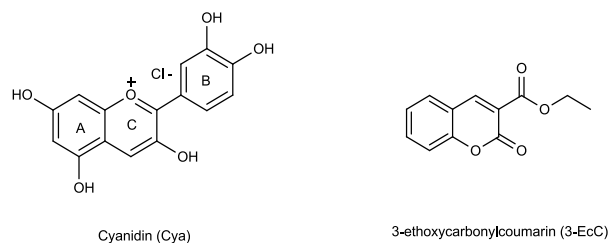


Figure 1. Ligands used in this study.

7.1 Coumarin (3-EcC) and Glia at neutral pH

7.1.1 Raman and IR vibrational results

Figure 2A reports the Raman spectra of lyophilized **Glia** before and after treatment with **3-EcC** at neutral pH; the spectrum of **3-EcC** is reported for comparison. In both treated and untreated samples, several bands are characteristic of specific amino acids. The bands prevalently due to phenylalanine (F), tyrosine (Y), tryptophan (W), glutamine (Q) and proline (P) have been indicated.¹⁴ In addition, the spectrum of the treated sample shows several bands (indicated with an asterisk) due to the bonded **3-EcC**; some of them appeared slightly shifted in their wavenumber positions.

The Raman spectrum of untreated **Glia** at neutral pH shows Amide I and III components at 1661 and 1276 cm⁻¹, respectively. These spectral features, together with the presence of the bands at about 1340, 1100 and 930 cm⁻¹ (δCCaH , νCN and skeletal stretching modes, respectively), diagnostic for alpha-helix,^[14,15,16,17,18] showed that the secondary structure of **Glia** is dominated by the α -helix conformation, in agreement with previously reported data.^[18]

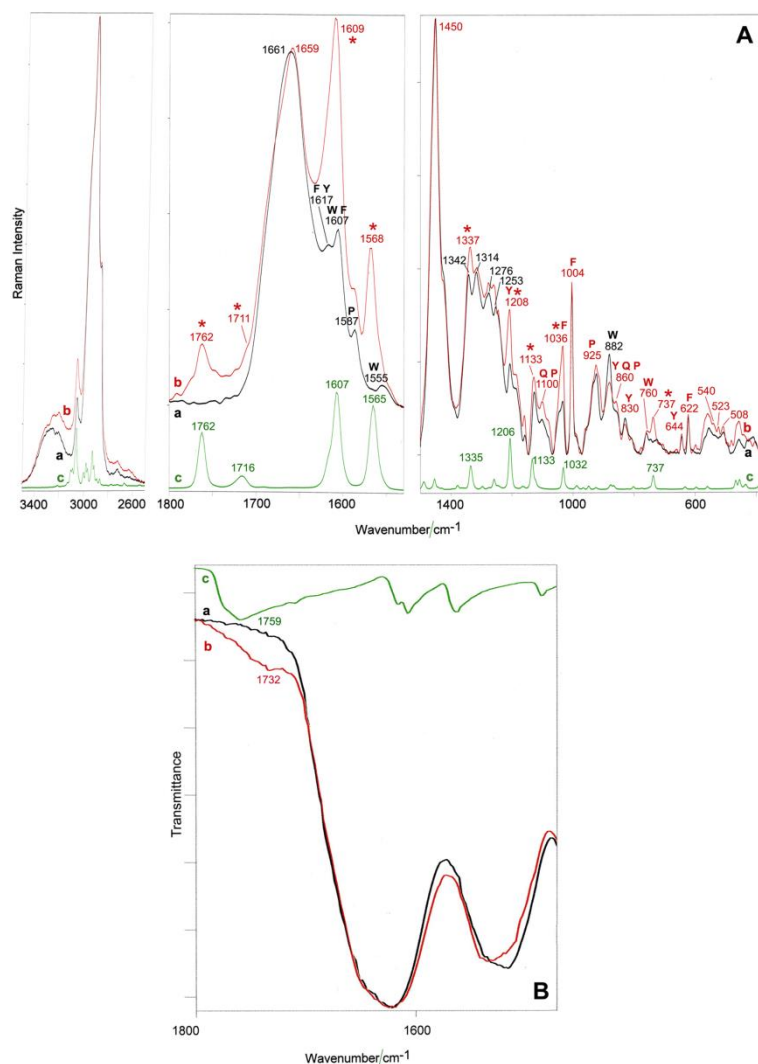


Figure 2. Raman (A) and IR (B) spectra of lyophilized Glia before (black) and after treatment with 3-EcC (red) at neutral pH; the spectra of 3-EcC (green) are reported for comparison. The bands prevalently due to phenylalanine (F), tyrosine (Y), tryptophan (W), glutamine (Q) and proline (P) are indicated. The bands due to the bonded 3-EcC are marked with an asterisk.

In the Amide III range, the band at about 1315 cm^{-1} , assignable to polyproline II PPII helical structure,^[17,19] revealed the presence of this conformation, according to other studies;^[17] the component at 1253 cm^{-1} is ascribable to turns/unordered conformations.^[14] The quantitative data obtained by the method of Alix *et al.* (Table 1) confirmed that the prevalent conformation was α -helix. Actually, it has been demonstrated that large amounts of proline make the

formation of long runs of residues in the β -sheet conformation more unlikely.^[20]

On the other hand, glutamine residues have been found to favor the α -helix region of the Ramachandran surface,^[21] although glutamine residues have also been reported to have a high PPII helix-forming propensity.^[22]

Upon treatment with **3-EcC**, the Amide I band shifted to lower frequency, i.e. at 1659 cm^{-1} (Figure 2A). The quantitative data reported in Table 1 suggested that the treatment with **3-EcC** induced a conformational rearrangement that involved an increase in α -helix and a parallel decrease in β -sheet (the content of turns and unordered structures remained nearly constant).

The Amide III spectral range confirmed the increase in α -helix content: in fact, the band at about 1275 cm^{-1} , assignable to this conformation increased in intensity, as well as the bands at about 1340 , 1100 and 930 cm^{-1} . Conformational rearrangements can also explain the changes observed in the $3500\text{-}3000\text{ cm}^{-1}$ range (where νNH and νOH stretching modes fall), ascribable to the development of different hydrogen bonding patterns.

Table 1. Percentages of secondary structure conformations as determined by applying the method of Alix et al.^[56] to the Amide I Raman band; full width at half maximum (FWHM) of the δCH_2 band at 1450 cm^{-1} and I_{855}/I_{830} intensity ratios as determined from the Raman spectra of the analyzed samples.

Sample	α -	β -	turns	unordere	FWHM ₁₄₅	I_{855}/I_{83}
Glia at neutral pH	47	26	16	11	35.5	1.10
Glia+3-EcC at neutral pH	53	21	16	10	35	2.02
Glia at acidic pH	44	28	17	11	37.1	1.10
Glia+3-EcC at acidic pH	55	20	15	10	34.9	1.08
Glia+Cya at acidic pH	60	16	14	10	unreliable	0.60
Glia+Cya+3-EcC at	64	12	14	10	unreliable	0.84
Glia at neutral pH	47	26	16	11	35.5	1.10
Glia+3-EcC at neutral pH	53	21	16	10	35	2.02

According to other authors,^[23] the increase of the α -helix content can be interpreted as an increased folding of the protein; the same authors explained the decrease in α -helix content in terms of unfolding of the protein.

The full width at half maximum (FWHM) of the δCH_2 band at 1450 cm^{-1} has been used as a marker of the relative order of the hydrophobic component as suggested for phospholipid assemblies;^[24,25,26] a certain increase of order occurred also in the hydrophobic component, as suggested by the slight sharpening of the δCH_2 band upon complexation with **3-EcC** (FWHM decreased from 35.5 to 35 cm^{-1} , Table 1).

The tryptophan band at 760 cm^{-1} has been proposed as indicator of the hydrophobicity of the environment of the indole ring. The addition of **3-EcC** caused a slight strengthening of the 760 cm^{-1} ; this result suggests a little increment in the “buriedness” of the tryptophan residues in the protein, which contributes to the formation of a more ordered structure.^[27,28] The intensity change of the band at 880 cm^{-1} , assignable to Trp besides other amino acid residues, confirmed a change in Trp environment; upon the treatment with **3-EcC**, the effect was opposite to that observed by other authors upon complexation with arabic gum.^[18] Some authors suggested that the intensity of the Raman bands of phenylalanine at about 1000 and 1035 cm^{-1} are sensitive to the environment of this amino acid, besides its content.^[18] In particular, the variations in the band at about 1000 cm^{-1} have been attributed to the environmental influences on the benzene ring π - electron clouds since Phe could not be involved in specific hydrogen-bonding or other polar interactions; a weakening of this band has been explained in terms of exposure to water, while a strengthening to hydrophobic environments.^[29,30] In our spectrum, the above mentioned bands appeared strengthened upon the treatment with **3-EcC**, particularly that at 1035 cm^{-1} , partly due to the contribution of the **3-EcC** ligand, which shows a band at a similar wavenumber position (Figure 2A).

The Raman bands at about 855 and 830 cm^{-1} (Fermi resonance between the ν_1 ring breathing vibration and the $2\nu_{16a}$ overtone of an out-of-plane ring bending vibration) can be used to investigate the H-bonding state of the Tyr phenoxyl.^[14,31]

The intensity ratio between the two components (I_{855}/I_{830}) has been extensively used to evidence the Tyr interactions in globular proteins, their assemblies and the degree of exposure to water.^[14] In fact, the I_{855}/I_{830} ratio achieves its minimum value of about 0.3 when tyrosine residues are buried and the phenolic OH group acts as a strong hydrogen-bond donor to an electronegative acceptor, such as carboxyl oxygen.^[31] When tyrosines are exposed at the surface of the protein, the phenolic OH acts as both a donor and an acceptor of moderate hydrogen bonds and the I_{855}/I_{830} is approximately 1.25.^[31] If the phenoxyl oxygen is the acceptor of a strong hydrogen bond from an electropositive group, such as a lysyl NH_3^+ group, and does not participate in significant hydrogen bond donation, the I_{855}/I_{830} approaches a presumed maximum value of 2.5.^[31] More recent studies on filamentous virus capsids,^[32,33,34,35] and silk fibroin in Silk I form,^[36] allowed to refine the correlation and to verify that the I_{855}/I_{830} intensity ratio can even exceed the latter value, indicating a strongly hydrophobic local environment for tyrosine residues, a state not represented in any previous study on globular proteins.

To obtain more reliable I_{855}/I_{830} intensity ratios, a curve-fitting procedure was used. As an example Table 1 reports the I_{855}/I_{830} values obtained from the Raman spectrum (region 970-790 cm^{-1}) of lyophilized **Glia** at neutral pH fitted into its components. In the spectrum of untreated **Glia**, the I_{855}/I_{830} intensity ratio was 1.10, suggesting that phenolic OH groups acting as both donor and acceptor of moderate hydrogen bonds,^[31] according to the amino acid composition of **Glia**.

Upon treatment with **3-EcC**, the I_{855}/I_{830} intensity ratio of **Glia** increased from 1.10 to 2.02 suggesting a change towards a more exposed state of tyrosine residues. The ν_{SS} disulphide stretching vibration (500-550 cm^{-1}) is commonly used to evaluate conformational changes, since disulphide bridges play a fundamental role in determining the tertiary structure of a protein. The symmetrical stretching vibration of the S-S bond is influenced by the conformation of the C atoms in the disulphide bridge. Components at about 510, 520 and 540 cm^{-1} have been identified as diagnostic for *gauche-gauche-gauche* (g-g-g), *gauche-gauche-trans* (g-g-t) and *trans-gauche-trans* (t-g-t) $\text{C}_\alpha\text{-C}_\beta\text{-S-S-C}_\beta\text{-C}_\alpha$ conformations, respectively.^[14,37]

In the spectral profile of the untreated **Glia** (Figure 2A), the most evident component appeared at 508 cm^{-1} , suggesting that the $C_{\alpha}\text{-}C_{\beta}\text{-S-S-C}_{\beta}\text{-}C_{\alpha}$ linkage took the lowest potential energy conformation (i.e. *gauche-gauche-gauche*). However, components at about 520 and 540 cm^{-1} were detected as shoulders.

To obtain more reliable information on the distribution of the disulphide bridge conformations, a curve-fitting procedure was adopted; as an example **Figure 3** shows the percentages obtained for the *g-g-g*, *g-g-t* and *t-g-t* conformations in the analysed samples.

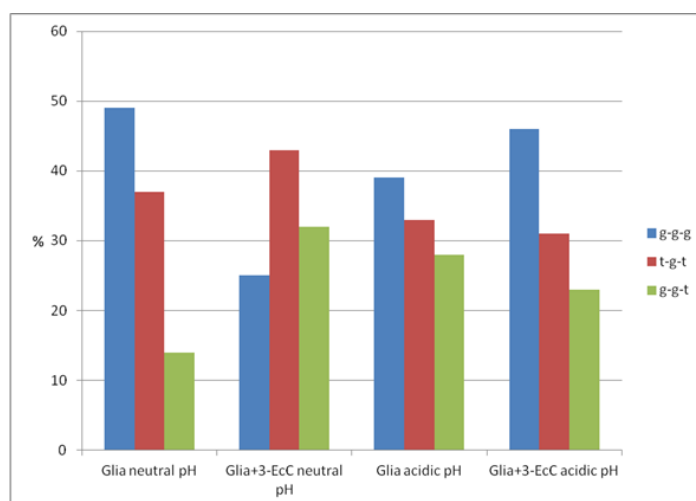


Figure 3. Percentages of *gauche-gauche-gauche* (*g-g-g*), *gauche-gauche-trans* (*g-g-t*) and *trans-gauche-trans* (*t-g-t*) $C_{\alpha}\text{-}C_{\beta}\text{-S-S-C}_{\beta}\text{-}C_{\alpha}$ conformations, as obtained by fitting the $585\text{-}485\text{ cm}^{-1}$ Raman spectra of the analysed samples.

The curve fitting analysis (**Figure 3**) confirmed that the prevalent conformation of the cystine disulphide bridges was *gauche-gauche-gauche* (49%). Significant amounts of *trans-gauche-trans* conformation were present (37%); the *gauche-gauche-trans* conformation was the least represented (14%). Upon the treatment with **3-EcC**, the bands at 540 and 523 cm^{-1} clearly appeared as distinct components (Figure 2A). The curve-fitting analysis showed that the *trans-gauche-trans* and *trans-gauche-trans* conformations increased their contents at the expenses of the *gauche-gauche-gauche* conformation (attaining percentages of 43, 32 and 25%, respectively, **Figure. 3**). An analogous behavior was observed by

other authors on gluten proteins treated with emulsifying agents,^[38] they interpreted this result as a marker of protein folding phenomena. Our findings suggest that the conformation of the disulphide bridges was strongly altered upon interaction with **3-EcC**.

The changes observed in the secondary structure as well as in Tyr, Trp and S-S bridges were analogous to those observed by other authors for gluten proteins treated with locust bean gum.^[23]

In the light of the obtained results, it can be affirmed that the interaction with **3-EcC** determined significant conformational rearrangements in the gliadins (**Glia**).

The IR and Raman region near 1700 cm^{-1} allowed to better clarify the nature of the interactions between **Glia** and **3-EcC**. As can be seen in the IR spectra reported in Figure 2B, the C=O stretching vibration of the ligand was found to shift to lower wavenumber values upon interaction with **Glia**, i.e. from 1759 to 1732 cm^{-1} ; analogously, the other C=O stretching vibration shifted in the Raman spectra from 1716 to 1711 cm^{-1} (Figure 2A) These trends would show that both the C=O groups of **3-EcC** should be involved in hydrogen bond interactions. At the same time, the shift of the **3-EcC** band from 1565 to 1568 cm^{-1} , assignable to C=C stretching vibrations, would suggest that also hydrophobic interactions occur.

7.1.2 NMR Results

In order to study by NMR gliadins-coumarin interaction in neutral conditions, methanol-d₄ was chosen as solvent instead of a more complicated mixture of solvents. The gliadins (**Glia**) are less soluble in methanol-d₄ than under acidic conditions or in the 60:40 ethanol/water mixture, but the STD technique permits to have binding site information even in the case of very dilute protein solutions. STD spectra of the reaction mixture show that the entire **3-EcC** molecule interacts because all its signals are involved in Overhauser effect, in particular the methyl moiety ($\delta = 1.40\text{ ppm}$) has a strong interaction with **Glia** (Figure 4)

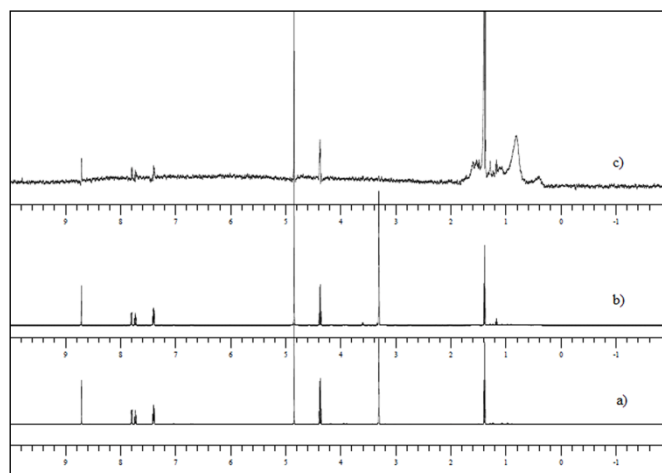


Figure 4. a) ^1H -NMR spectrum of 3-EcC in CD_3OD ; b) ^1H -NMR spectrum of 3-EcC and Glia in CD_3OD ; c) STD spectrum of 3-EcC and Glia CD_3OD .

7.2 Coumarin (3-EcC) and Glia at acidic pH

7.2.1 Raman Results

The pH conditions appeared to significantly influence the conformation of **Glia**. The differences observed are consistent with the findings reported in the literature,^[18] in particular, at decreasing pH, in the Amide I range, the center of the band appeared slightly up-shifted, and a shoulder at higher wavenumber values appeared more prominent. Interestingly, the Amide I broadened (going from neutral to acidic pH its FWHM increased from 55.5 to 59.8 cm^{-1}), suggesting a wider distribution of secondary structure conformations. At the same time, in the Amide III range, the bands at about 1340 and 1270 cm^{-1} appeared decreased in intensity with respect to those at about 1315 and 1250 cm^{-1} , respectively; in agreement with Chourpa *et al.*,^[18] the obtained trends can be explained in terms of a reduced α -helix content, as confirmed by the quantitative data reported in Table 1. At decreasing pH, the δCH_2 band at 1450 cm^{-1} increased its FWHM from 35.5 to 37.1 cm^{-1} (Table 1), suggesting an increased disorder also in the hydrophobic component.

According to Chourpa *et al.*,^[18] the Raman bands of phenylalanine at about 1000 and 1035 cm^{-1} were found to increase in intensity upon pH decrease, suggesting a change in the environment of this amino acid.

Upon pH decrease, the 880 cm^{-1} band decreased in intensity, while no changes were detected in the intensity of the 760 cm^{-1} band. At acidic pH, the I_{855}/I_{830} intensity ratio was the same as at neutral pH (Table 1). In contrast, the distribution of the disulphide bridges conformations was significantly affected by the pH value (Figure 3). At acidic pH, although the *gauche-gauche-gauche* (g-g-g) conformation remained the prevailing one, its content appeared significantly decreased if compared with neutral pH (39% *versus* 49%); the *trans-gauche-trans* conformation underwent a less pronounced decrease (from 37 to 33%), while the *gauche-gauche-trans* (g-g-t) conformation doubled its content (from 14 to 28%). By decreasing pH, also the hydrogen bonding patterns were found to vary, as suggested by the changes in the 3500-3200 cm^{-1} range.

Figure 5A reports the Raman spectra of lyophilized **Glia** before and after treatment with the **3-EcC** at acidic pH; the spectrum of **3-EcC** is reported for comparison. The spectrum of the treated sample showed also the bands due to the bonded **3-EcC**, with a lower relative intensity than at neutral pH, suggesting a higher protein/**3-EcC** ratio and thus a lower affinity towards the ligand. The IR spectra (Figure 5B) confirmed this finding.

The trend of the spectra showed that also at acidic pH, the complexation with **3-EcC** favoured an enrichment in α -helix conformation, as confirmed by the trend of the above mentioned marker bands of this structure at about 1340 and 930 cm^{-1} , and the quantitative data reported in Table 1. At acidic pH the extent of transformation into α -helix appeared more pronounced, in consideration of the fact that in the untreated sample the content of this conformation was lower.

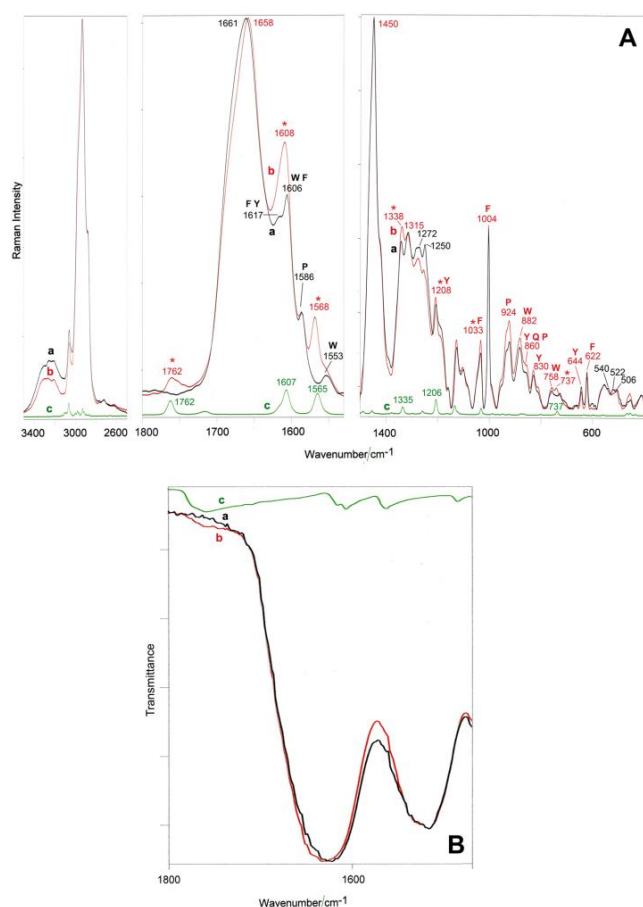


Figure 5. Raman (A) and IR (B) spectra of lyophilized Glia before (black) and after treatment with 3-EcC (red) at acidic pH; the spectrum of 3-EcC (green) is reported for comparison. The bands prevalently due to phenylalanine (F), tyrosine (Y), tryptophan (W), glutamine (Q) and proline (P) are indicated. The bands due to the bonded 3-EcC are marked with an asterisk.

At the same time, the contents of β -sheet and turns conformations decreased (Table 1). The FWHM of the δCH_2 band showed a more pronounced decrease (from 37.1 to 34.9 cm^{-1}), attaining values similar to those obtained at neutral pH (Table 1).

The changes in Phe and Trp environment were less pronounced than at neutral pH (the bands at about 1033, 1004, 880 and 760 cm^{-1} changed less significantly than at neutral pH); the I_{855}/I_{830} remained constant upon the treatment, suggesting that no changes in Tyr environment occurred (Table 1). With regards to disulphide conformations, the spectra clearly showed a weakening

of the components at about 540 and 520 cm^{-1} . The curve fitting analysis confirmed this qualitative result, showing a decrease of the contents of the *trans-gauche-trans* and *gauche-gauche-trans* conformations and a parallel increase in the more stable *gauche-gauche-gauche* conformation (Figure 3).

7.2.2 NMR Results

The spectra reported in Figure 6 show that under acidic conditions **3-EcC** interacts with **Glia**. By analyzing the spectra c), it is possible to note that the entire molecule is involved in the interaction as reported in the case of **Cya** with **Glia**.^[6] To gain more insights into the differences of interaction with the ligands (**Cya** versus **3-EcC**), Raman spectroscopy was used.

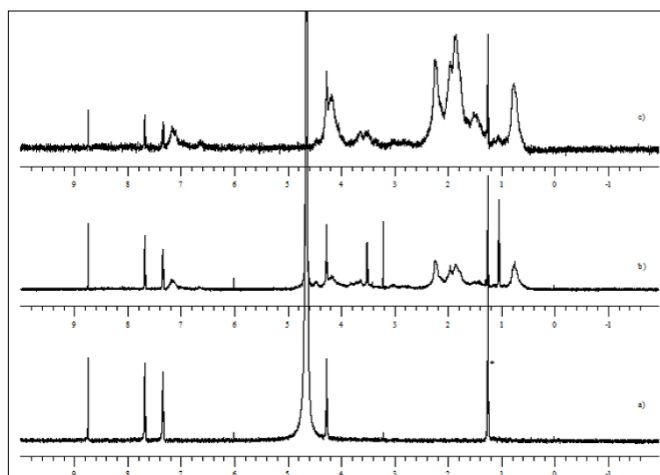


Figure 6. a) $^1\text{H-NMR}$ spectrum of **3-EcC** in $\text{D}_2\text{O/DCl}$; b) $^1\text{H-NMR}$ spectrum of **3-EcC** and **Glia** in $\text{D}_2\text{O/DCl}$ c) STD spectrum of **3-EcC** and **Glia** in $\text{D}_2\text{O/DCl}$

7.3 Cyanidin (Cya) and Glia at acidic pH

7.3.1 Raman Results

Figure 7A reports the Raman spectra of lyophilized **Glia** before and after treatment with **Cya**; the spectrum of **Cya** is reported for comparison.

Upon treatment with **Cya**, some new bands ascribable to the anthocyanidin appeared (marked with a circle), although often significantly shifted with respect to their position in pure **Cya**. As can be easily seen, the strongest band of **Cya** appeared at 1331 cm^{-1} and was assigned to an inter-ring bond stretching mode,^[39,40,41] in the treated **Glia** sample, no band was observed at a similar wavenumber. Therefore, it may be considered that this band, possibly shifted in frequency contributes to the strengthening of the band at 1320 cm^{-1} . This result would suggest, according to Merlin *et al.*,^[41] a change in the delocalized π -electron density.

The quantitative data reported in Table 1 suggest that the interaction with **Cya** determined an enrichment in the α -helix content more pronounced than upon **3-EcC** complexation. This result was confirmed by the trend of the bands at 1270 and 1100 cm^{-1} , which significantly increased in intensity. At the same time, the contents of β -sheet and turns conformations decreased, as observed upon **3-EcC** complexation (Table 1).

Due to the contribution of the anthocyanidin to the band at about 1450 cm^{-1} , it could not be used to normalize the spectra. Therefore, no information can be obtained on the possibly changed environment of Trp and Phe. In contrast, curve-fitting analyses allowed to gain insight into the changes of Tyr environment. Upon treatment with **Cya**, the I_{855}/I_{830} ratio decreased to 0.60 (Table 1), i.e. to a more buried Tyr state, differently from what observed for the other samples. Also Linlaud *et al.*^[23] have observed a different behavior of the Tyr intensity ratio depending on the kind of hydrocolloid added to gluten proteins.

The distribution of the disulphide conformations cannot be evaluated due to the contribution of **Cya**, which showed bands at 540 , 520 and 505 cm^{-1} .

Also the treatment with the anthocyanidin altered the hydrogen bonding patterns, as suggested by the changes in the $3500\text{-}3000\text{ cm}^{-1}$ range, where νOH and νNH modes fall.

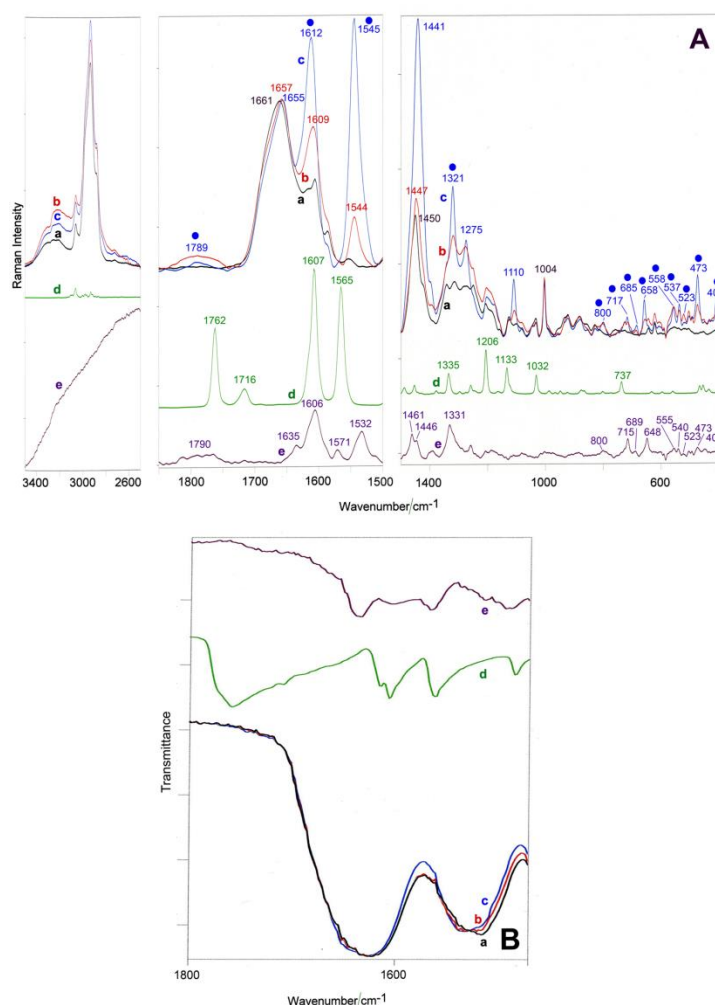


Figure 7. Raman (A) and IR (B) spectra of lyophilized GliA before (a) and after treatment with Cya (b) and with Cya and 3-EcC (c) at acidic pH; the spectra of Cya (e) and 3-EcC (d) are reported for comparison. The bands prevalently due to phenylalanine (F), tyrosine (Y), tryptophan (W), glutamine (Q) and proline (P) are indicated. The bands ascribable to Cya are marked with a circle.

7.4.1 NMR Results

NMR experiments on **GliA** and **Cya** are reported in a previous paper and showed that the entire molecule of **Cya** interacts with **GliA**.⁶ No favorite binding site was detected by STD experiments. It is possible to suppose that **Cya** is completely included in a cavity of the gliadins (**GliA**) networks.

7.4 A complex between coumarin and cyanidin? Influence on gliadin (Glia) secondary structure

7.4.1 Raman Results

Figure 7A shows the Raman spectrum of lyophilized **Glia** after treatment with **Cya** and **3-EcC** (Figure c) at acidic pH. The bands assignable to **Cya** (marked with a circle) appeared even more intense than in the spectrum of **Glia** treated only with **Cya**. Interestingly, no bands due to **3-EcC** were observed (in particular, no band at about 1760 cm^{-1} was detected and no strengthening near 1205 cm^{-1} was observed). The IR C=O stretching vibration range confirmed this finding: no band above 1700 cm^{-1} was detected (Figure 7B). Upon treatment with the anthocyanidin, the enrichment in α -helix and the decrease in β -sheet and turns were even more pronounced than upon treatment with the only **3-EcC**, as suggested by the above discussed spectral features, as well as by the quantitative data reported in Table 1.

Upon treatment with **Cya** and **3-EcC**, the I_{855}/I_{830} ratio decreased to 0.84, i.e. Tyr residues appeared more buried than in **Glia**, but less than in **Glia** treated with **Cya** alone ($I_{855}/I_{830} = 0.60$, see Table 1). Also the treatment with **Cya** and **3-EcC** altered the hydrogen bonding patterns, as suggested by the changes in the $3500\text{-}3000\text{ cm}^{-1}$ range, where νOH and νNH modes fall. The vibrational results would suggest that the species prevalently interacting in the complex is **Cya**; however, **3-EcC** indirectly favored the complex formation with **Glia**.

To gain more insights into this behavior, the possible formation of a complex between **Cya** and **3-EcC** has been investigated. Actually, by mixing **Cya** and **3-EcC** in the HCl aqueous solution in a 1:1 molar ratio, an insoluble solid is formed; this could indicate the existence of an interaction between **Cya** and **3-EcC**. To clarify this aspect, the aqueous solution was lyophilized and the obtained solid was analyzed by Raman and IR spectroscopy; the spectra are reported in Figure 8. The theoretical Raman spectrum of the complex was calculated by summing the normalized spectra of the ligands.

The experimental Raman spectrum reported in Figure 8A showed bands of both ligands and no significant shifts in their wavenumber position were observed (in particular, for the C=O stretching bands of **3-EcC** at about 1760 and 1715 cm^{-1}). The major differences between the experimental and theoretical spectra were observed in the δCH_2 bending region, i.e. near 1450 cm^{-1} , suggesting that hydrophobic interactions occur between the two molecules; moreover, the difference in intensity of the band at 1334 cm^{-1} may be interpreted as above, i.e. as marker of a change in the delocalized π -electron density, according to Merlin *et al.*^[41]

Complementary information was obtained by IR spectroscopy; the spectrum of the complex (Figure 8B) was highly dominated by the bands of **3-EcC**. Most of them did not appear shifted in their wavenumber positions; however, significant changes were observed in the C=O stretching region of **3-EcC**.

Upon interaction, the band at 1758 cm^{-1} was found to slightly shift and change its profile while the component at 1709 cm^{-1} appeared less distinct. These trends would suggest the involvement of the C=O groups into the complex formation. Only few bands ascribable to **Cya** were distinctly observed (indicated with a circle); upon interaction, the C=C ring stretching vibration of **Cya** appeared significantly shifted in wavenumber position (from 1635 to 1641 cm^{-1}); the band assignable to an inter-ring bond stretching mode at 1327 cm^{-1} shifted to 1332 cm^{-1} , confirming a change in the delocalized π -electron density. Moreover, new bands, absent in the spectra of the ligands, were detected in the C=C ring stretching range at 1581, 1538 and 1519 cm^{-1} . Vibrational results are in agreement with the theoretical calculations reported below.

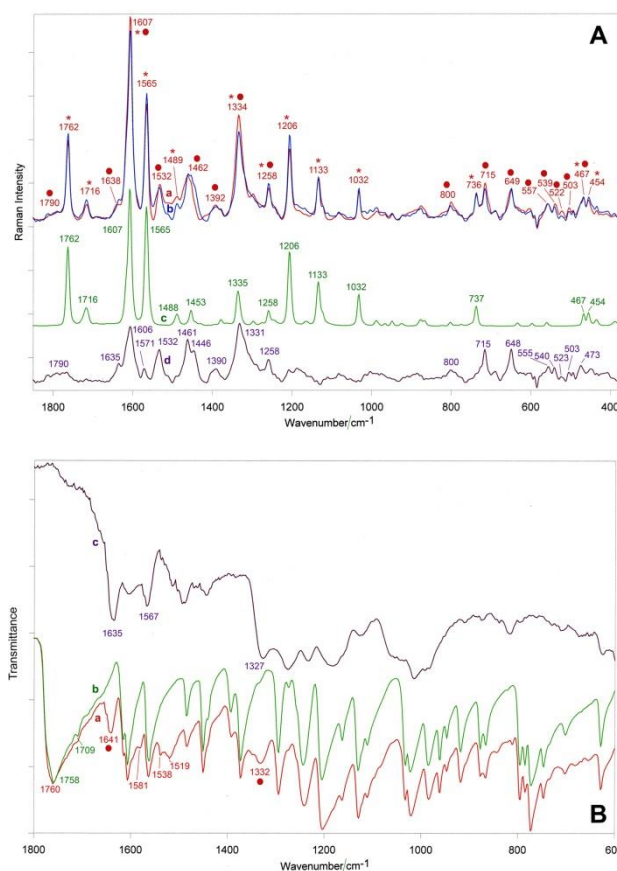


Figure 8. (A) Experimental (a) and theoretical (b) Raman spectra of the Cya+3-EcC complex; the theoretical spectrum was obtained by summing the normalized spectra of the ligands (Cya (d), normalized to the 1390 cm⁻¹ band; 3-EcC (c), normalized to the 1762 cm⁻¹ band); (B) Experimental IR spectra of the Cya+3-EcC complex (a), Cya (c) and 3-EcC (b). The bands ascribable to Cya and 3-EcC are marked with a circle and an asterisk, respectively.

7.4.2 NMR Results

Attempts to dissolve in a different solvent the solid obtained in the HCl aqueous solution (and also in the D₂O/HCl solution) by mixing **3-EcC** and **Cya** led to a different ratio of the two molecules in the solution. To avoid the formation of the solid compound upon interaction between **3-EcC** and **Cya**, at first **3-EcC** was mixed with **Glia** and the ¹HNMR and STD spectra were recorded (Figure 9 b,c). The spectrum in Figure 9c shows the interaction between **Glia** and **3-EcC**.

After the addition of **Cya**, we did not observe the formation of any insoluble solid because it is possible that the inclusion in **Glia** networks of **Cya** and **3-EcC** did not permit the formation of the complex.

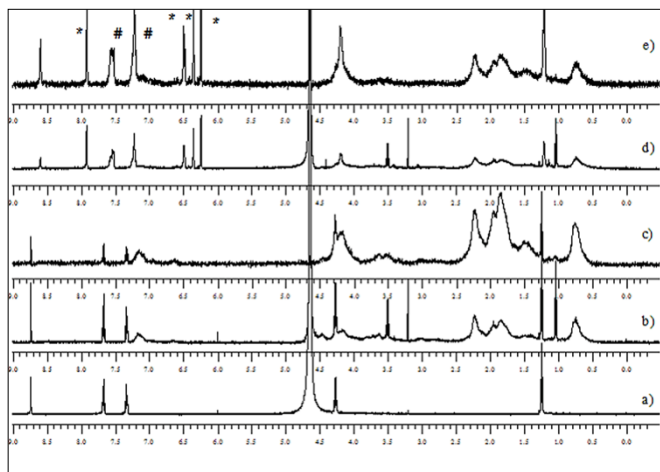


Figure 9. a) $^1\text{H-NMR}$ spectrum of **3-EcC** in $\text{D}_2\text{O/DCl}$; b) $^1\text{H-NMR}$ spectrum of **3-EcC** and **Glia** in $\text{D}_2\text{O/DCl}$; c) STD spectrum of **3-EcC** and **Glia** in $\text{D}_2\text{O/DCl}$; d) $^1\text{H-NMR}$ spectrum of **3-EcC**, **Glia** and **Cya** in $\text{D}_2\text{O/DCl}$; e) STD spectrum of **3-EcC**, **Glia** and **Cya** in $\text{D}_2\text{O/DCl}$.
(*signals belonging to **Cya**; # signals belonging to **Cya** and **3-EcC**)

The $^1\text{H-NMR}$ spectrum of this solution (Figure 9d) shows the signals of both **Cya** and **3-EcC**, even if **3-EcC** signals are broader than in the absence of **Cya** (Figure 9b), The STD NMR spectrum of **Glia-Cya-3-EcC** complex (Figure 9e) shows that both **Cya** and **3-EcC** completely interacts with **Glia**; also in this case, the **3-EcC** signals were broad and slightly shifted to high fields. This shift is in agreement with the data reported in literature for the complex formed between malvin chloride (an anthocyan) and esculin (a coumarinic derivative) named co-pigment,^[42] even if the interaction between **Cya-3** and **EcC** gives broader NMR signals.

7.4.3 UV-Vis analysis

As shown in Figure 10, the UV-vis spectrum of **Cya** displays an intense absorption maximum at about 510 nm which is responsible for its red color, while the **3-EcC** spectrum shows absorption bands only in the UV region, i.e. at about 296 nm. The spectrum of the solution containing both compounds was compared with the simple arithmetical sum of the spectra of the isolated species; as shown in Figure 10, no significant differences can be observed. The copigmentation usually shows both bathochromic and hyperchromic shift, while in our case only a slight hypochromic effect in the UV region of the spectrum is appreciable (Figure 10). This is not a good reason to discard the hypothesis of the formation of a complex. Actually, the above mentioned shifting effects are mainly due to the formation of complexes dominated by charge transfer interactions, while, for example, complexes dominated by hydrogen bonding interactions do not show strong absorption shifting.

With the aim to better understand the nature of the interactions between **Cya** and **3-EcC**, a theoretical investigation was carried out.

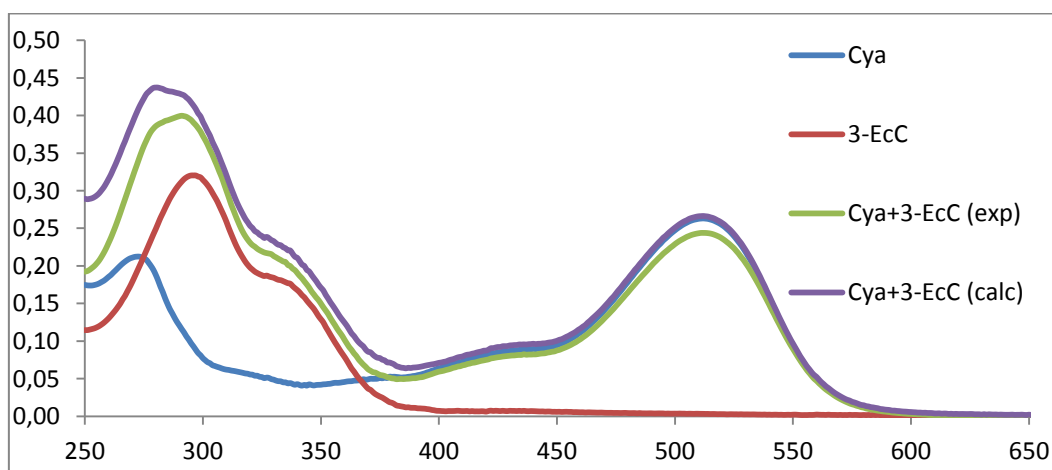


Figure 10. Experimental UV-vis spectra of the aqueous acidic solutions containing **Cya**, **3-EcC**, **Cya** and **3-EcC**. The calculated spectrum was obtained by summing the spectra of **Cya** and **3-EcC**.

7.4.4 Theoretical calculation

All DFT calculations were carried out with the Gaussian 09 program package.^[43] All geometries were fully optimized by using the ω B97X-D/6-31G(d) level of theory,^[44] which is known to produce reliable geometries for molecules bonded by non-covalent interactions. Frequencies were calculated at the same level as the geometry optimization to verify the nature of the stationary points and to obtain zero-point vibrational corrections. The basis set superposition error (BSSE) corrections was calculated by using the Boys-Bernardi counterpoise correction scheme,^[45] with the automated procedure available in the Gaussian 09 software package.

Solvent (water) effects were introduced during the optimization step by using the PCM model.^[46] Binding energies were calculated as the difference between the energy of the complexes and the sum of the energy of the isolated species. The chlorine counterion of the cyanidine moiety was not taken into account during the calculations since the inclusion of such kind of fragment usually does not improve the final results; we only balance the global charge by adding a positive charge in the cyanidine moiety.

We performed the geometry optimization for both molecules and we calculated their relative energies; then we optimized the geometries of some complexes that could be intuitively hypothesized to be formed. Only the complex with the lowest energy was taken into account; its structure is reported in Figure 11.

As depicted in Figure 11, the aromatic rings of **Cya** and **3-EcC** are in a stacked conformation; however, the non-complete overlap (probably due to the high number of oxygen atoms which favour electrostatic repulsions) does not allow for charge transfer interactions, which are usually accompanied by bathochromic shifts in the visible region of the electromagnetic spectra. It is also possible to note some hydrogen bonding interactions, which are promoted by the high content of hydroxyl functions present in both **Cya** and **3-EcC**.

The results of the calculations also show that the binding energy of the complex is about 13 Kcal/mol, which is compatible with all the different kinds of interactions observed.

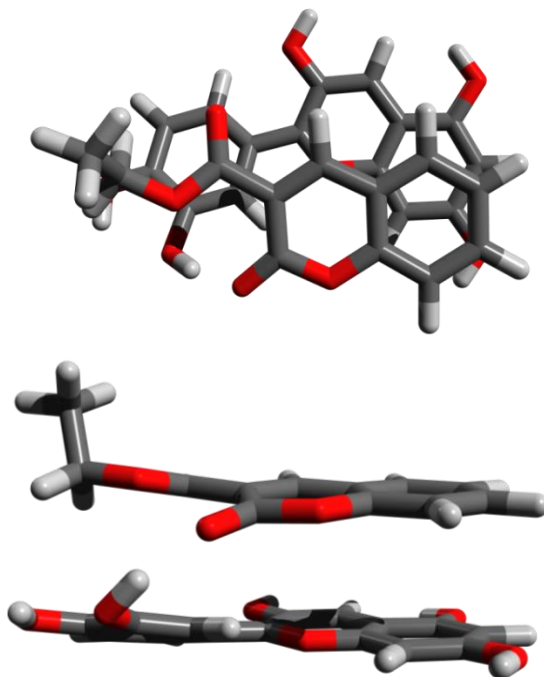


Figure 11. Geometry of the Cya-3EcC complex, obtained as the lowest energy-structure by DFT calculations.

The theoretical findings are in agreement with the results obtained by both UV-Vis and vibrational spectroscopies. Actually, the former technique only displayed a slight hypochromic shift in the UV region, while the latter showed a change in the C=C ring stretching (caused by hydrophobic or stacking interactions) and in the **3-EcC** C=O stretching (caused by hydrogen bonding interactions).

Conclusion

The interaction between **Glia** and **3-EcC** and/or **Cya** leads to a change in the secondary structure of the proteins; in particular, Raman spectra showed that both molecules produce a similar effect on the **Glia** structure (Table 1).

3-EcC proved to be useful in the evaluation of the **Glia** conformational changes at neutral pH because it is structurally similar to **Cya**, but is not so sensitive to pH changes. In fact, it was not possible to use **Cya** in neutral conditions as it is not stable at this pH value. Furthermore, **3-EcC** allowed to screen the change in the disulphide bridge conformation both in neutral and acidic conditions (Figure 3). These bridges are mostly present in α -gliadin (main responsible for coeliac disease) and the change in the distribution of the disulphide bridge conformations seems to confirm that the interaction involved this type of **Glia**.^[47] The interaction of **Glia** with **3-EcC** and/or **Cya** led to an increase in α -helix conformation and a decrease in β -sheet and turns (Table 1). In the presence of both molecules, this effect was more marked.

The obtained NMR data showed that both **Cya** and **3-EcC** interact with **Glia**. In the STD NMR spectrum (Figure 9e), the signals belonging to the aromatic ring of **3-EcC** were quite large and slightly shifted to higher field. This would suggest that **3-EcC** and **Cya** form a complex. Raman spectroscopy did not detect the **3-EcC** bands in the **Glia-3-EcC-Cya** system; however, the secondary structure of **Glia** underwent changes more significant than in the presence of **Cya** alone, suggesting that **3-EcC** plays a significant role in the **Glia-Cya-3-EcC** complex formation. The results obtained in this study provide new insights into anthocyanidins–gliadins (**Glia**) interactions and may have relevance to human health, in the field of the attempts to modify gluten proteins to decrease allergen immunoreactivity. As reported in a recent review,^[47] three significant protein structure elements may be identified as responsible for allergenicity. The first is short “toxic” amino acid sequences that probably function as antibody-binding epitopes in immunological reactions. Other significant structural elements to be considered are β -turns, giving allergen particles a specific conformation, and disulphide (SS) bonds which stabilize that structure. Any treatment able to alter

these structural elements may potentially decrease allergen immunoreactivity. In this light, the investigated ligands (modifying the secondary structure and in particular the turns content, as well as the disulphide bridge conformation) may be of interest to decrease allergen immunoreactivity.

References

- [1] A. S. Tatham, and P. R. Shewry, *Journal of Cereal Science*, 1995, **22**, 1.
- [2] H. Weiser, *Food Microbiology*, 2007, **24**, 115.
- [3] K. Bürk, A. Melms, J.B. Schulz, J. Dichgans, *Ann. Neurol.*, 2001, **50**, 827.
- [4] E. Varjonen, E. Vainio, K. Kalimo, *Allergy*, 2000, **55**, 386.
- [5] H. Wieser, *Acta Paediatrica*, 1996, Suppl. **412**, 3.
- [6] P. Mazzaracchio, S. Tozzi, C. Boga, L. Forlani, P. G. Pifferi, and G. Barbiroli, *Food Chemistry*, 2011, **129**, 1100.
- [7] D. S. Antal, G. Garban, and Z. Garban, *The Ann Univ. Dunarea de Jos of Galati, Food Tech*, 2003, **VI**, 106–115.
- [8] S. A. Brown in *The Biochemistry of Plants*, Vol. 7 Academic Press, Inc., New York, 1981, 269.
- [9] K.C. Fylaktakidou, D. J. Hadjipavlou-Litina, K.E. Litinas, D. N. Nicolaidis, *Current Pharmaceutical Design*, 2004, **10**, 3813.
- [10] S.S. Bhattacharyya, S.Paul, S.K. Mandal, A. Banerjee, N.Boujedainib, A.R. Khuda-Bukhsh, *European Journal of Pharmacology*, 2009, **614**, 128.
- [11] I. Kostova, S. Bhatia, P. Grigorov, S. Balkansky, V.K. Parmar, A. Prasad, L.Saso, *Current Medicinal Chemistry*, 2011, **18**, 3929.
- [12] R.G. Kalkhambkar, G.M. Kulkarni, C.M. Kamanavalli, N. Premkumar, S.M.B. Asdaq, C.M. Sun, *European Journal of Medicinal Chemistry*, 2008, **43**, 2178.
- [13] J.R.S. Houlst, and M. Paya, *General Pharmacology: The vascular system*, 1996, **27**, 713.
- [14] A.T. Tu, in *Raman Spectroscopy in Biology: Principles and Applications*, John Wiley and Sons, Ltd., Chichester, 1982
- [15] R. J. Tuma, *Raman Spectroscopy*, 2005; **36**, 307.
- [16] B.G. Frushour, J.L. Koenig, *Biopolymers* 1974; **13**: 455.
- [17] E.W. Blanch, D.D. Kasarda, L. Hecht, K. Nielsen, and L.D. Barron. *Biochemistry*, 2003, **42**, 5665.
- [18] I. Chourpa, V. Ducel, J. Richard, P. Dubois, and F. Boury. *Biomacromolecules* 2006, **7**, 2616.

-
- [19] B. Bochicchio, A. Aït-Ali, A.M.Tamburro, A.J. Alix, *Biopolymers*, 2004, **73**(4) 484.
- [20] C. K. Smith, and L. Regan, *Acc. Chem. Res.*, 1997, **30**, 153.
- [21] D.Pal, and P. Chakrabarti, *Acta Crystallographica*, 2000, **D56**, 589.
- [22] M.A. Kelly, B.W. Chellgren, A.L. Rucker, J.M. Troutman, M.G. Fried, A.F. Miller, and T.P. Creamer, *Biochemistry* 2001, **40**, 14376.
- [23] N. Linlaud, E. Ferrer, M.C. Puppo, C. Ferrero. *Journal of Agriculture and Food Chemistry*, 2011, **59**, 713.
- [24] A. Tinti, M. Di Foggia, P. Taddei, A. Torreggiani, M. Dettin, C. Fagnano, *Journal of Raman Spectroscopy*, 2008, **39**, 250.
- [25] M. Di Foggia, P. Taddei, C. Fagnano, A. Torreggiani, M. Dettin, S. Sanchez-Cortes, A. Tinti, *Journal of Molecular Structure*, 2009, 924-926, 120.
- [26] I.W. Lewin *In Advances in Infrared and Raman Spectroscopy*, vol. 11, Chapter 1, Clark RJH, Hester RE (eds). John Wiley & Sons: New York, 1984.
- [27] S.W. Ellepola, S.M. Choi, D.L. Phillips, C.Y. Ma. *Journal of Cereal Science*, 2006, **43**, 85.
- [28] T. Kitagawa, T. Azuma, K. Hamaguchi. *Biopolymers*, 1979, **18**, 451.
- [29] M. Xu, V.V. Ermolenkov, W. He, V.N. Uversky, L. Fredriksen, I.K. Lednev. *Biopolymers*, 2005, **79**, 58.
- [30] P.G. Hildebrandt, R.A. Copeland, T.G. Spiro, J. Otlewski M. Laskowski Jr., F.G. Prendergast, *Biochemistry* 1988, **27**, 5426.
- [31] M.N. Siamwiza, R.C. Lord, M.C. Chen, T. Takamatsu, I. Harada, H. Matsuura and T. Shimanouchi, *Biochemistry*, 1975, **14** 4870.
- [32] S.A. Overman, K. Aubrey, N.S. Vispo, G. Cesareni and G.J. Thomas Jr., *Biochemistry*, 1994, **34**, 1039.
- [33] Z.Q. Wen, A. Armstrong and G.J. Thomas Jr., *Biochemistry*, 1999, **38**, 3148.
- [34] Z. Arp, D. Autrey, J. Laane, S.A. Overman and G.J. Thomas Jr., *Biochemistry*, 2001, **40**, 2522.
- [35] G.J. Thomas Jr., *Biopolymers (Biospectroscopy)*, 2002, **67**, 214.
- [36] P. Taddei, T. Asakura, J. Yao and P. Monti, *Biopolymers*, 2004,**75**, 314.
- [37] E.A. Carter, J.S. Church, R.J. Denning, P.M. Fredericks, *Spectrochimica Acta*, 1994, **50A**, 1927.
- [38] E.G. Ferrera, A.V. Gómez, M.C. Anòn, M.C. Puppo. *Spectrochimica Acta Part A*, 2011, **79**, 278.
- [39] M. Foster, R.B. Girling, and R.E. Hester, *Journal of Raman Spectroscopy*, 1982, **12**, 36.
- [40] D.J. Barker, R.P. Cooney, and L.A. Suners, *Journal of Raman Spectroscopy*, 1985, **16**, 265.
- [41] J.-C. Merlin; A. Statoua, J.-P. Cornard. M. Saidi-Idrissi, R. Brouillard, *Phytochemistry*, 1994, **35** ,227.

- [42] E. Haslam, T.V. Mistry, Y. Cay, T.H. Lilley, *Journal of Chemical Society. Perkin Transaction 2*, 1991, 1287.
- [43] Gaussian 09, Revision B.01, Frisch, M. J.; Trucks, G. W.; Schlegel, H. B.; Scuseria, G. E.; Robb, M. A.; Cheeseman, J. R.; Scalmani, G.; Barone, V.; Mennucci, B.; Petersson, G. A.; Nakatsuji, H.; Caricato, M.; Li, X.; Hratchian, H. P.; Izmaylov, A. F.; Bloino, J.; Zheng, G.; Sonnenberg, J. L.; Hada, M.; Ehara, M.; Toyota, K.; Fukuda, R.; Hasegawa, J.; Ishida, M.; Nakajima, T.; Honda, Y.; Kitao, O.; Nakai, H.; Vreven, T.; Montgomery, Jr., J. A.; Peralta, J. E.; Ogliaro, F.; Bearpark, M.; Heyd, J. J.; Brothers, E.; Kudin, K. N.; Staroverov, V. N.; Kobayashi, R.; Normand, J.; Raghavachari, K.; Rendell, A.; Burant, J. C.; Iyengar, S. S.; Tomasi, J.; Cossi, M.; Rega, N.; Millam, J. M.; Klene, M.; Knox, J. E.; Cross, J. B.; Bakken, V.; Adamo, C.; Jaramillo, J.; Gomperts, R.; Stratmann, R. E.; Yazyev, O.; Austin, A. J.; Cammi, R.; Pomelli, C.; Ochterski, J. W.; Martin, R. L.; Morokuma, K.; Zakrzewski, V. G.; Voth, G. A.; Salvador, P.; Dannenberg, J. J.; Dapprich, S.; Daniels, A. D.; Farkas, Ö.; Foresman, J. B.; Ortiz, J. V.; Cioslowski, J.; Fox, D. J. Gaussian, Inc., Wallingford CT, 2009.
- [44] J. D. Chai and M. Head-Gordon, *Phys. Chem. Chem. Phys.*, 2008, **10**, 6615.
- [45] S. F. Boys and F. Bernardi; *Mol. Phys.*, 1970, **19**, 553.
- [46] J. Tomasi, B. Mennucci, R. Cammi, *Chem. Rev.*, 2005, **105**, 2999.
- [47] J. Waga *Pol. J. Food Nutr. Sci.* 2004, **13/54** (4), 327.

Chapter 8

Theoretical study on the spectroscopic properties of iron complexes

Over the past decades dye-sensitized solar cells (DSSC) have attracted remarkable attention as one of the most promising technologies toward cost-effective light to energy conversion.^[1-3] There is actually an increasing demand, both from academic and industrial domains, for the research of new dyes that can improve the, still, not high efficiency, especially compared to the one obtained by silicon based solar cell³. Indeed, one has to consider that the latter are more efficient in terms of photon to electricity but show the disadvantage of high cost and high energy consumption production process, implying a long pay-back time. DSSCs are composed of different elements^[1-3]: a nanocrystalline semiconductor film, a dye sensitizer, a redox electrolyte and a counter electrode. Among these the dye sensitizer represents one of the critical components to achieve a high power conversion efficiency. Strictly speaking an ideal dye should absorb as much visible light as possible and channel the electrons in the conduction band of the semi-conductor. Together with direct DSSC in the last years there has been some interest also in the so called inverse Grätzel solar cells.^[4] In the latter upon light excitations a hole, instead of an electron, is injected in the semi-conductors by the dye.

Most of high efficiency DSSCs, starting from the original works of Grätzel^[1], are based on Ruthenium(II)-polypyridyl complexes^[3], which shows wide absorption range from the visible to the near infrared (NIR) region with, for the last generation devices, an overall power conversion efficiency approaching 12%.^[3] The high efficiency showed by ruthenium based dyes has implied an active field of research on such compounds, and many different ligands are proposed and tested.^[5-31] The disadvantage of these complexes is related to the use

of Ruthenium, a rare and expensive metal that can limit its use in large scale production. Because of this, many works are focused in finding cheaper dyes, such as full organic, polymeric or cheaper metal-based complexes.^[32] Let us also cite that, one important point in building efficient DSSCs relies on the proper combination of the redox mediator with the proper dye, since the two components can interplay leading to a considerable variation in the efficiency of the cell.^[16]

In some recent works Welter and co-workers synthesized two complexes of iron with salicyloylhydrazono dithiolane ligand (Figure 1), which can show interesting properties and potential application as dye sensitizers for solar cells.^[33-35] These two new colored complexes undergo spontaneous photo-reduction and photo-isomerization following a rather complex mechanism.

In particular the photo-isomerization coupled with a photo-reduction could be exploited in order to store energy produced from light conversion. To be used as efficient DSSC sensitizers the complex should show charge transfer excitations, appearing in the visible and near infrared region, and inducing charge separation and hence a possible holes or electrons injections. Obviously the interest on such a system will mainly arise from the use of a cheap and ubiquitous metal, like iron, that could strongly diminish economic costs and environmental impact.

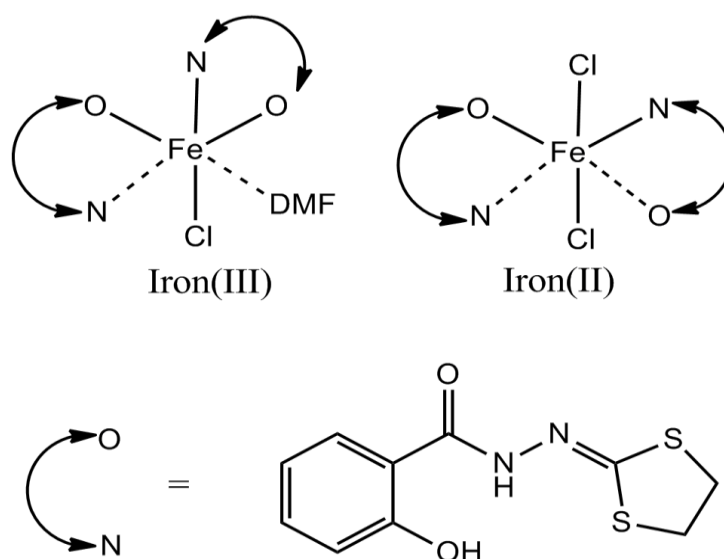


Figure 1. Iron(III) and iron(II) complexes molecular structures; note the different coordination between the two oxidation states.

The interest and the possible use of iron in DSSC was, for instance, evidenced by recent works of Ferrere that have synthesized and tested iron complexes with bipyridyl ligands which shown relatively high quantum yield.^[32]

In order to maximize the performance of iron-based complexes two aspects should be considered, first of all ligands should be able to enlarge the spectral width as much as possible, in particular toward the near infra-red region, maintaining relatively high absorption intensities. Secondly the electron, or hole in the case of inverse DSSC, transfer should be made as easy and efficient as possible, while, at the contrary, the unwanted recombination with the mediator leading to dark current phenomena should be avoided. A rationalization of this latter aspect, and the role played by ligands modification, can be realized by a carefully analysis of the electron density reorganization from ground to excited state.^[6, 17, 18]

Obviously quantum chemistry deploys there all its strength and can ultimately lead to efficient and rational molecular design.

In this work we studied at density functional theory (DFT) and at time dependent density functional theory (TD-DFT) levels of theory the properties of the originals iron II and iron III complexes (Figure 1). The absorption spectrum, inside the Franck-Condon approximation, has been considered to show the possibility to reproduce experimental results for this kind of complicated systems. The complex nature of the excited states has also been considered and tackled by using Natural Transition Orbitals (NTO) formalism.^[36-38]

The complex interplay between different phenomena taking place in the photo-isomerization and photo-reduction process^[33-35], crucial for energy storage, will instead make the object of a future contribution. Iron, in both +2 and +3 oxidation states, has a partially filled *d* shell and can therefore exhibit different multiplicities, often depending on the strength of the ligands field. For this reasons, even if experimentally the two complex have been found to have the maximum spin, all the possible spin multiplicities have been considered in the present work.

Because of the rather peculiar spectroscopic properties of this class of complexes, and the need to correctly reproduce crucial details, an analysis of the performance of different exchange-correlation functionals will be presented. In particular we will focus on the role of long-range corrected functionals, since we are mostly interested in charge transfer transitions that dominate the visible part of the spectrum and are crucial for charge injection process. Moreover, we will also analyze the subtle interplay between the functional used to obtain the equilibrium geometry and the one used to compute vertical transitions.

8.1 Computational methods

All computations have been performed by using Gaussian09 code^[39] at DFT and TD-DFT level. Environment effects have been taken into account by using PCM model^[40] for geometry optimization and for excited states calculations. Coherently with experimental procedure *n,n*-dimethylformamide parameters have been used to simulate the solvent.

Transition states energies and oscillator strengths (intensities) have been computed in the framework of the Franck-Condon principle from the optimized ground state geometry. In order to incorporated in a trivial way vibrational and other experimental effects, vertical transitions have been convoluted with Gaussian functions of fixed half-length width of 0.3 eV.

Geometry optimization have been performed using the LANL2DZ^[41] basis set as developed by Hay et al., the latter includes electron core pseudopotentials (ECP) for heaviest atoms such as iron. Geometry optimization has been performed for all the possible spin states in order to verify the relative stability.

Optimizations have been performed using the B3LYP^[42] exchange correlation functionals and the long range corrected CAM-B3LYP.^[43]

Excited states have been computed at TD-DFT level using the LANL2DZ basis. To assess for the quality of the basis some tests have been performed using an augmented triple zeta basis. Since the difference between the spectra obtained

with the two basis is negligible, in particular for the visible region of the spectrum, in the following we will present results obtained with the smaller double zeta basis set only.

Excited states have been computed as vertical excitations using TD-DFT approach. The number of the calculated excited states is chosen for every functional tested in order to span the experimental absorption spectrum range (between 80 and 120 singlet states). We also performed a benchmark of different functionals checking their reliability in reproducing absorption spectra, in particular we considered: B3LYP, PBE0^[44] and M06-2X^[45] hybrid functionals, the long-range corrected CAM-B3LYP, LC- ω PBE^[46] and the long-range and dispersion corrected functional ω B97X-D.^[47]

The nature of the main excitation has been analyzed with the help of the Natural Transition Orbitals (NTOs)^[36-38], in which a transition is represented, most of the time, by a simple couple of orbitals: the occupied orbital, i.e. the orbital left empty from the electron upon excitation, and the virtual orbital, i.e. the orbital which describes the electron in the excited state. NTOs have been obtained by a proper post-processing of the Gaussian output file using Nancy-EX (<http://nancyex.sourceforge.net/>) a GPL code developed in our laboratory.

8.2 Functionals benchmarking

As previously cited, we performed a benchmark to evaluate the performance of the different classes of functionals on the calculation of the UV/VIS spectra. Moreover, the effect of the functional chosen for the geometry optimization, and therefore of the different equilibrium geometries, on the final absorption spectrum was also considered.

Since the experimental spectrum of the iron(II) complex is missing we performed this benchmark only on the iron(III) complex to compare the computed spectrum with the experimental one.

Starting from the geometry obtained by X-Ray diffraction analysis we optimized the structure of the complex at B3LYP and CAM-B3LYP level of theory for the three possible spin states.

As shown in Table 1 both functionals give the same energy order for the different multiplicities. In agreement with experimental data, the sextuplet is always the ground state. The doublet and the quartet are between 0.4 and 0.5 eV higher energy than the sextuplet. Note that the energy difference between doublet and quartet is much less important and close to 0.1 eV

Table 1. Relative energies (eV) of Iron(III) complex for different multiplicity states with respect to the sextuplet ground state obtained with different functionals.

	B3LYP	CAM-B3LYP
Doublet	0.38	0.38
Quartet	0.45	0.49
Sextuplet	0.00	0.00

In Figure 2 we report the experimental spectrum together with the TDDFT calculated ones. Different combinations of functionals were used to compute optimized geometry and vertical transitions, as a convention, in the following nomenclature, we will indicate first the functional used for TD calculations followed by the one used for geometry optimization. Notice that the experimental spectrum presents an intense and broad maximum in the UV region of the spectrum extending from 250 to 350 nm. Moreover a much lesser intense absorption band is present in the visible region centered at about 520 nm (see the zoom panel in Figure 2). If we concentrate on the visible part of the spectrum one can see that the choice of the functional used for geometry optimization is much more important than the choice of the functional used for the TD calculations.

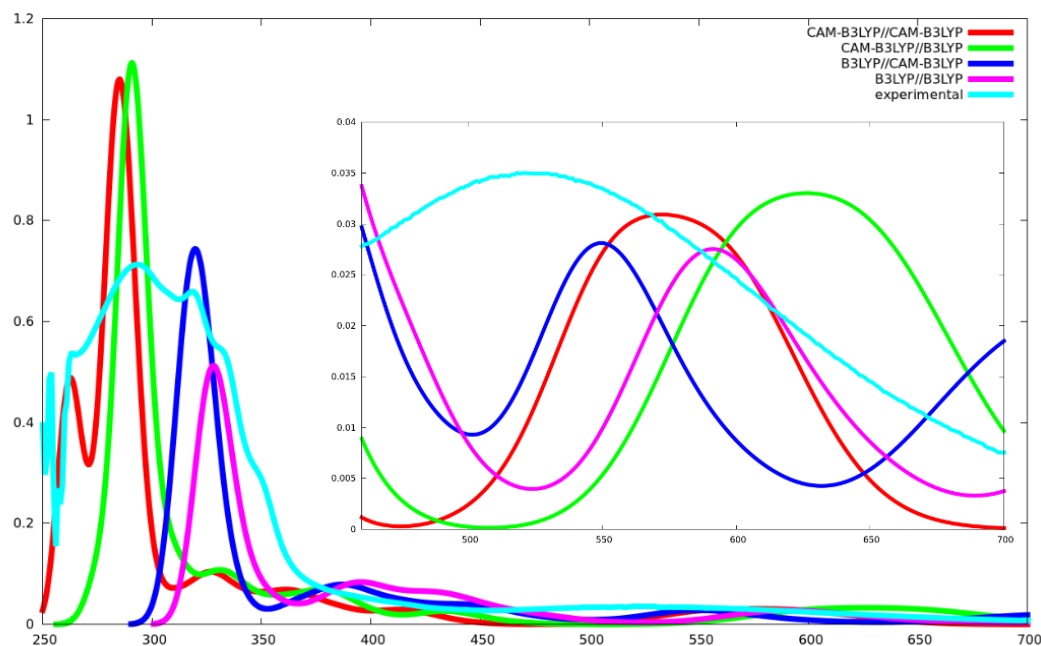


Figure 2. Absorption spectrum of Iron(III) complex calculated with different functionals vs the experimental one. On the left the functional used for TD calculation and on the right the functional used for geometry optimization (wavelength in nm, intensities in arbitrary units).

Indeed when using the CAM-B3LYP optimized geometry we obtain an absorption maximum in better agreement with experimental results whatever functional is used for the calculation of the excited states, with a deviation of about 25 nm for B3LYP. On the other hand when using B3LYP for geometry optimization the value of the absorption maximum is significantly red-shifted, with deviations going from 70 to 100 nm. The worst result is the one obtained using CAM-B3LYP for vertical excitations and B3LYP for geometry optimization. Note anyway that long-range corrected functionals overperform the hybrid one in giving a much broader absorption band, coherently with experimental evidences. As far as the near UV region is considered none of the methods is able to correctly reproduce the broad absorption spectrum. In that case the influence of the optimized geometry appears less important than in the

previous one with the role of the functional used for TDDFT calculation being the dominant one. Indeed B3LYP gives absorption maximum at about 330 nm, whatever functional used for geometry optimization, while CAM-B3LYP maximum appears at about 280 nm. The somehow worse agreement shown in the UV region can be due to the limited size of the basis set used as well as to the necessity to compute more excited states.

These results show that the choice of the functional for the geometry optimization, that is sometimes not sufficiently addressed, can bring important differences on the final calculated absorption spectrum, even when the deviations between the optimized geometries are quite small. This effect may be due to the internal π conjugation of salicyloylhydrazono dithiolane ligands as well as to the interaction of the ligands with iron, that necessitate of long-range corrected functionals to recover the long-range $1/R$ behavior.

Considering the previous results we decided to assess for the performance of different functionals in computing absorption spectrum starting from CAM-B3LYP optimized geometries. As described in computational detail, we want to consider functionals built using different strategies and including different effects, such as long-range corrections, in order to understand how taking into account these contributions can improve the accuracy in reproducing the experimental spectrum.

In Figure 3 we report the TD-DFT absorption spectrum computed with all the different functionals. If, in particular, we analyze in detail the visible region of the spectrum we can see that the M06-2X and LC-wPBE functionals perfectly fit the absorption maximum. Moreover M06-2X give a pretty broader absorption band with a general shape and intensity that are in a very good agreement with the experimental one.

On the other hand PBE0 functional show a blue shift of about 50 nm, while B3LYP, wB97XD and CAM-B3LYP experience a significant red shift going up to 50 nm. Notice, as already underlined, that B3LYP experiences a less pronounced deviation (about 25 nm) from the experimental maximum than long-

range corrected functionals, even if the band shape and intensities are less well reproduced.

Again none of the used functionals is able to correctly reproduce the large and intense experimental band in the near UV, with again hybrid functionals (B3LYP and PBE0) presenting maxima at shorter wavelengths than the others, while long range-corrected as well as M06-2X fail in reproducing the absorption at about 350 nm, showing slightly blue-shifted maxima.

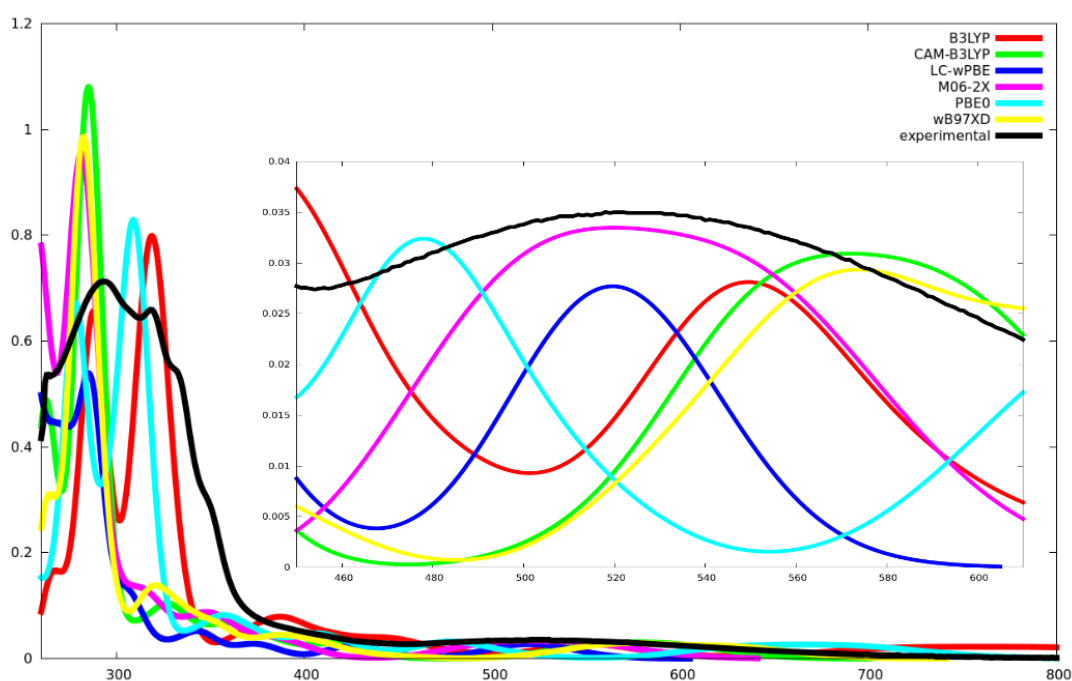


Figure 3. Comparison between absorption spectrum of iron (III) complex calculated with different functionals vs the experimental one. In the inset an expansion of the visible region (wavelength in nm, intensities in arbitrary units).

This functionals benchmark for TD calculation show that although M06-2X and LC-wPBE represent very well the visible part of the absorption spectrum their performance is worse in the near UV part. However, in photovoltaic

applications the visible region, constituted of charge-transfer type transitions, will be the most important and therefore the one to which we will pay most attention.

As stated previously the present iron complex undergoes a photoisomerization and photoreduction, it will be quite interesting to reproduce the spectrum of the iron(II) complex even if it has not been reported experimentally. UV/VIS spectrum has been calculated using the optimized CAM-B3LYP of the most stable isomer for these oxydation state. Note that like the case of iron(III) also the reduced specie is a high spin complex, the maximum multiplicity state being the most stable. Like in the case of iron(III) DFT calculations also correctly reproduce the energy order of the different spin states, with the quintet state being the ground state, triplet and singlet are quasi-degenerate among us and lay at about 1 eV higher energy. The convoluted spectrum is reported in Figure 4 for the visible region only, and one can again see a slight important variation of the absorption maximum with the functional used, the latter assuming values comprised between 370 and 410 nm. Hybrid functionals experience an important red-shift, while M06-2X appears the most blue-shifted. Note also that intensity (oscillator strengths) are much lower than in the case of iron(III), and vary quite a lot between functionals with wB97XD giving the lowest and B3LYP the highest ones.

In the work of Welter *et al.* [33-35] the absorption spectrum of the iron(II) complex is not reported because of its air-sensitive behavior leading to oxidation, even though they were able to isolate it as a yellow crystals. The computed low intensity peaks are coherent with such observation, and moreover the small values of the oscillator strengths are also coherent with the fact that the crystal and the solution are only very weakly colored.

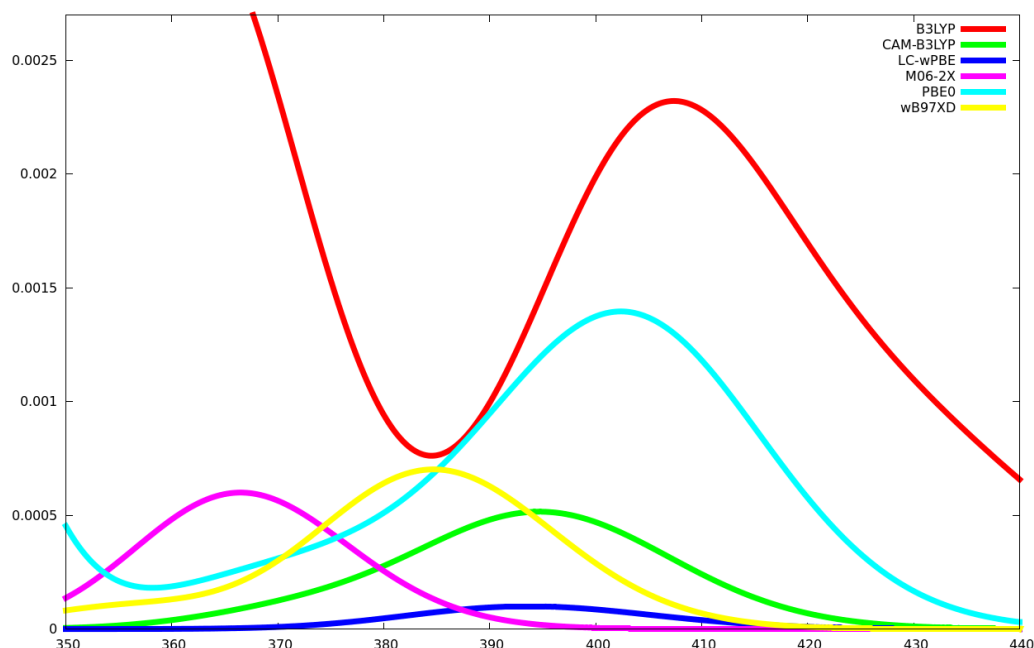


Figura 4. Expansion of the visible region of the spectrum of iron (II) complex calculated with different functionals (wavelength in nm, intensities in arbitrary units).

8.3 Transition analyses

One important possibility offered by quantum chemistry is to have a direct access to the analysis of the individual electronic transitions, composing the experimental spectrum, in terms of electron density rearrangement. Hence it can be extremely helpful to show the role of the different ligand in the physical process and to orient the synthesis of optimized dyes.

This analysis has been conducted in terms of NTO and allows to graphically visualize the topology of the orbital involved in the transition and the type of excitations, that can be a Metal-to-Ligand (MLCT), Ligand-to-Ligand (LLCT) or Ligand-to-Metal (LMCT) Charge Transfer.

We decided to extract NTO from the TD-B3LYP calculation since it shows a good overall performance, compared with the experimental iron(III)

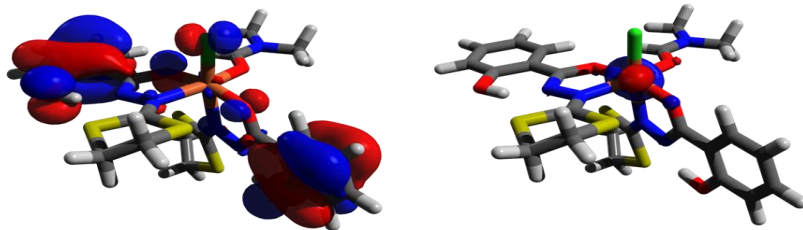
spectrum, in all the spectral regions. However NTOs obtained with the other functionals show the same qualitative behavior.

In Table 2 are reported the wavelengths of the most important vertical transitions in terms of oscillator strength and in figure 5 some NTOs for the iron(III) complex.

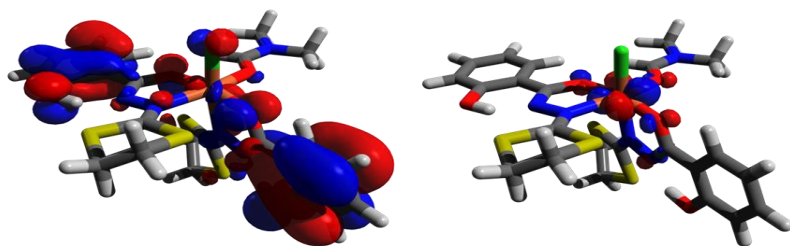
Table 2. Main electronic transition of iron(III) complex with B3LYP. The transition index indicates the excited state involved in the transition.

Transition	Wavelength (nm)	f
9	553	0.0129
10	550	0.0026
11	544	0.0082
12	542	0.0032
13	516	0.0021
17	480	0.0056
20	451	0.0081
22	444	0.0099
42	390	0.0155
43	387	0.0113
44	384	0.0207
74	323	0.0599
75	322	0.2134
76	319	0.1214
78	317	0.2374
80	312	0.1034
94	288	0.3950
95	287	0.0748

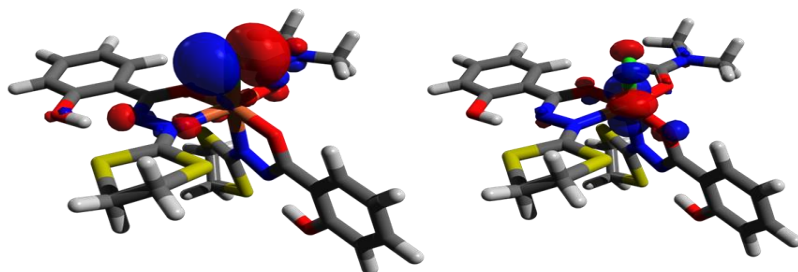
Transition 9



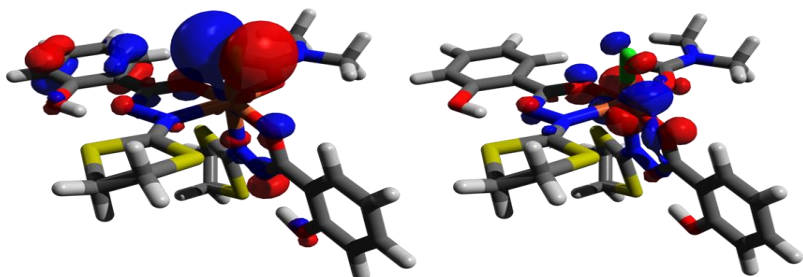
Transition 11



Transition 17



Transition 22



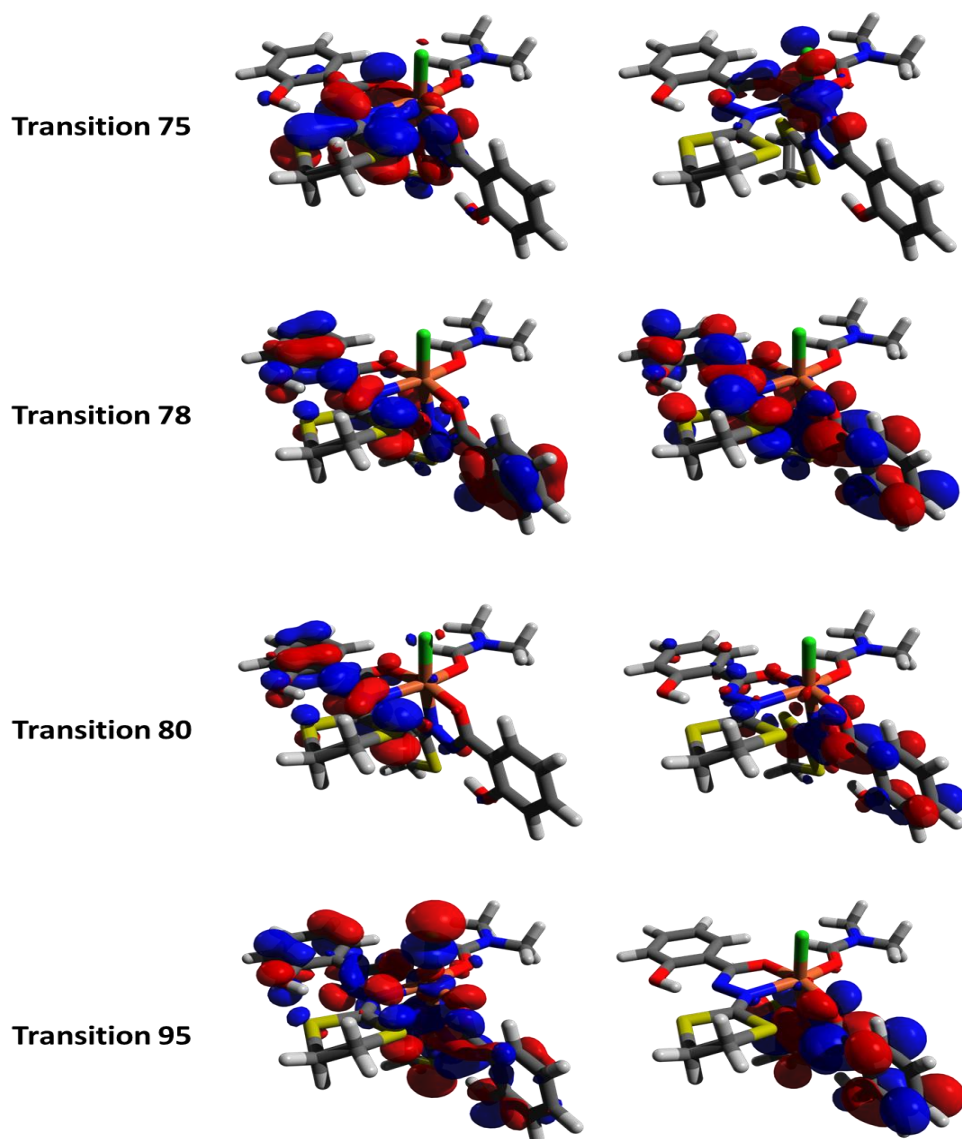


Figure 5. Occupied (left) and Virtual (right) NTO for iron III complex selected transitions

By analyzing the selected NTOs reported in figure 5 one can notice the presence of LMCT transitions in the visible part of the spectrum (transitions 9, 11, 17, 22). In particular the lowest lying transitions involves the creation of a hole on the salicylic ligands, while higher energy transitions draw electron density from the chlorine. Notice that some transitions appearing at relative high energy (transition 75, 322 nm) can still be qualified as LMCT. The other most important

transition in Figure 5 can be seen whether as LLCT (transition 80, 95) or as strongly delocalized p-p type (transition 78). Note that no MLCT transitions appears to have significant intensity.

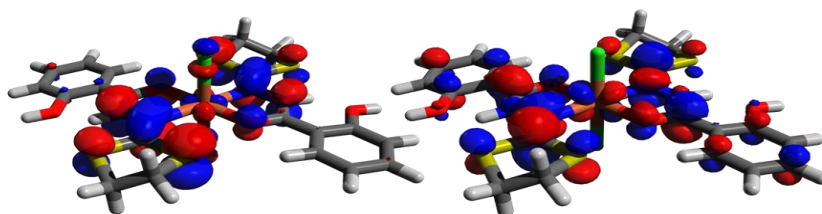
In Table 3 the main vertical transitions of iron(II) complex are reported while in Figure 6 some representative selected NTOs for the same system are shown.

Table 3. Main electronic transition of iron(II) complex with B3LYP. The transition index indicates the excited state involved in the transition.

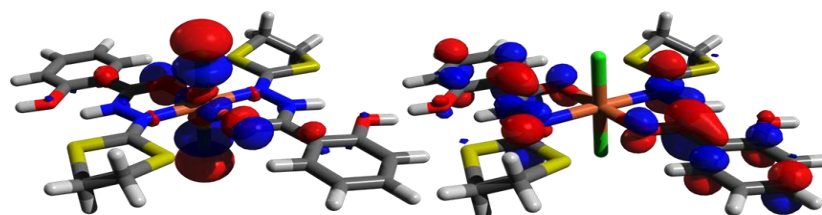
Transition	Wavelength (nm)	f
6	431	0.0007
8	406	0.0022
9	364	0.0013
11	362	0.0004
12	354	0.0009
16	330	0.0752
22	319	0.2189
27	311	0.2270
38	296	0.0229
50	284	0.0775
56	275	0.1785

Again one can clearly see that the visible part of the spectrum is characterized by LMCT transitions (8, 9, 16) notice also the more important role played by the chlorine atoms in the low energy transitions, and notice also the presence of a chlorine-to-metal charge-transfer transition at quite high energy values (transition 56, 276 nm). All the other evidenced transitions are of LLCT type and always show an extremely important role of the chlorine in the occupied NTO, i.e. chlorine definitively acts as the principal electron donor group.

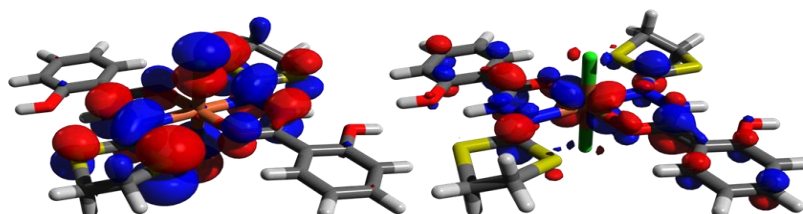
Transition 8



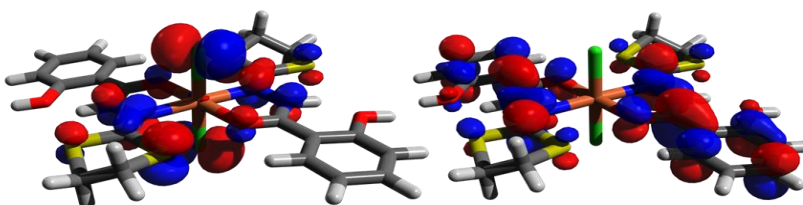
Transition 9



Transition 16



Transition 22



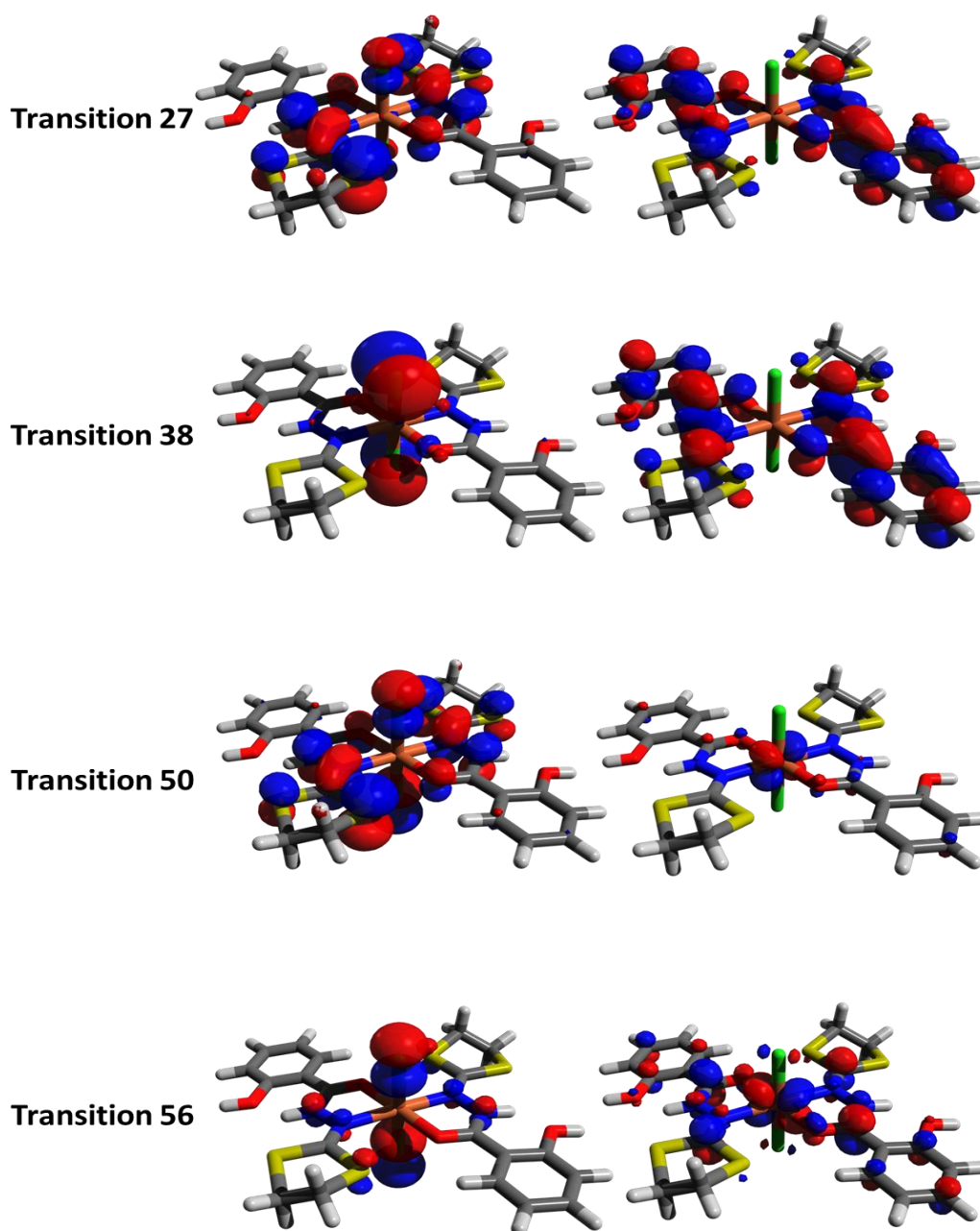


Figure 6. Occupied (left) and Virtual (right) NTO for iron II complex selected transitions

The presence of LMCT that leaves holes on the ligand can be extremely beneficial in the case of the application as dyes in inverse DSSC, since in that paradigm is the semiconductor that is supposed to inject electron into the dye following excitation. Obviously the presence of important electron deficiency on

the ligand that are directly grafted to the surface can favor such a process.

However the weak absorption intensities, as well as the important role played by the chlorine atom can limit the performance of the system. The introduction of more delocalized chelating ligand can help in overcoming such limitations.

Conclusion

The electronic excitation spectrum of an iron complex known to experience photoisomerization and photoreduction has been performed at TDDFT level for both +3 and +2 oxidation states. The performance of different functionals has been accounted for, and in particular the dependence of the functional used for geometry optimization has been particularly evidenced. In particular B3LYP appears unable to provide equilibrium geometries from which one can safely extract vertical excitation energies. At the other hand the use of long-range corrected CAM-B3LYP for geometry optimization allows to reliably reproduce the absorption spectrum. New generation M06-2X functional as well as LC-wPBE appears to be the ones better reproducing the visible region of the spectrum, although their performance is less good in the near UV. Quite surprisingly, for vertical excitations, B3LYP performs better than some of long-range corrected functionals, namely CAM-B3LYP. This occurrence even in the case of charge-transfer states can be related to the limited size of the complex and therefore to the presence of a small charge separation. It is known that in such conditions CAM-B3LYP may experience important deviations from experience, and in general has a worse performance than B3LYP in reproducing excitation energies.^[48,49] This evidence has also already been pointed out, for instance by Ruud et al.^[50] in the calculation of circular dichroism as well as by some of us in computing absorption spectra of ruthenium organo-metallic complexes.^[51,52] The topological analysis of the transition has clearly shown that the absorption spectrum is dominated by LMCT transition type, leaving a hole in the ligands. This occurrence is confirmed for both iron(III) and iron(II) complexes, moreover an important participation of

the ancillary chlorine ligands has been evidenced. The necessity to modify the ligands in order to enhance the absorption intensities and to favor transitions potentially leading to efficient charge injection in the domain of DSSC has been also evidenced. In particular the use of more p-delocalized ligands and a substitution of the chlorine, for instance by NCS, should be considered. In the future we plan to perform a systematic computational study on possible candidates in order to optimize the ligand choice in a molecular design approach.

Part of this chapter is reproduced with permission from “*Journal of Physical Chemistry A*” by American Chemical Society. The complete study here described can be found in the paper “N. Zanna, A. Monari, X. Assfeld, *J. Phys. Chem. A*, **2012**, 48, 11905-11912” fully available at <http://pubs.acs.org> .

References

- [1] O'Regan, B.; Grätzel, M. *Nature*, **1991**, 353, 737
- [2] Hagfeldt, A.; Grätzel, M. *Acc. Chem. Res.*, **2000**, 33, 269
- [3] Hagfeldt, A.; Boschloo, G.; Sun, L.; Kloo, L.; Pettersson, H. *Chem. Rev.*, **2010**, 110, 6595
- [4] Nattestad, A.; Mozer, A. J.; Fischer, M. K. R.; Cheng, Y.-B.; Mishra, A.; Bäuerle, P.; Bach, U. *Nature Mat.*, **2010**, 10, 31
- [5] Hagfeldt, A.; Grätzel, M. *Chem. Rev.* **1995**, 95, 49
- [6] Labat, F.; Le Bahers, T.; Ciofini, I.; Adamo, C. *Acc. Chem. Res.* **2012**, 45, 1268
- [7] Grätzel, M. *Nature* **2001**, 414, 338
- [8] Grätzel, M. *Inorg. Chem.* **2005**, 44, 6841
- [9] Ardo, S.; Meyer, G. *J. Chem. Soc. Rev.* **2009**, 38, 115
- [10] Peter, L. M. *J. Phys. Chem. C* **2007**, 111, 6601
- [11] Peter, L. M. *Phys. Chem. Chem. Phys.* **2007**, 9, 2630
- [12] Bisquert, J.; Cahen, D.; Hodes, G.; Ruhle, S.; Zaban, A. *J. Phys. Chem. B* **2004**, 108, 8106
- [13] O'Regan, B. C.; Durrant, J. *Acc. Chem. Res.* **2009**, 42, 1799
- [14] Hagfeldt, A.; Boschloo, G.; Sun, L.; Kloo, L.; Pettersson, H. *Chem. Rev.* **2010**, 110, 62595
- [15] Robertson, N. *Angew. Chem., Int. Ed.* **2006**, 45, 2338
- [16] Grabulosa, A.; Martineau, D.; Beley, M.; Gros, P. C.; Cazzanti, S.; Caramori, S.; Bignozzi, C. A. *Dalton Trans.* **2009**, 63

- [17] Noureen, S.; Caramori, S.; Monari, A.; Assfeld, X.; Bignozzi, C. A.; Beley, M.; Gros, P. C. *Dalton Trans.* **2012**, *41*, 4833.
- [18] Monari, A.; Assfeld, X.; Beley, M.; Gros, P. C. *J. Phys. Chem. A*, **2011**, *115*, 3596.
- [19] Preat, J. *J. Phys. Chem. C* **2010**, *114*, 16716
- [20] Preat, J.; Jacquemin, D.; Perpète, E. A. *Energy Environ. Sci.* **2010**, *3*, 891
- [21] Preat, J.; Jacquemin, D.; Michaux, C.; Perpète, E. A. *Chem. Phys.* **2010**, *376*, 56
- [22] Preat, J.; Jacquemin, D.; Perpète, E. A. *Environ. Sci. Technol.* **2010**, *44*, 5666
- [23] Preat, J.; Michaux, C.; Jacquemin, D.; Perpète, E. A. *J. Phys. Chem. C* **2009**, *113*, 16821
- [24] Pastore, M.; De Angelis, F. *ASC Nano* **2010**, *4*, 556
- [25] Fantacci, S.; De Angelis, F.; Selloni, A. *J. Am. Chem. Soc.* **2005**, *125*, 16835
- [26] De Angelis, F.; Fantacci, S.; Selloni, A.; Grätzel, M.; Nazeruddin, M. K. *J. Am. Chem. Soc.* **2007**, *129*, 14157
- [27] Lundqvist, M. J.; E. Galoppini, E.; Meyer, G. J.; Persson, P. *J. Phys. Chem. A* **2007**, *111*, 1487
- [28] Jacquemin, D.; Perpète, E. A.; Laurent, A. D.; Assfeld, X.; Adamo, C. *Phys. Chem. Chem. Phys.* **2009**, *11*, 1258
- [29] Martineau, D.; Beley, M.; Gros, P. C.; Cazzanti, S.; Caramori, S.; Bignozzi, C. A. *Inorg. Chem.* **2007**, *46*, 2272
- [30] Grabulosa, A.; Beley, M.; Gros, P. C.; Cazzanti, S.; Caramori, S.; Bignozzi, C. A. *Inorg. Chem.* **2009**, *48*, 8030
- [31] Nazeeruddin, M. K.; Wang, Q.; Cevey, L.; Aranyos, V.; Liska, P.; Figgemeier, E.; Klein, C.; Hirata, N.; Koops, S.; Haque, S. A.; Durrant, J. R.; Hagfeldt, A.; Lever, A. B. P.; Grätzel, M. *Inorg. Chem.* **2006**, *45*, 787
- [32] Ferrere, S. *Inorg. Chim. Acta*, **2002**, *329*, 79
- [33] Bouslimani, N.; Clément, N.; Rogez, G.; Turek, P.; Bernard, M.; Dagorne, S.; Martel, D.; Cong, H. N.; Welter, R. *Inorg. Chem.* **2008**, *47*, 7623.
- [34] Bouslimani, N.; Clément, N.; Toussaint, C.; Hameury, S.; Turek, P.; Choua, S.; Dagorne, S.; Martel, D.; Welter, R. *Eur. J. Inorg. Chem.*, **2009**, *2009*, 3734.
- [35] Bouslimani, N.; Clément, N.; Rogez, G.; Turek, P.; Choua, S.; Dagorne, S.; Welter, R. (2010). *Inorg. Chim. Acta*, **2010**, *363*, 213.
- [36] Martin, R. L. *J. Chem. Phys.* **2003**, *118*, 4775.
- [37] Monari, A.; Very, T.; Rivail, J.-L.; Assfeld, X. *Comp. Theor. Chem.*, **2012**, *990*, 119.
- [38] Monari, A.; Very, T.; Rivail, J.-L.; Assfeld, X. *Theor. Chem. Acc.*, **2012**, *131*, 1221.
- [39] Gaussian 09, Revision **B.01**, Frisch, M. J.; Trucks, G. W.; Schlegel, H. B.; Scuseria, G. E.; Robb, M. A.; Cheeseman, J. R.; Scalmani, G.; Barone, V.; Mennucci, B.; Petersson, G. A.; Nakatsuji, H.; Caricato, M.; Li, X.; Hratchian, H. P.; Izmaylov, A. F.; Bloino, J.; Zheng, G.; Sonnenberg, J. L.; Hada, M.; Ehara, M.; Toyota, K.; Fukuda, R.; Hasegawa, J.; Ishida, M.;

- Nakajima, T.; Honda, Y.; Kitao, O.; Nakai, H.; Vreven, T.; Montgomery, Jr., J. A.; Peralta, J. E.; Ogliaro, F.; Bearpark, M.; Heyd, J. J.; Brothers, E.; Kudin, K. N.; Staroverov, V. N.; Kobayashi, R.; Normand, J.; Raghavachari, K.; Rendell, A.; Burant, J. C.; Iyengar, S. S.; Tomasi, J.; Cossi, M.; Rega, N.; Millam, J. M.; Klene, M.; Knox, J. E.; Cross, J. B.; Bakken, V.; Adamo, C.; Jaramillo, J.; Gomperts, R.; Stratmann, R. E.; Yazyev, O.; Austin, A. J.; Cammi, R.; Pomelli, C.; Ochterski, J. W.; Martin, R. L.; Morokuma, K.; Zakrzewski, V. G.; Voth, G. A.; Salvador, P.; Dannenberg, J. J.; Dapprich, S.; Daniels, A. D.; Farkas, Ö.; Foresman, J. B.; Ortiz, J. V.; Cioslowski, J.; Fox, D. J. Gaussian, Inc., Wallingford CT, 2009.
- [40] Tomasi, J.; Mennucci, B.; Cammi, R. *Chem. Rev.* **2005**, *105*, 2999.
- [41] Wadt, W. R.; Hay, P. J. *J. Chem. Phys.* **1985**, *82*, 284.
- [42] a) Becke, A. D. *J. Chem. Phys.* **1993**, *98*, 1372 b) Lee, C.; Yang, W.; Parr, R. G. *Phys. Rev. B* **1993**, *37*, 785.
- [43] Yanai, T.; Tew, D. P.; Handy, N. C. *Chem. Phys. Lett.* **2004**, *393*, 51
- [44] Adamo, C.; Barone, V. *J. Chem. Phys.* **1999**, *110*, 6158
- [45] Zhao, Y.; Truhlar, D. G. *Theor. Chem. Acc.* **2008**, *120*, 215
- [46] a) Vydrov, O. A.; Heyd, J.; Krukav, A. V.; Scuseria, G. E. *J. Chem. Phys.* **2006**, *125*, 074106
b) Vydrov, O. A.; Scuseria, G. E. *J. Chem. Phys.* **2006**, *125*, 234109
- [47] Chai, J.-D.; Head-Gordon, M. *Phys. Chem. Chem. Phys.* **2008**, *10*, 6615
- [48] Peach, M. J. G.; Benfield, P.; Helgaker, T.; Tozer, D. J. *J. Chem. Phys.* **2008**, *128*, 044118.
- [49] Jacquemin, D.; Perpète, E. A.; Wathélet, V.; Adamo, C. *J. Chem. Theory Comp.* **2009**, *5*, 2420
- [50] Scherbin, D.; Ruud, K. *Chem. Phys.* **2008**, *349*, 234.
- [51] Very, T.; Despax, S.; Hébraux, P.; Monari, A.; Assfeld, X. *Phys. Chem. Chem. Phys.* **2012**, *14*, 12496
- [52] Chantzis, A.; Very, T.; Monari, A.; Assfeld, X. *J. Chem. Theory Comp.*, **2012**, *8*, 1536.

